Order Number 9417473

Investigation of heterogeneous electron transfer on a mercury oblate spheroidal microelectrode and liquid chromatography with electrochemical detection for chloroquine and metal ions

Huang, Zuopeng, Ph.D.

City University of New York, 1994

U·M·I
300 N. Zeeb Rd.
Ann Arbor, MI 48106

Investigation of Heterogeneous Electron Transfer on a Mercury Oblate Spheroidal Microelectrode and Liquid Chromatography with Electrochemical Detection for Chloroquine and Metal Ions

by

Zuopeng Huang

A dissertation submitted to the Graduate Faculty in Chemistry in partial fulfillment of the requirements for the degree of Doctor of Philosophy, The City University of New York.

1994

This manuscript has been read and accepted for the Graduate Faculty in Chemistry in satisfaction of the dissertation requirement for the degree of Doctor of Philosophy.

1/20/94
date

Ronald L. Birke
Chairman of Examining Committee

1/26/94
date

Executive Officer

Supervisory Committee

The City University of New York

Abstract

Investigation of Heterogeneous Electron Transfer on a Mercury Oblate Spheroidal Microelectrode and Liquid Chromatography with Electrochemical Detection for Chloroquine and Metal Ions

by

Zuopeng Huang

Adviser: Professor Ronald L. Birke

A mercury microelectrode formed by electroreduction of mercury on an inlaid platinum microdisk is experimentally shown to be well modeled by oblate spheroidal geometry when the ratio of the semiminor axis to the semimajor axis of the protruding drop is less than one. The validity of the geometry is established by comparison of the experimentally determined coefficient in the steady state diffusion current equation with the theoretical value for oblate spheroidal geometry. Spherical cap geometry is also shown to be an equally valid geometric model; however, theoretical treatment for this system is more difficult. The theory of a quasi-reversible electrode process is developed and applied to the determination of the electrode parameters of the $Ru(III)(NH_3)_6$ /$Ru(II)(NH_3)_6$ electrode reaction on a mercury oblate spheroidal

microelectrode. Results agree well with others found in the literature for the same process on a mercury electrode.

Liquid chromatography with a static mercury electrode has been studied to detect chloroquine based on the catalytic hydrogen wave. Both the electrochemical properties and optimal conditions of chromatography have been studied in this set of experiments. The results have shown this method can be used as an electrochemical detector for HPLC trace determination because of its high sensitivity and good reproducibility. Since nitrogenous compounds are widely used and many of these compounds have been reported to exhibit catalytic hydrogen wave at mercury electrode, the method should quite general.

Liquid chromatography with thin-layer cell electrochemical detection has been investigated as a method for the simultaneous determination of copper, nickel, and cobalt in rock samples. This detection was based on formation, separation, and subsequent oxidation of dithiocarbamate complexes. The complex formation, reproducibility, interferences, and an analytical procedure for the detection are presented. Limits of detection of less than 1 ng can be obtained for all of these metals. The analysis results are in good agreement with the values from atomic absorption spectroscopy.

Acknowledgment

I would like to express my sincere gratitude to my thesis advisor Professor Ronald L. Birke for his advice, guidance, encouragement, and continuous support throughout the course of this work. I would like to thank Professor David C. Locke and David K. Gosser, my thesis members, for their advice and for finding time in their busy schedules to serve on my thesis committee. I am also indebted to my friends and colleagues, George D. Sukenick, Vimal T. Kumar, Qingdong Huang, Feng Zhang and others for their friendship and assistance during my years at City College. Finally, I would like to thank my wife, Lihua Chen, without her love, patience, and encouragement, this work could never have been done.

Table of Contents

List of Figure

List of Table

Part I

Theoretical and Experimental Investigation of Steady State Voltammetry for Quasi-reversible Heterogeneous Electron Transfer on a Mercury Oblate Spheroidal Microelectrode

1.1 Introduction

Various electrode geometries have been characterized for the investigation of steady state currents at microelectrodes including the inlaid microdisk embedded in a nonconducting plane, the microsphere and microhemisphere, and the microline and microband electrode [1]. Recently, using oblate spheroidal geometry, an equation was derived for steady state diffusion controlled current for a reversible electrode reaction on an oblate microspheroidal electrode embeded in a nonconducting basal plane [2]. This current-potential relationship has the interesting feature that it contains both the hemispherical and inlaid microdisk geometry as limiting cases. In this thesis, it is shown that oblate spheroidal geometry can be used to accurately model an electrode made by depositing Hg on an inlaid microdisk electrode and then the current-potential relationship is developed for quasi-reversible heterogeneous electron transfer (ET) on this electrode. Finally, the theory is applied to an experimental determination of a heterogeneous ET rate constant.

Spheroidal geometry is characterized by an altitude, b, above the basal plane of the electrode and by a radius, a, of a microdisk (circular area) in the basal plane of the microelectrode, Figure 1.1. For an oblate spheroid a and b are the major and minor semiaxes, respectively. The diffusion current equation for oblate spheroidal geometry becomes the equation for the inlaid microdisk as the altitude, b, goes to zero or the microhemisphere in the other limit when b becomes equal to the radius, a [2]. According to Myland and Oldham [3] oblate spheroidal microelectrodes belong to a more general class of electrode geometry referred to as "conforming microelectrodes" [3]. Along with the oblate spheroid and its limiting forms of inlaid disk and hemisphere, conforming microelectrodes include the hemitoroid, the hemicylinder, the spherical segment (sphere-cap family), and the prolate spheroid. All of these electrodes contain a conducting circular area in the basal plane of the electrode which intersects an infinite insulating plane, the simplest case being a conducting disk inlaid in a nonconducting plane. Furthermore, they are all solids of revolution formed by rotation of a curve segment about an axis which is in the center of and perpendicular to the conducting circular area in the basal plane. For example, the oblate spheroid conforming electrode is formed by rotation of an ellipse about its minor axis, b (see Figure 1.1).

In order to use equations developed for oblate spheroidal geometry, it must be confirmed that this geometry is a good model for mercury mircoelectrodes formed by electrodeposition of Hg(I) from solution on to an inlaid metal microdisk electrode. It is clear that the resulting electrodes will be of the above described conforming type. Colyer, Oldham and Fletcher [4] point out that in an idealized system the mercury would adopt a

spherical segment shape which minimizes the surface area of mercury, and thus minimizes the interfacial energy of the mercury-solution interface. However, the surface area of the oblate spheroid will be very close to that of a spherical segment for the same volume of mercury drop and for non ideal conditions (imperfections in the disk surface, etc) it is not certain a priori which shape is the best model. Furthermore, there are many different ways that a mercury overlayer could form by electrodeposition on an inlaid disk depending on the interfacial energies [4]. In this study, it was assumed that for b/a ratios larger than 0.2 and less than 1.0 the mercury completely covers the inlaid disk electrode and does not form on the insulating plane.

It has been shown by Wehmeyer and Wightman [5] that fabricated mercury microelectrodes have good properties in that the electrodes are durable and can be used in aqueous or nonaqueous media. Considering the advantages of the smooth surface of mercury and the large number of studies in the literature for redox processes on mercury, it would be an advantage to have a well-characterized Hg microelectrode for the determination of redox parameters.

In this investigation, both the spherical cap and oblate spheroidal geometry have been examined. It is clear that both are equally good approximations to the geometry of our Hg microelectrode. These results are for microelectrodes made by electrodeposition of Hg from solution when the b/a ratio is less than unity. Furthermore, the oblate spheroidal geometry has the advantage that a closed form steady state diffusion current equation is available while a numerical integration is necessary to evaluate the current equation for diffusion to a spherical cap microelectrode. Additionally, it is straightforward to develop the steady

state current-potential equation for the quasi-reversible case at the oblate hemispheroid microelectrode.

After it was verified that a Hg conforming microelectrode can be described by steady state diffusion to an oblate microhemispheroid, the quasi-reversible current-potential relation for this geometry was developed. From this general (quasi-reversible) expression, current-potential relations can also be found as the geometry takes the limiting forms of an inlaid microdisk and a microhemisphere. The equations are then applied to the determination of the standard heterogeneous rate constant for the $Ru(III)(NH_3)_6$ /$Ru(II)(NH_3)_6$ electrode reaction on the oblate hemispheroidal microelectrode. In addition, the most appropriate methodology for determining unknown parameters of the electrode kinetic system is discussed.

1.2 Experimental Section

The ruthenium hexa-ammine trichloride (ICN Biomedicals, Inc. Cleveland, Ohio) and the mercury(I) perchlorate (Alfa products, Danvers, MA) were used as received. Ferricyanide was obtained from J.T. Baker Chemical Co., Phillipsburg, NJ. All chemicals used in electrolyte preparation were analytical reagent grade. Electrodes were polished with 0.05 micron Micropolish II (Buehler Ltd., Lake Bluff, IL). Pure water was obtained by passing tap water through a carbon filter, multiple ion exchange system and then distilling. Solutions were degassed with prepurified nitrogen.

Steady state currents were obtained with linear scan voltammetry from a 3.0mM ruthenium(III) hexa-ammine trichloride solution in deoxygenated 0.1M phosphate buffer (pH=7.0). The phosphate buffer contained 0.06M KH_2PO_4 and 0.04M Na_2PO_4 and was adjusted to pH 7.0 with dilute H_3PO_4. The mercury microelectrodes were washed with deionized-distilled water after deposition and then transferred to the ruthenium ion solution. The scan potential range was from 0.0V to -0.50 V vs. SCE with a scan rate of 10 mV/sec.

Chronoamperometric electrodeposition of mercury onto a gold microdisk electrode and linear scan experiments were made with a Tacusel PRG 5, Pulse Polarographic instrument and a Houston Model 200 XY recorder. The gold microdisk electrode (10 micron in diameter) was obtained from Bioanalytical Systems (BAS). The experimentally determined surface area of deposited mercury microelectrodes ranged from 84 $x10^{-8}$ cm^2 to 157 x 10^{-8} cm^2 for calculations based on a perfect oblate hemispheroid. A saturated calomel electrode (SCE) and a platinum electrode served as the reference and auxiliary electrodes, respectively. Before each experiment, the working microelectrode was polished with 0.05 micron Micropolish II and washed with copious amounts of deionized-distilled water. At the end of each experiment, the electrode was polished and dipped into concentrated nitric acid to prevent etching of the gold by the mercury [6].

Numerical computations such as the solution of cubic equations and numerical integration were done with the internal functions of Mac II - MATLAB on a Macintosh SE/30 computer. Linear least squares analysis was performed with Cricket Graph on a variety of Macintosh computers

and nonlinear least squares analysis was performed with a FORTRAN 77 version of the subroutine NLLSQ on a Vax 11/780 computer. The latter subroutine was written at Bell Telephone Laboratories and is an implementation of the Marquardt iterative scheme for nonlinear least squares fitting which employs both gradient and Taylor series methods.

1.2.1 Mercury Electrode Formation

A large number of examples of electrodeposited mercury covered carbon and solid metal electrodes have appeared in the literature (see [7] and references within). It is important to insure smooth spreading of the mercury during the electrodeposition process. As the following discussion shows the choice of electrode material influences the fabrication of a well covered electrode. At a platinum disk, the wetting process is slow and the mercury electrodeposition process may form one or more isolated drops which do not cover the entire surface, especially on larger microelectrodes such as one with a 10 micrometer diameter [6]. Stojek and Osteryoung [8] sought to increased the rate of the wetting process on Pt by cycling the potential between 0.0 and 0.8V to form a thin layer of $HgPt_2$, HgPt, and Hg_2Pt compounds to speed up the wetting process; however, they still obtained behavior on the i-t curve that displayed sudden drops in current characteristic of the coalescence of mercury droplets. For mercury deposition on a carbon disk electrode, the deposition process was very nonreproducible and usually resulted in failure of the drop to adhere to the carbon [5]. Silver is more easily wettable by mercury than platinum because silver solubility in mercury is larger than platinum [9]; however, to

enhance the rate of wetting for a silver microdisk, it was necessary to apply an oxidizing prepulse to form Ag^+ [8]. Au is easily wet by Hg and its wetting process is fast and quite simple. After polishing the electrode, it can be directly wetted without any other pretreatment.

Based on the previous discussion, a Au microdisk was selected as the best electrode surface to use for electrodeposition. A deoxygenated solution of 0.25 M $HClO_4$ containing 5.0 mM or 25.0 mM $Hg_2(ClO_4)_2$ was used for the mercury deposition. Mercury deposition on the gold microdisk electrode was carried out by application of a constant potential of 0.0V vs. SCE for various times depending on the desired size of the conforming microelectrode. This applied potential insures Hg(I) reduction but is too low for the reduction of most other metal ions. The chronoamperometric i-t curve was followed to insure proper coverage of the Hg on the Au microdisk. The conforming mercury microelectrode prepared in this way is relatively durable and rugged. The electrode can normally be washed repeatedly with distilled water or left in solution while deoxygenating with a nitrogen stream without loss of the mercury. The altitude b was determined using the charge obtained from the i-t curve to calculate the volume of mercury from Faraday's law. Then b was calculated from the volume equations for the oblate spheroid or spherical segment geometry.

1.2.2 Evaluation of the Steady State Diffusion Current Equation for Oblate Spheroidal and Spherical Cap Microelectrodes

The steady state current for the conversion of soluble oxidized species, O, to soluble reduced species, R, in a reversible electrode reaction

involving n electrons per molecule at a conforming microelectrode can be formulated [2] as

$$i = \frac{knF\,a D_O C_O^b}{(1+\theta)} \qquad (1\text{-}1)$$

with $$\theta = \frac{D_O}{D_R} \exp\left(\frac{nF}{RT}(E - E^{0'})\right)$$

where a is the radius of the disk in the basal plane, k is a coefficient which depends on the geometry of the conforming microelectrode and thus on the parameters a and b, C_0^b is the bulk concentration of species O, θ is the Nernst factor given above , E is the electrode potential and $E^{o'}$ the formal potential, D_o and D_R are diffusion coefficients of the indicated species, and F is the Faraday constant [10]. The value of k is well known for various geometries. It will be between the limiting cases of 4 (embedded disk) and 2π (hemisphere) for either an oblate hemispheroid or hemispherical cap microelectrode depending on the ratio b/a.

Although the hemispherical electrode case, k= 2π, is well described theoretically, Wehmeyer and Wightman [5] did not find highly accurate agreement between radii determined from deposition times and those determined by measuring steady state limiting currents assuming hemispherical diffusion. These experiments were conducted by electrodeposition of Hg on various sizes of inlaid Pt disks where the radius of the microdisk was usually much smaller than the measured radius of the deposited Hg. Stojek and Osteryoung [8] experimentally estimated the altitude to basal radius ratio, b/a, of deposited Hg conforming electrodes by

measuring the volume of Hg deposited on Pt and Ag inlaid microdisks and assuming spherical cap geometry. This procedure allowed them to measure the coefficient k of the steady state diffusion current equation (1-1) for spherical cap electrode geometry. However, since they did not have a theoretical relationship for k in terms of a and b, they could not verify whether the assumed geometry was a good model for the microelectrode. Colyer, Luscombe and Oldham [7] investigated growing electrodeposited Hg drops based on the spherical segment (cap) model using an earlier theoretical treatment of Bobbert [11]. Their experiments for the charge flowing during Hg deposition were performed with deposition on platinum microdisks for radii between 0.5μm and 12.5 μm. They did not find good agreement of this theory with the data of Stojek and Osteryoung [8] except for the case when a is nearly equal to b, and their own experimental data [7] only show good agreement with theory for deposition times in 100s to 600s range for microdisks of radii less than 2.5 μm. However, for short deposition times (<150s), the theory seemed to fit the data for all of their microdisks [7]. The deposition times used in the present experiments, consistent with the condition b<a, are in this short time range.

After investigating both oblate spheroid and spherical cap microelectrode geometries using a similar experimental approach to those discussed above [7, 8], the Hg electrode was formed by electrodeposition and the value of the b axis determined from the deposition charge. However, the deposition current (charge) was not used to evaluate k in the steady state current equation (1-1), rather the Hg microelectrode was transferred to a fresh solution and linear sweep voltammetric reduction used to measure the limiting steady state currents and thus the steady state

diffusion current coefficients, k. The test solutions contained $Ru(NH_3)_6Cl_3$ and the electrode process was outer sphere reduction of Ru(III) to Ru(II). This procedure gave a better fit to theory than evaluation using the Hg deposition current. The steady state limiting current results were used to compare measured and calculated values of k for the two geometries.

For an oblate hemispheroid, the coefficient k can be expressed [2] as

$$k = \frac{4\,(b/a)}{\xi_0(1-(2/\pi)\tan^{-1}\xi_0)} \qquad (1\text{-}2)$$

and where ξ is an oblate spheroidal coordinate (see Figure 1.1) given by $\xi = b/\sqrt{a^2-b^2}$ and at electrode surface $\xi = \xi_0 = b_0/\sqrt{a_0^2-b_0^2}$. In general values of a and b may be used to refer to any ξ position in the coordinate space; however, in this experiment, only values which refer to the geometric parameters of the metal electrode are needed, and thus the zero subscripts on a and b are dropped. It can be shown [2] that the value of k will be 4 in equation (1-2) when b=0 , which is the microdisk case, while at b=a the value of k will be 2π, which is the hemisphere case. As the ratio of b/a changes from 0 to 1, the microelectrode geometry goes from inlaid disk to oblate hemisphere to hemisphere and the value of k varies from 4 to 2π.

Values of a and b were determined electrochemically in a straight forward manner. First, the radius, a, on the microdisk was measured experimentally using the limiting form of equation (1-1) with k=4 and Θ =1 with a reversible redox system of known D_0 and C_0^b. Then the value of the

altitude, b, was found from the volume of the deposited Hg obtained by coulometric measurement. If an oblate spheroid is assumed as the electrode geometry then the volume formula $V=(2/3)\pi a^2 b$ can be used to calculate b.

On the other hand, the same experiment can be interpreted assuming that the geometry is that of a spherical cap (segment). Recently, a relation has been given which can be used to calculate k in equation (1-1) for the case of steady state diffusion to a spherical cap electrode. For this case [3]

$$k = 2\pi \int_0^{\infty} \frac{\cosh\{x\tan^{-1}(b/a)\}dx}{\cosh\{x\cot^{-1}(b/a)\}\cosh(\pi x/2)} \qquad (1\text{-}3)$$

Thus if a spherical cap microelectrode is assumed then b is calculated from the volume expression for such a geometry,

$V= \pi b(3a^2 + b^2)/6$ which is a cubic equation in b.

The above developments are necessary for comparison of experimentally determined coefficients, k, with values calculated by equations (1-2) and (1-3) for the two geometric models. After establishing the appropriateness of the oblate spheroidal model, only its volume formula was used for determining geometric parameters.

1.3 Results and Disscusion

1.3.1 Determination of Steady State Diffusion Equation Coefficients

The value of k in equation (1-1) for various values of b/a were determined experimentally and then compared to values calculated from either equation (1-2) for the oblate hemispheroid or equation (3) for the spherical cap microelectrode. To evaluate the coefficient k in equation (1-1) by experiment, several different sizes of conforming microelectrodes were made by controlling the deposition time in a chronoamperometric experiment. A typical i vs t curve obtained with a gold microdisk is shown in Figure 1.2 in which the smooth curve shows the smooth spreading of mercury during the electrodepositing process. The current increases with increasing time which is due to the increase in electrode area as the mercury is deposited. It takes about 60 seconds to get a near hemisphere at a 5 μm radius microdisk electrode.

As mention before, the value of the microdisk radius, a, can be determined by using the limiting current from the equation (1-1) for the case where k=4. For 5.00 mM ferricyanide solution in 0.100M potassium chloride, a steady state current of 7.34 nA was found at a gold disk microelectrode . Using a diffusion coefficient for ferricyanide of 7.6×10^{-6} cm^2/s [12], this current gives a radius value of 5.01 μm for the 10 μm diameter electrode, as reported by BAS.

The value of the altitude b was evaluated from the total charge passed for a given time of mercury deposition. For example, in 5.0 mM $Hg_2(ClO_4)_2$, a total charge of 0.666 μC is found at t=30.0 s from the area under the curve in Figure 1.2. A value of b=1.95 μm is found based on the oblate spheroidal volume formula $V = (2/3)\pi a^2 b$ while a value b= 2.42 μm is found based on the spherical cap volume formula $V= \pi b(3a^2 + b^2)/6$. After preparing conforming Hg microelectrodes of different b/a ratios, they were transferred to 3.00mM Ru(III) solution. Steady state voltammograms at 10 mV/s were run and compared with the voltammogram of the same solution on the bare gold microdisk electrode before mercury deposition. Figure 1.3 shows typical curves. Both voltammograms are sigmoidal in shape rather than the customary peak-shaped curve obtained for linear diffusion , and a return sweep tracks back on its self. The current is larger following mercury deposition indicative of the increased size of the electrode. The limiting steady state current from these voltammograms was directly used to evaluate the k coefficient of equation (1-1) using a diffusion coefficient for ruthenium(III) hexa-ammine in 0.1M phosphate buffer solution (pH=7.0) of 5.93 $x10^{-6}$ cm^2 s^{-1} obtained from steady state current at the bare 5.01 μm gold disk electrode. This value is close to that of $6.0x10^{-6}$ cm^2 s^{-1} reported in the literature for the same redox system [5].

Coefficient k values using equations (1-2) and (1-3) are shown in Table 1.1 for various b/a ratios assuming either an oblate hemispheroid or spherical cap microelectrodes. To avoid error with a freshly prepared mercury electrode from the first voltammogram [5], limiting currents from the next three scans were averaged to find experimental coefficient values, k_{exp}. This parameter is actually the current function, $l_{lim}/nFDaC_o^b$. The relative standard deviation for the three runs averaged over the ten values

of b/a was 1%. Table 1.1 shows a comparison of k_{exp} with coefficients calculated from equation (1-2) for the oblate hemispheroid, k_{ob}, and with coefficients calculated from equation (1-3) for the spherical cap, k_{sp}. It is seen that at the two lowest ratios of b/a both cases show their largest relative deviations (up to 5%), but the hemispherical cap seems to be a better model based on lower deviations of k_{exp}- k_{model}. However, at these low ratios the Au disk microelectrodes may not be completely covered with Hg and these two low ratios were disregarded.

For the next highest eight values of b/a, the oblate spheroid model has a lower sum of absolute deviations, $|k_{exp}- k_{model}|$, than the spherical cap microelectrode model. In order to see if one geometry is a better model than the other, a least squares fit of k_{exp} versus k_{model} to the relationship $Y = b_1X$ was used, again for the eight highest values of b/a. The slope b_1, sum of squares of the residuals, SS_r, and linear correlation coefficient, r, and the standard error in the slope, s_b, can be found from the data in Table 1.1. Of course a perfect fit to the model in the absence of experimental error would have b_1= r = unity with a zero value of SS_r. For the oblate spheroid model: b_1=1.007, SS_r=0.0312, r=0.9866, and s_b=0.057, while for the spherical cap model: b_1=1.010, SS_r =0.0471, r=0.9780 and s_b=0.066. Clearly, theory and experiments are both well correlated, although there is undoubtable random error in both k_{exp} and k_{model} values. Furthermore, an approximate t test shows there is no statistical difference in the slopes for the two geometries. Since the models fit the experimental coefficients equally well and there is a closed form analytical expression for the steady state current in the oblate spheroidal case, this case was taken to be a superior model to use for the type of conforming Hg electrodes that have

been fabricated. The average relative deviation of the experimental coefficient from the theoretical value for the oblate spheroid geometry is 1% for the last eight values of b/a which is about the same magnitude as the relative standard deviation of the experimentally measured steady state limiting current values. Thus, to within this experimental precision, the oblate spheroidal geometry is taken as an adequate model for Hg electrodeposited microelectrodes with b/a ratios between 0.4 and 1.0.

1 . 3. 2 Theory of a Quasi-reversible Electrode Reaction on an Oblate Spheroidal Microelectrode

The steady state current-potential relationship at an oblate microhemispheroid electrode for the general quasi-reversible case can be derived based on the oblate spheroidal geometry, which then gives the reversible and irreversible cases under limiting conditions. The results for oblate spheroidal geometry are exact and can be simply expressed just as in the case of a hemispherical electrode. These desirable qualities may result from the fact that concentration profiles in the two cases can be expressed in terms of a single geometric coordinate, the radius r for the spherical case and the spheroidal coordinate ξ in the oblate spheroidal case [13]. The theory will be used for the measurement of the standard heterogeneous rate constant for the ruthenium hexa-ammine electrode reaction at a Hg oblate spheroidal microelectrode made as previously described.

For a simple quasi-reversible electrode reaction of the solution soluble redox couple O, R involving n electrons

$$O + ne^- \rightleftarrows R \qquad (1\text{-}4)$$

the electrode current can be expressed as

$$i = nFA\{k_f(E)C_O^s - k_b(E)C_R^s\} \qquad (1\text{-}5)$$

where C_O^s and C_R^s are the surface concentrations of species O and R, $k_f(E)$ is the forward heterogeneous rate constant and $k_b(E)$ is the backward heterogeneous rate constant, F is the Faraday constant, and A is the electrode area [10]. Furthermore, under equilibrium conditions (i=0), the system obeys the Nernst equation with the surface concentrations expressed as

$$\frac{C_O^s}{C_R^s} = \exp\left(\frac{nF}{RT}(E - E^{0'})\right) = \frac{D_R\,\theta}{D_O} \qquad (1\text{-}6)$$

where in this case R is the gas constant, T the temperature in degrees Kelvin, and $E^{0'}$ has the usual meaning in the electrochemical literature of the formal electrode potential [10]. For microelectrodes the right hand side(RHS) in equation (1-6) is set equal to the ratio of diffusion coefficients times the potential dependent factor θ. Since under Nernst conditions $k_f(E)C_O^s = k_b(E)C_R^s$, we can use the RHS of equation (1-6) to express the i vs. E equation in a form used by Saveant and Tesser [14]

$$i = nFA\, k_f(E)\, [\, C_O^s - C_R^s \frac{D_R \theta}{D_O}\,] \qquad (1\text{-}7)$$

For a steady state oblate spheroidal electrode, we have previously derived the concentration profile $C_i(\xi)$ as [2]

$$C^b_i - C_i(\xi) = \frac{(C_i^b - C_i^s)(1-(2/\pi)\tan^{-1}\xi)}{(1-(2/\pi)\tan^{-1}\xi_0)}\,, \quad i = O, R \qquad (1\text{-}8)$$

Using equation (1-8) and the proper flux equations and metric coefficients(see [2]), the total current can be expressed in terms of the surface concentrations. The results are current expressions which have the correct form for steady state mass transport, i.e. radial like diffusion. Thus

$$i = \frac{4nFD_O f(C_O^b - C_O^s)}{\kappa_O} \qquad (1\text{-}9)$$

$$i = \frac{4nFD_O f C_R^s}{\kappa_O} \qquad (1\text{-}10)$$

where $f = \sqrt{a^2 - b^2}$ and $\kappa_O = (1-(2/\pi)\tan^{-1}\xi_0)$. Rearranging equations (1-9) and (1-10), we find expressions for the surface concentrations in terms of the steady state current ,i, and the limiting steady state current, i_L, where $i=i_L$ when $C_o^s = 0.0$

$$C_o^s = \frac{i_L - i}{K_O} \qquad (1\text{-}11a)$$

and

$$C_R^s = \frac{i}{K_R} \qquad (1\text{-}11b)$$

where $K_O = 4nFD_Of/\kappa_O$ and $K_R = 4nFD_Rf/\kappa_O$. Substituting equations (1-11) into (1-7) gives the quasi-reversible steady state current

$$i = \frac{i_L}{[1 + \theta + \frac{4fD_O}{A\kappa_O k_f(E)}]} \qquad (1\text{-}12)$$

This form of the current-potential curve can be used to experimentally measure values of k_f as a function of potential without assuming a relationship for the potential dependency. On the other hand, if we let $k_f = k^o \exp[-\alpha \frac{nF}{RT}(E-E^{o'})]$ as in the Butler-Volmer equation, the effect of k^o, the apparent standard heterogeneous rate, on the current - potential curve can be illustrated (Figure 1.4). In this plot the charge transfer coefficient α is taken as 0.5 and a typical geometry for the oblate spheroid microelectrode is chosen. It can be seen from the plot that the shape of the curve is strongly influenced by the magnitude of k^o. This type of dependence is similar to other geometries which give steady- state behavior, e.g., the disk and hemisphere microelectrodes [15,16].

The characteristic size of the oblate spheroid electrode is contained in the reciprocal of the factor $f/A\kappa_O$. As this characteristic size gets smaller, it introduces more irreversibility in the quasi-reversible equation (1-12) since the third term in the denominator of (1-12) becomes larger. This third term must not be negligible with respect to $1+\theta$, if k^o is to be measured with any accuracy. To illustrate this effect of the size of an oblate spheroid microelectrode on the magnitude of the third term, we take the case where

$D_O = D_R$, $E = E^{o'}$, $k_f = k^o$, and plot in Figure 1.5 the variable $(1 + \theta + \frac{4fD_O}{A\kappa_O k^o})$ vs log k^o. Actually for these conditions $\theta=1$, and thus the greater the curves deviate from 2 the more accurate the measurement of k^o. Only, curve d (Figure 1.5) shows a significant deviation of the term $(4f D_o/A\kappa_O k^o)$ from zero. Thus, these curves show that to measure a k^o of 1 cm/s, for instance, an electrode is needed with a=1μm. In fact, the term $(4f D_o/A\kappa_O k^o)$ must be greater than around 0.03 to get any measure of the value of k^o. Since the reciprocal of $f/A\kappa_O$ is a characteristic length, the smaller it gets the more accurately one can measure k^o.

It is straightforward to calculate the dimensionless quantity $4fD_o/A\kappa_O k_f$ from which one can determine the size electrode needed for a given measurement. The electrode surface area, A, for the oblate hemispheroid electrode is needed and is easily obtained from a formula such as [3]

$$A = \pi a^2 \left[1 + (b^2/a^2) \frac{\cosh^{-1}(a/b)}{\sqrt{1 - (b^2/a^2)}}\right].$$

An equivalent formula for the surface area in terms of the readily calculated logarithmic function is also given later in equation (1-22). Using the above formula for A and an expressions for κ_O and f it can be seen that :

$$\frac{4fD_O}{A\kappa_O k^o} = \frac{4D_O F(b/a)}{\pi a k^o}$$

with $k_f = k^o$. The function F(b/a) actually does not vary much as b/a goes from zero to one. For example, it can be shown that F(0)= 1 which is the case for an inlaid disk and $F(1)=\pi/4=0.7854$ which is the case for a

hemisphere. For other values of b/a such as 0.40, 0.60, 0.80, 0.90, and 0.98, F(b/a) equals 0.975, 0.907, 0.842, 0.813, and 0.791, respectively. Therefore, it can be appreciated that it is the size of the radius, a, of the disk in the basal plane of the oblate hemispheroidal microelectrode that is the characteristic length of the electrode. Thus it is radius a and not the ratio b/a which has the possibility of influencing whether a voltammetric process is in a reversible, quasi-reversible, or totally irreversible region. This fact is also brought out by Figure 1.5 where the effect on the various curves of changes in the radius a at constant b/a can be dramatically seen.

Following a similar definition used by Oldham et al. [16], let the parameter

$$\kappa_{obl} = \frac{\pi k^o a}{4 D_0 F(b/a)}$$

define the three voltammetric regimes. This parameter is just the reciprocal of the dimensionless quantity which appears in equation (1-12) and was discussed above. Thus $\kappa_{obl} > 40$ is effectively reversible, $0.2 < \kappa_{obl} < 20$ is usefully quasi-reversible, and $\kappa_{obl} < 0.1$ is effectively irreversible, following Oldham et al.[16]. To calculate a value of radius, a, needed for a given value of k^o, one must chose a magnitude for $1/\kappa_{obl}$ for the accuracy desired. If we say that $1/\kappa_{obl}$ must be at least 0.1, then $a \leq 40 D_0 F(b/a)/\pi k^o$ and for $D_0 = 1 \times 10^{-5}$ cm, F(0.9) =0.813, and k^o = 2 cm/s, then $a \leq 2.1 \times 10^{-4}$cm or 2.1 μm. Since F(b/a) is not much different form one, its value can be ignored in the calculation. A possible constraint for this type of consideration is the difficulty of making the inlaid microdisks smaller than around 0.2 μm.

1.3.3 Reversible Case

For a reversible electron transfer process, the third term in the denominator of (1-12) is much less than 1 + θ and thus

$$i = i_{rev} = i_L/(1 + \theta) \qquad (1\text{-}13)$$

where $i_L = \frac{4nFD_O f C_O^b}{\kappa_0}$. By rearranging (1-12), it can be

$$\frac{i_L - i}{i} = \theta = (D_O/D_R)\exp\left(\frac{nF}{RT}(E - E^{0'})\right) \qquad (1\text{-}14)$$

or

$$E = E_{1/2} + \frac{RT}{nF} \ln \frac{i_L - i}{i} \qquad (1\text{-}15)$$

which is the typical form of a reversible polarographic or steady state voltammetry expression at a microelectrode [15]. $E_{1/2}$ is the value E when $i=i_L/2$ and is given by

$$E_{1/2} = E^{0'} - (RT/nF)\ln(D_O/D_R) \qquad (1\text{-}16)$$

As previously pointed out in the literature , these equations are similar to the classical polarographic results except that the diffusion coefficient ratio D_R/D_0 does not appear under a square root sign [15].

1.3.4 Irreversible Case

In the current-potential curve of a totally irreversible electron transfer process , the reduction wave is shifted negatively from the formal potential to such an extent that for all points on the voltammogram, the term $\exp(\frac{nF}{RT}(E - E^{0'}))$ is negligible in comparison with unity [15,16]. In this case

$\theta << 1 + \frac{4fD_O}{A\kappa_O k_f(E)}$ and equation (1-12) becomes

$$i_{irr} = \frac{i_L}{[1 + \frac{4fD_O}{A\kappa_O k_f(E)}]} \qquad (1\text{-}17)$$

Equation (1-17) shows again that the nature of the voltammetric i vs. E curve depends on a characteristic size for the oblate hemispherical microelectrode, and it is this size factor $A\kappa_O/f$ which influences the extent of electrochemical reversibility for the steady state system.

Assuming as before the usual exponential form for k_f, one obtains from equation(1-17) a logarithmic expression for the current potential curve

$$E = E_{1/2} + \frac{RT}{\alpha nF} \ln \frac{i_L - i_{irr}}{i_{irr}} \qquad (1\text{-}18a)$$

where

$$E_{1/2} = E^{o'} - \frac{RT}{\alpha nF} \ln \frac{4fD_o}{A\kappa_o k^o} \qquad (1\text{-}18b)$$

and α is the transfer coefficient for the electrode process. As expected, equations (1-18) resembles the irreversible equation for other microelectrode geometries except that the geometric parameters are again in terms of the more general oblate spheroid microelectrode.

1.3.5 Limiting Forms for the Hemisphere and Inlaid Disk

Since the limiting forms of the oblate hemispheroid are the hemisphere and inlaid disk, equation (1-12) represents the quasi-reversible i vs E relationship for these microelectrodes also. Note that the factor $4f/A\kappa_0$ in the denominator of this equations only depends on the semimajor and semiminor axes, a and b, which can be measured independently of kinetic measurements as discussed above. For a hemisphere (a=b) this factor becomes 1/a [2], and equation (1-12) becomes

$$i = \frac{i_L}{1 + \theta + \frac{D_O}{ak_f(E)}} \qquad (1\text{-}19)$$

which is same result as equation (1-9) of [15].

As b goes to 0 (b/a=0), which is the case for a disk, the factor $4f/A\kappa_0$ becomes $4/\pi a$ [2], and equation (1-12) becomes

$$i = \frac{i_L}{1 + \theta + \frac{4D_0}{\pi a k_f(E)}} \qquad (1\text{-}20)$$

This form of the current-potential relationship is equivalent to that given by Galus et al. [17] except their equation was derived for reduced species only in the bulk and is based on assuming a linear concentration profile.

Bond, Oldham, and Zoski [18] have derived expressions for the steady state current to an inlaid disk microelectrode based on cylindrical geometry and a separation of variables method. This method does not give a closed form solution for the quasi-reversible case and tabulated numerical results are presented [18]. It is interesting to note that these tabulated results can be represented [15] by an empirical equation which only differs from equation (1-20) by a factor which multiplies the third term in the denominator of equation(1-20). In our notation this factor is $(2\pi a k_f + 12\pi D_o / 4a k_f + 12\pi D_o)$ which gives values that are not greatly different from one. In fact the maximum difference between values of equation (1-20) with and without this factor is 4%.

The extent of irreversiblity for the three geometries is shown in Table1. 2 in terms of the deviation of $E_{1/2} - E^o$ from 0.0 where $E = E_{1/2}$ at $i/i_L = 0.5$. In this calculation, let $D_0 / D_R = 1$ in equation (1-12) with a=5μm and b=0, 2.5, and 5μm for disk, oblate spheroid and hemisphere cases, respectively. Under these conditions, the values of E^o and $E_{1/2}$ are very close for k^o values greater than 2 cm/sec which we take as the onset of reversibility. Here the reversible case is defined as the value of k^o at which

the difference $E_{1/2}$ -E^o is so close that they can not be distinguished experimentally in a voltammetry experiment, i.e, $|E_{1/2} - E^o| \leq 0.3mV$. This value of k^o of course depends on the size of the microelectrode. Values in Table 1.2 show that for comparable sized microelectrodes, the oblate spheroid introduces more irreversibility than the hemisphere but less than the disk microelectrode. In order to calculate α and k^o ,we show in the next section that the value of E^o must be known accurately even when $E_{1/2} \approx E^o$. When k^o is smaller than 0.001 cm/s, for the present conditions, the difference between E^0 and $E_{1/2}$ become large enough so that θ is much less than one and the system tends to the irreversible case.

1.3.6 Determination of a Heterogeneous Rate Constant

A particular form of $k_f(E)$ such as the Butler-Volmer form [10] can be assumed to investigate i vs. E behavior; however, it is not necessary to choose a model a priori since equation (1-12) can be solved directly for $k_f(E)$:

$$k_f(E) = \frac{(4fD_O/A\kappa_O)}{\frac{i_L - i}{i} - (D_O/D_R)\exp\{nF/RT(E-E^{0'})\}} \qquad (1\text{-}21).$$

If $E^{o'}$ is known a value of k_f can be calculated from (1-21) using the current data, i(E), at each value of E and i_L, allowing the potential dependence of k_f to be determined experimentally [10,14].

If the Butler-Volmer exponential dependence is assumed then the apparent standard heterogeneous rate constant k^o and the charge transfer coefficient α are found by plotting $\ln k_f$ vs E, since $\ln k_f(E) = \ln k^o - (\alpha nF/RT)$

$(E-E^{0'})$. However, for the quasi-reversible case unless $E^{o'}$ is known accurately, this procedure may lead to errors in the analysis since the terms in the denominator of equation (1-21) can be very close in value leading to erroneous results. One possible approach is to use a large size electrode where the system becomes reversible to obtain an accurate value of $E^{o'}$. Another approach is to use a nonlinear curve fitting procedure to calculate optimized values of α, k^o, and $E^{o'}$.

The geometric factor $4f/A\kappa_0$ in equation (1-21) can be calculated with given a, b values, using $\kappa_0 = (1 - \frac{2}{\pi}\tan^{-1}\xi_0)$, $f = \sqrt{a^2 - b^2}$, $\xi = b/f$ with $\xi = \xi_0$ at the electrode surface, and the oblate sphere surface area, A. The surface area for the oblate spheroid can be found [19] from the formula

$$A = \pi a^2 + \frac{\pi b^2}{2\varepsilon} \ln \frac{1+\varepsilon}{1-\varepsilon} \qquad (1\text{-}22)$$

where $\varepsilon = \frac{\sqrt{a^2 - b^2}}{a}$.

As a test of the oblate hemispheroidal Hg microelectrode, electrochemical rate parameters were obtained for the quasi-reversible ruthenium hexa-ammine trichloride redox system in deoxygenated 0.1M phosphate buffer (pH=7.0). For electrode kinetics experiments, microelectrodes (a=5.01μm) with two b/a ratios (0.752 and 0.914) were used. Theoretical consideration [20] suggested that steady-state assumptions were very close to being fulfilled under the experimental conditions with a sweep rate of 10 mV/s. The diffusion coefficients were assumed to be equal, $D_O=D_R$, and a value of $D_0 = 5.93\text{x}10^{-6}$ cm^2/s was taken from limiting current experiments. First, equation (1-21) was used to calculate values of k_f as a function of potential. The results of a plot of $\ln(k_f)$ vs E for nine

values on the i vs E curve are shown in figure 1.6. The Hg microelectrode in this case had b/a=0.914 and the data was calculated twice with two different values of $E^{o'}$. For curve (b) in Figure 1.6, a value of $E^{o'}$ =-0.265V was used which is the $E_{1/2}$ value obtained experimentally from the i vs E curve. This curve gives α =0.64 and k^o = 0.22 cm/s. In order to illustrate the sensitivity of this calculation of k_f on $E^{o'}$, a very slightly different value of $E^{0'}$ (-0.2648V) was used to calculate k_f. The results lead to plot (a) in Figure 1.6. This set of data gives noticeably different parameters, α =0.69 and k^o = 0.19 cm/s. Since the correlation coefficient for both sets of data is 0.999, there is no way to decide on the correct parameter set from this statistic.

For comparison, the Marquardt method was employed in a nonlinear least squares regression analysis using equation (1-12). The results of the above method and the nonlinear least squares method are summarized in Table 1.3. The curve fitting procedure gives values of α= 0.604 ± 0.064, k^o = 0.244± 0.055 cm/s, and $E^{o'}$ = - 0.2651V ± 0.0003 vs SCE with the sum of squares of the residuals = 2.1×10^{-6} and a reduced chi square = 3.5×10^{-7}. The uncertainties are the standard errors in the parameters as calculated by the Marquardt program assuming all data points have equal uncertainties. A second experiment with a different Hg microelectrode(b/a =0.752) was also conducted. In this case only the nonlinear least squares analysis was reported, which gives values of α = 0.645 ±.015, k^o = 0.217± 0.012 cm/s and $E^{o'}$ = -0.2650V ± 8.3×10^{-5} vs SCE with the sum of squares of the residuals = 1.3×10^{-7} and a reduced chi square = 2.2×10^{-8}. The curve fitting procedure gives the same $E^{o'}$ as the $E_{1/2}$ value, and thus the ln(k_f) vs. E plot should give the same values as the curve fitting procedure. Since the goodness of fit statistics are better for the case of b/a=0.752 microelectrode, it can be seen these values are more likely to be closer to the true values. An

average of all of the above determined values(Table 1.3) or use of the values for b/a=0.752 assuming only two significant figures are reliable gives k^o =0.22 cm/s (α = 0.65). this can be compared with a value of k^o = 0.35 cm/sec (α = 0.65± 0.02) determined for the same redox system on Hg with the ac voltammetry [21] and a value 0.45 cm/sec (α=0.63) determined for the same redox system on Hg with fast scan voltammetry [22]. Different supporting electrolyte systems were used in these studies which accounts for the slight differences in the measured rate constants. All alpha values, on the other hand, are very close in value. Since specific adsorption and double layer potential will have an effect on the value of the apparent standard heterogeneous rate constant, k^o, it can be seen that the agreement between these measurements and those cited from the literature is quite good.

1.4 Conclusion

The results of this investigation show that a well described Hg conforming microelectrode can be made by electrodeposition. These microelectrodes are adequately modeled by an oblate hemispheroid for b/a ratios (semiminor axis to semimajor axis) which are between about 1/2 and 1. It is not necessary to fabricate a perfect hemisphere or to use the more involved spherical cap geometry to have both a good model for the geometry and an accurate theory for the electrode system. From this work, it can be seen that the oblate hemispheroidal electrode is easily fabricated by electroplating mercury on a Au microdisk. Furthermore, the oblate

hemispheroid steady state theory is general in that it also describes the hemisphere and inlaid disk cases. Finally, the results also show that for electrode reactions which are close to reversible, the value of $E^{0'}$ used in the data analysis by a $\ln(k_f)$ vs. E plot will have a strong effect on the results for the other ET parameters. This fact suggests that a nonlinear curve fitting procedure is the best approach to measuring kinetic values.

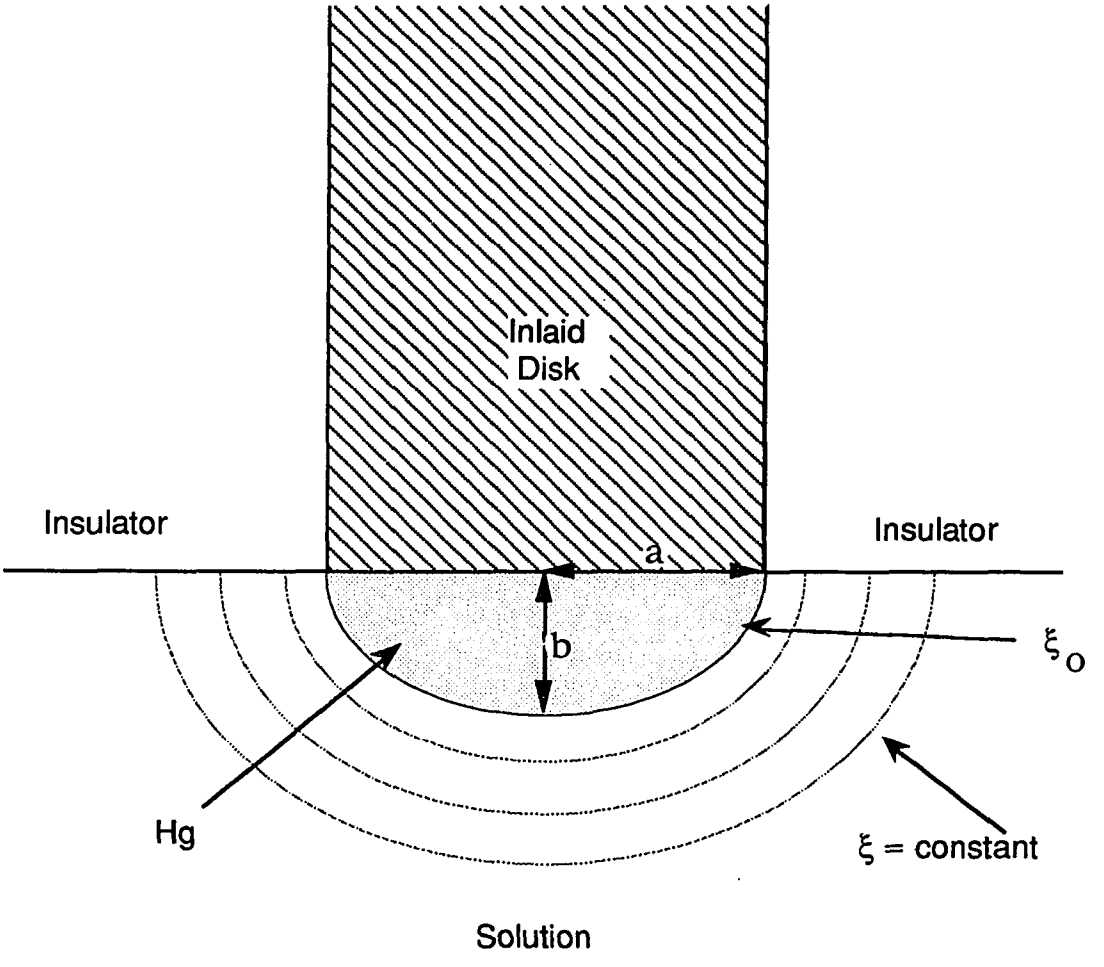

Figure 1.1 Geometry of the Oblate Hemipheroidal Microelectrode.

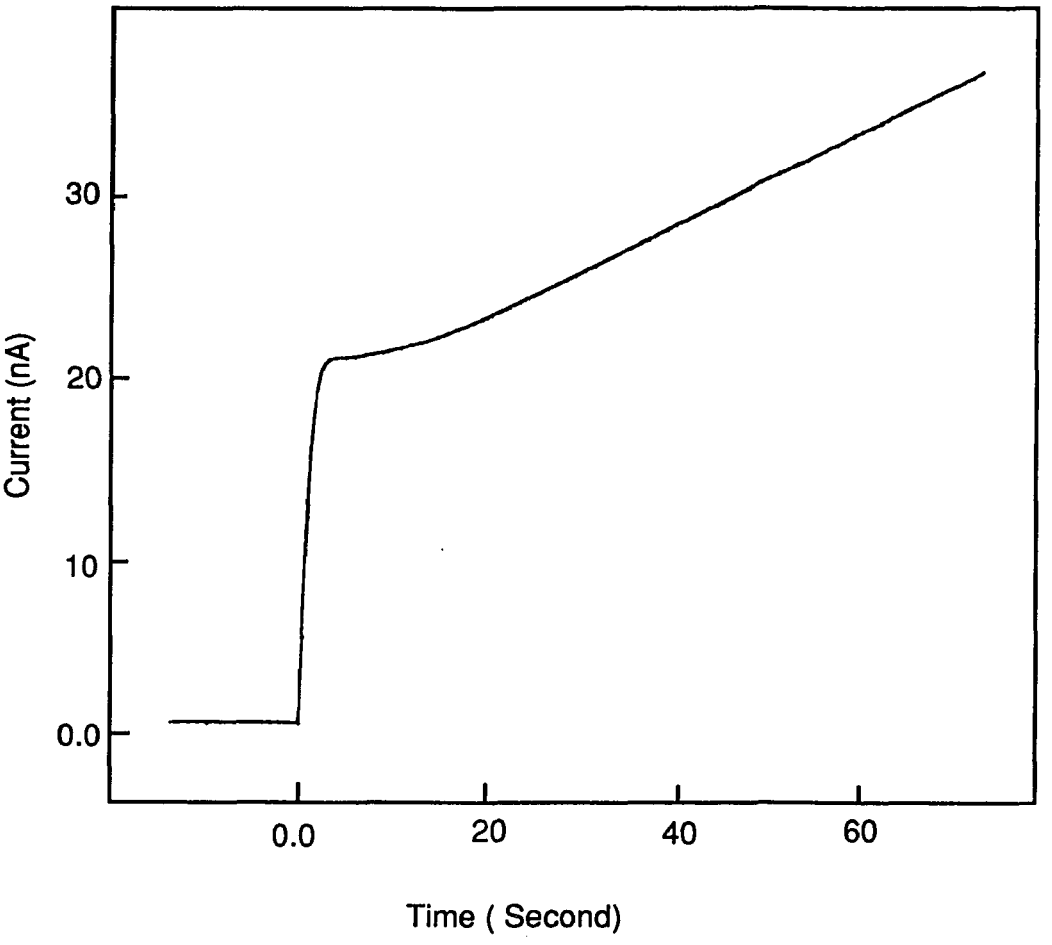

Figure 1.2 Chronoamperometric current vs. time curve for deposition of Hg on a Au disk microelectrode. 5.0 mM $Hg_2(ClO_4)_2$ in 0.25M $HClO_4$ solution on an embedded disk with r=5.01μm. E=0.0V vs. SCE.

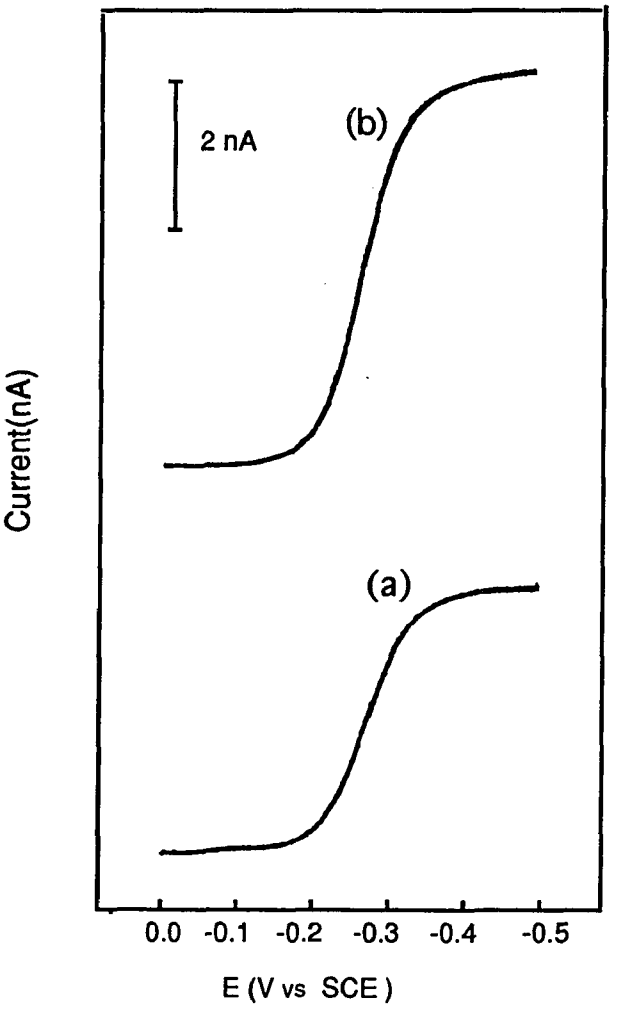

Figure 1.3 Steady state voltammograms on microelectrodes 3.0 mM ruthenium hexa-amine chloride at (a) 5.01μm Au disk and (b) oblate spheroidal electrode (mercury deposited on same Au disk); scan rate 10mV/sec.

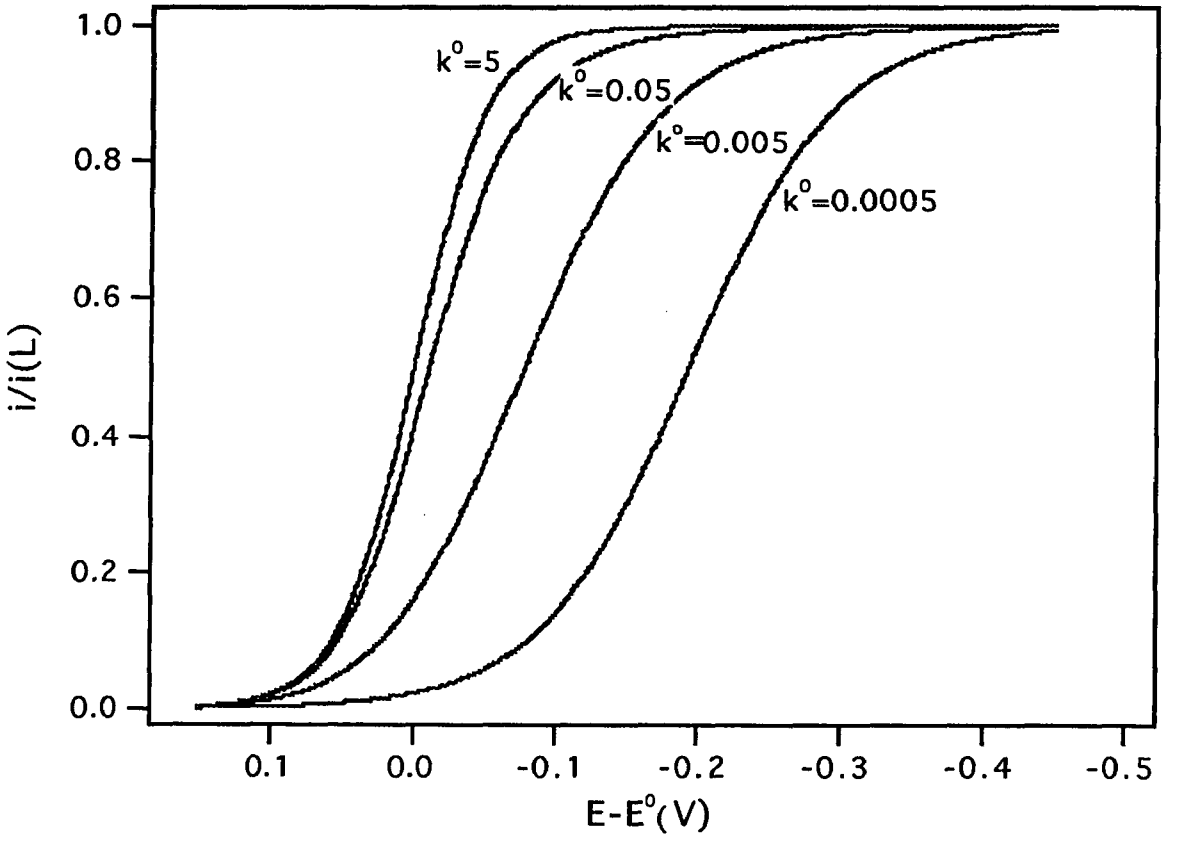

Figure 1.4 Quasi-reversible steady-state voltammograms as a function of standard heterogeneous rate constant, k^0, for an oblate spheroid microelectrode. The parameter values are: a=5μm, b=2.5μm D_O/D_R =1, α=0.5, and D_O=9.0 x 10^{-6} cm^2 /s.

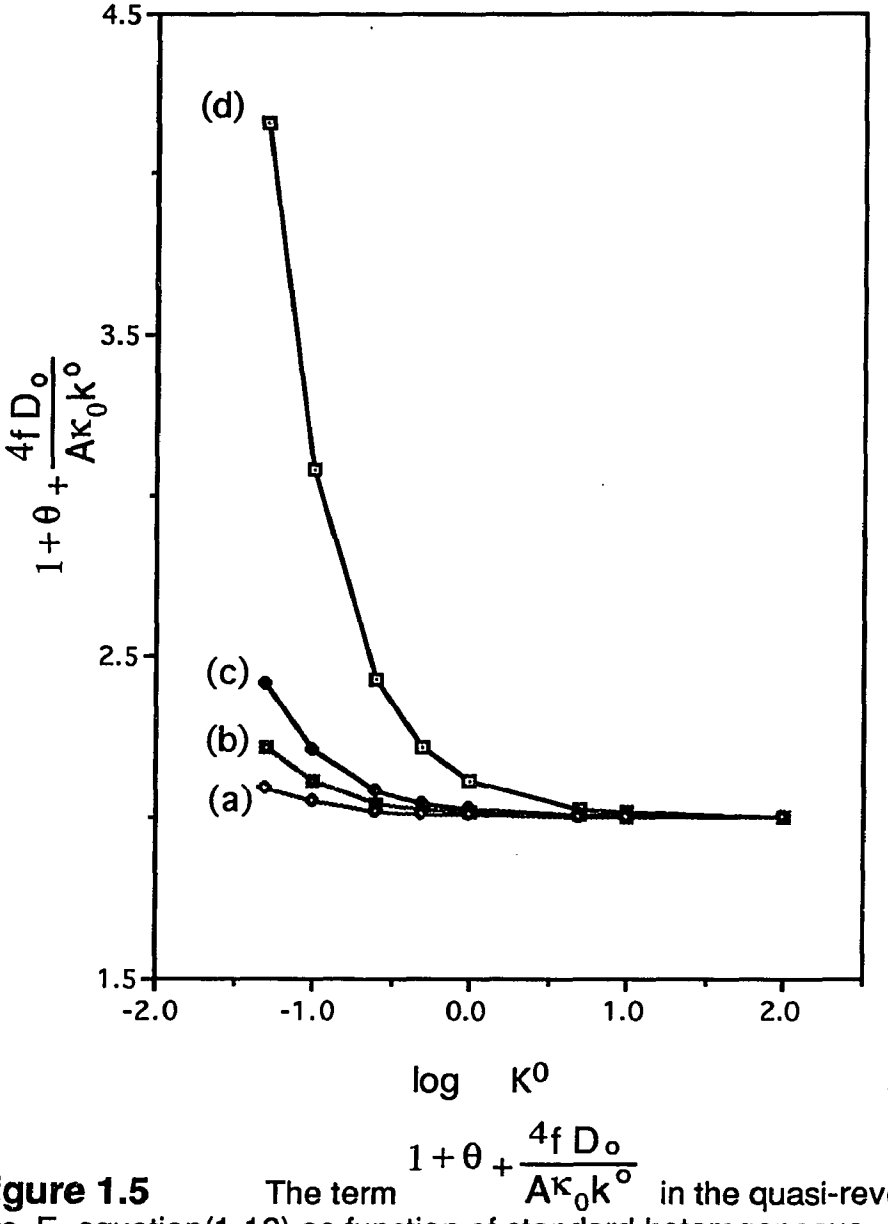

Figure 1.5 The term $1+\theta+\frac{4f D_o}{A\kappa_0 k^o}$ in the quasi-reversible i vs. E equation(1-12) as function of standard heterogeneous rate constant, k_0, at different size oblate spheroidal electrodes. (a) a=25μm, b=12.5μm; (b) a=10μm, b=5.0μm; (c)a=5.0μm, b=2.5μm; (d) a=1.0μm, b=0.5μm. The parameter values: E =E_0, k_f =k_0, D_O/D_R =1, α=0.5, D_O=9.0 x10^{-6} cm^2/s.

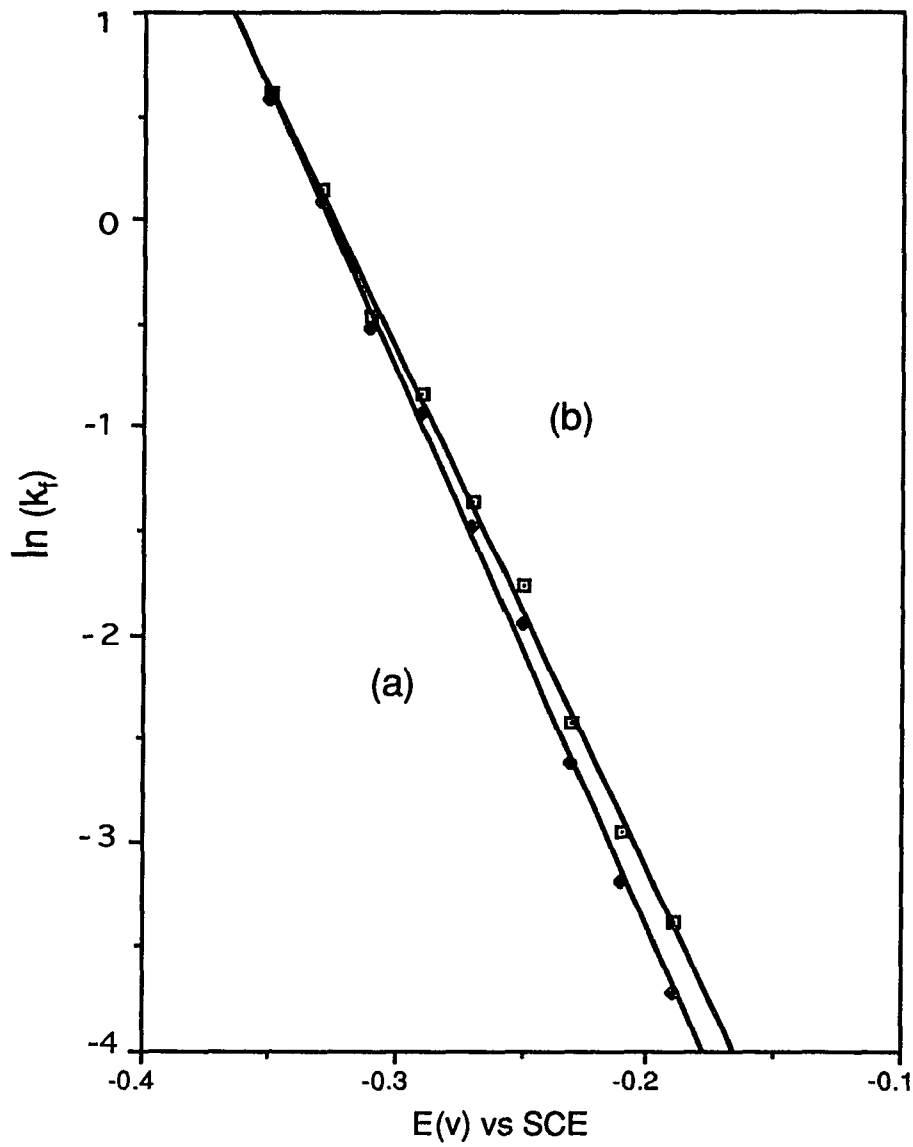

Figure 1.6 Plot of $\ln(k_f)$ vs. potential for different values of $E^{o'}$. Data calculated using equation (1-21) and experimental voltammogram for 3.0 mM ruthenium hexamine chloride in 0.1M phosphate buffer at a Hg oblate spheroid microelectrode, b/a= 0.914.
(a) $E^{o'}$= -0.2648V vs. SCE, (b) $E^{o'}$ = -0.2650V vs. SCE.

Table 1.1 Comparison of coefficients calculated from equation(1-2), $k_{ob.}$, and equation (1-3), $k_{sp.}$, with experimental values, $k_{exp.}$.

Ob. Spheroid b/a	Spherical Cap b/a	$k_{exp.}$	$k_{ob.}$	$k_{sp.}$
0.1824	0.2387	4.24	4.46	4.36
0.2523	0.3250	4.43	4.62	4.52
0.3606	0.4504	4.87	4.87	4.79
0.4873	0.5835	5.21	5.17	5.10
0.5579	0.6516	5.43	5.33	5.28
0.6237	0.7464	5.57	5.47	5.53
0.7338	0.8047	5.80	5.72	5.70
0.8184	0.8710	6.01	5.90	5.89
0.9036	0.9336	6.02	6.08	6.07
0.9823	0.9981	6.22	6.25	6.28

Table 1.2 Comparison of the extent of irreversibility for the three geometries in terms of the deviation of $E_{1/2} - E_0$ from 0.0 where $E = E_{1/2}$ at $i/i_L = 0.5$. The parameter values: $D_O/D_R = 1$, $\alpha = 0.5$, $D_O = 9.0 \times 10^{-6}$ cm^2/sec were assumed.

k_o(cm/sec)	$E_{1/2} - E_0$ (mV)		
	oblate spheroid*	hemisphere**	disk***
5	0.10	0.10	0.11
2	0.29	0.23	0.30
1	0.56	0.44	0.60
0.5	1.1	0.88	1.2
0.2	2.8	2.3	3.0
0.1	5.6	4.6	6.0
0.05	11	9.2	12
0.02	27	22	28
0.01	48	42	50
0.005	78	69	81
0.002	123	114	126
0.001	158	148	161
0.0005	194	184	197
0.0002	241	231	244
0.0001	276	267	279

*a=5μm, b=2.5μm; ** a=b=5μm; *** a=5μm, b=0μm.

Table 1.3 Estimation of kinetic parameters by different methods

Method	b/a	k_o (cm /s)	α	E_o' (V vs. SCE)
Ln(k_f) vs E Plot	0.914	0.22	0.64	-0.2650*
	0.914	0.19	0.69	-0.2648*
Nonlinear Least Sq.	0.914	0.244±.055	0.604±.064	- 0.2651±.0003
	0.752	0.217±.012	0.645±.015	- 0.2650±.00008

* Value assumed in the calculation of k_f

Part II

Liquid Chromatography with Mercury Electrode for Electro-catalytic Detection of Chloroquine

High-performance liquid chromatography (HPLC) is one of the most rapidly expanding techniques in analytical chemistry. HPLC bears a close resemblance to gas chromatography, GC. It arose in the late 1960s out of the experience in GC and from the application to LC of theories developed for GC. The major theoretical influence came from the work of Giddings [1], although Hamilton [2] had been a pioneer in his work on ion exchange chromatography. The major experimental advances, which brought about practical HPLC systems, were made by Lipsky in 1967 [3], Huber in 1967 [4] and Kirkland in 1969 [5]. HPLC complements GC, being able to separate substances that cannot readily be volatilised, and is particularly suitable for the separation of compounds having high molecular weight, high polarity, thermal instability and tendency to ionize in solution. Since a liquid in place of a gaseous eluent has high viscosity and since column particles are small, the operating pressure is high. The equipment for HPLC must be designed to withstand the high column inlet pressure. The column and particle dimensions and connecting tubing must be minimized. In HPLC, the operating conditions, namely, column temperature, flow rates etc. are closely controlled. The sample for analysis is small and injected directly by valve onto the column; the separated solutes are detected as they emerge from the column by a detector, which gives a quantifiable record. HPLC can

be carried out in any of the classical modes, of which the most important are liquid-solid adsorption chromatography, liquid-liquid partition chromatography, liquid-organobonded phase chromatography, ion-exchange chromatography, and size-exclusion chromatography.

2.1 Basic introduction to detection systems

The function of the detector in any chromatograph is to monitor the concentration or quantity of the sample components emerging from the column. It should provide an electrical signal proportional to concentration or quantity, which can be processed with a potentiometric recorder, an electronic integrator, or a computer system. The main criteria of an ideal detector for liquid chromatography are 1) suitable selectivity for the problem being examined, 2) low limit of detection, 3) minimal effect on peak width, and 4) independence of the detector on chromatographic parameters such as the flow rate of eluent. The most commonly used detectors for HPLC are based on optical absorption, refractive index, fluorescence, and electrochemical reaction. The combination of liquid chromatographic separation with mass spectroscopic, infrared and chemiluminescence detectors are also available.

2.1.1 Absorbance detectors

This is the most common type of detector. It can be highly sensitive, has a wide linear range, is relatively unaffected by temperature fluctuations and is also suitable for gradient elution. The absorbance detectors work by passing light of a specific wavelength through a cell

connected to an HPLC system and measuring the absorbance in real time. There are four general types of absorbance detectors: (1) fixed wavelength employing a discrete wavelength source such as a low-pressure Hg lamp; (2) a filter photometer employing a continuous source (e.g., deuterium lamp) where the wavelength range of interest is selected by use of optical filters; (3) a variable - wavelength spectrophotometric detector with and without automatic wavelength change capability; (4) multichannel / rapid scan variable - wavelength detectors, usually based on linear photodiode arrays. Fixed-wavelength detectors are typically more sensitive and have lower noise and drift characteristics than variable wavelength detectors[1]. This is due to the use of specialized lamps or phosphor filters that emit one or two intense and narrow bands of UV or visible light. The narrow bands of emitted light provide maximum adherence to Beer's law. The filter photometric detector is a compromise between a fixed-wavelength and variable - wavelength detector. The major advantage of a filter photometric detector relative to a fixed-wavelength detector is the option of multiple wavelengths. However, the bandwidth of the selected wavelength is typically larger for the filter photometric detector than for the fixed-wavelength detector. Therefore, it gives lower sensitivity and higher noise and drift characteristics than the fixed wavelength detector. Variable - wavelength spectrophotometric detectors [6-8] have noise and drift characteristics approaching those of fixed-wavelength detectors. However, they provide a continuum of wavelengths from < 200 nm to the visible. Therefore, a variable - wavelength spectrophotometric detector is a commonly used detector for HPLC. The photodiode array detector (PDA) is inherently an information-rich detector [9-11]. Peak spectra can be compared with those of standards to confirm the identity of unknowns, thus

providing another dimension of information besides retention times. Peak purity can be easily ascertained through a variety of techniques to aid method development and to provide confidence in quantitative results. Chromatograms at multiple wavelengths can either be simultaneously stored or extracted post measurement from the three-dimensional data matrix to enable quantitation of multiple peaks at each of their optimum wavelengths of detection. Photodiode array detectors give similar sensitivity as filter photometric detectors if the detector parameters [i.e., wavelength, bandwidth, etc.] of the PDA are optimized correctly [12]. In general, novel separation approaches have been the driving force for new absorbance detection schemes. Absorbance detection is following the latest trends in liquid chromatographic separation instrumentation; for example, the growth of microbore, packed capillary, and open tubular HPLC columns has produced a trend toward the miniaturization of absorbance detector flow cells to reduce detector band broadening. Absorbance detection continues to be the forefront of the detection methodology for HPLC.

2.1.2 Refractive index detectors

A refractive index detector (RI) was generally considered to be the most common "universal" detector. The RI detector is a bulk property detector that measures very small differences between the refractive index of the eluent and solute. Unfortunately, the refractive index of liquids is a very sensitive function of temperature, pressure, and dissolved gases. Most commercially available RI detectors either have addressed the temperature control problem by providing for an external circulating bath or have built electronic thermal control into the internal design of the detector.

Therefore, the universality is not only the RI detector's biggest advantage but also its greatest source of problems. Much of the recent work has been directed toward minimizing these limitations in the RI detector. Refractive index gradient (RIG) detection is developing into a useful RI detection method [13-15]. It is a laser-based beam deflection sensor that measures the concentration gradient (refractive index gradient) of a chromatographic peak. This refractive index gradient (RIG) detector has the advantage that it can discriminate between long-term refractive index changes such as those caused by temperature change or gradient elution and short-term changes due to the elution of an analyte. The development of the RIG detector was reported to be applied to microbore LC. Low nanogram quantities were detectable at a nonabsorbing wavelength [16-17] by RIG detection following microbore LC. In other work [18], the RIG was successfully used in both mobile-phase gradient and thermal gradient microbore LC.

2.1.3 Fluorescence Detectors

Some compounds that absorb UV light can subsequently emit a fraction of the absorbed light as fluorescence. The wavelength of the emitted fluorescence is always higher than that of the absorbed light (Stokes'Law) and it is therefore possible to irradiate a solution with a wavelength at which the solute absorbs strongly (usually in the UV region) and observe the fluorescent emission through a filter that cuts out the irradiating light. In LC, fluorescence detectors are often preferred for trace analytical studies because of their good selectivity and excellent sensitivity. The sensitivity may be up to 1000 times greater than absorbance detection.

The principal limitation of fluorimetric detectors is low emitted light levels. Since the number of light quanta emitted is proportional to the absorbed light energy, an increase in intensity of the exciting radiation will increase the intensity of the fluorescence proportionally. Because of the high-photon flux and the excellent spatial resolution of the laser, the majority of papers have dealt with the modification and evaluation of new fluorometric detection systems based on the Laser-Induced Fluorescence (LIF). Many studies have been made on the incorporation of lasers and miniaturization to make this detector compatible with microbore and /or capillary HPLC [19-22]. Emission can also be stimulated by simultaneous absorption of two photons of lower individual energy [23]. The two-photon spectroscopy provides additional detector selectivity. The high photon density of lasers is required for the technique to be feasible since the two-photon event is much less probable than the one-photon event [24]. The approach of frequency doubling, and variable wavelength dye laser extends applicability of LIF [22,25].

2.1.4 Chemiluminescence detectors

Chemiluminescence detection in liquid chromatography has received increasing research effort as a result of the excellent sensitivity and selectivity of this technique. Many papers have reported that detection limits are superior to fluorescence determination. This is due to the reduced background since extraneous radiation associated with photolytic excitation, i.e. Rayleigh and Raman scattering and source instabilities are eliminated [26]. Moreover, chemiluminescence detectors cause less band broadening than fluorescence detectors and other detectors which require

going to larger cells [27]. Therefore, the chemiluminescence system is very suitable as a detection method for capillary liquid chromatography [28,29]. The fundamental work in chemiluminescence detection includes novel instrumentation for CL, theoretical studies of photolysis coupled with CL, new solid-phase and immobilized reagents and instrumentation. Recently, a sulfur-selective chemiluminescence detector (SCD) has been developed [30]. The analytes decompose into sulfur monoxide and react with ozone, thus creating chemiluminescence. This can be used to detect many sulfur-containing compounds such as environmentally interesting pesticides, and industrial surfactants which are not chromatographable by gas chromatography. Time resolved detection with a pulsed Xe lamp and a gated photomultiplier,using a long luminescence decay time (>0.1ms) has been developed [31]. The CL method can also be used in the analysis of trace metals. Metals separated by ion chromatography displace cobalt from a Co-EDTA postcolumn reagent. The liberated cobalt is detected by a luminol-peroxide reagent. Developments in instrumentation for CL have also been reported [32].

2.1.5 LC/MS detectors

The combination of liquid chromatographic and mass spectral detection is an important analytical technique. Both techniques have matured to the point that they represent two of the most important tools available for the characterization of wide range of compounds. LC/MS research has been focused strongly on interface technology. The first successful commercially available interface was the transport, or moving-belt system [33,34]. The operating principle can be separated into three

distinct steps: deposition of the eluent, removal of the solvent in a vacuum, and volatilization of the sample into the ion source. A shortcoming of this mode is the requirement of either reduced chromatographic flow rates or partial splitting of effluent away from the interface. The other popular mode of LC/MS has been called direct liquid introduction (DLI) [33,35,36]. The effluent from the liquid chromatograph is introduced directly into the MS ion source region. However, the gas burden from conventional LC flow rates (1 mL/min of water produces 1.2L/min of gas) creates nearly 20 times more gas than a cryopumped vacuum system can handle. Thus, DLI LC/MS often uses a splitter such that only 1-5% of the total effluent is introduced into the mass spectrometer. This, of course, sacrifices sensitivity. Although the above two interfaces were available in the late 1970s, they were not routine techniques such as GC/MS was at that time. Since then, however, advancement including the thermospray, fast atom bombardment, and electrospray, have increased the ease of accomplishing LC/MS. A wide variety of LC/MS applications have appeared and commercial mass spectrometers dedicated to LC/MS are available [37].

To be successful, an LC/MS interface must not only divert a large fraction of mobile phase from the mass spectrometer inlet but also must make possible the transformation of nonvolatile and fragile species from solutes in a liquid to ions in a vacuum ready for mass analysis. The thermospray interface is the most routinely used interface for LC/MS. Because the thermospray interface readily accommodates conventional reversed-phase HPLC at high flow rates which represent the majority of HPLC applications today, it is frequently applied to obtain molecular weight information [38,39]. The FAB interface for LC/MS has proved useful for the analysis of polar, nonvolatile, and thermally labile compounds and

can provide both molecular weight and structure information. The interfacing of FAB to microcolumn LC allowed high resolution multidimensional information to be obtained [40]. Electrospray has been used to study various positive ions including NH_4^+, Na^+, K^+, Cs^+, Ca^+, and the BH^+ of organic nitrogen bases. Detection limits in the subfemtomole to attomole range were achieved [41]. Inductively coupled plasma (ICP) and MS methods have been used to detect trace rare-earth elements as impurities in other rare-earth materials. The detection limits for the 14 rare earth elements ranged from 1 to 5 pg/ml in solution [42]. The role of chemistry in LC/MS has been small and is generally neglected, since often as a primary goal of LC/MS coupling it is formulated that analysis can be performed without the need to perform the kind of chemical modifications which are often necessary in gas chromatography. However, some of the interfaces strongly rely on chemistry in their LC/MS operation, such as thermospray, DLI and FAB. It is clear that the detection can be improved considerably if the chemistry is tuned properly [43, 44]. Therefore, the role of chemistry is becoming more important since many interfaces are linked with ionization conditions possesing an important chemistry component.

2.1.6 LC/FT-IR detectors

Despite the fact that mass spectrometry is the most commonly applied technique for characterizing substances chromatographically, it has certain drawbacks. For example, structural isomers can not be differentiated by MS and library searches can sometimes lead to erroneous identifications. Under these circumstances, the Fourier transform infrared (FT-IR) spectroscopy has emerged as the most generally useful alternative.

The interfaces which join LC and FT-IR generally fall into one of two categories. All early HPLC/FT-IR interfaces involved passing the column effluent through a flow cell and continuously measuring spectra [45-47]. Since all mobile phases absorb IR radiation at certain wavelengths and some, such as water, have intense absorption across most of the spectrum, the absorbance of incident radiation by the solvent must always be compensated. This compensation is almost impossible when the composition of the mobile phase is changing (i.e. during gradient elution). The absorbance of the solvent limits the use of a flow cell interface. The other category is to eliminate the solvent prior to the IR measurement. This approach is to vaporize the solvent, then depositing the dissolved analytes on some moving media, ideally as small spots which are then scanned. In the first stage, 80-90% of the solvent is evaporated, in the second stage, each solute is deposited onto a suitable substrate for measurement of its IR spectrum. During the deposition, the remaining mobile phase must be completely evaporated to obtain a spectrum free of solvent absorption bands. Detection limits achieved using this principle are about 2 orders of magnitude lower than can be obtained with a flow cell interface [48]. However, this interface is not without its drawbacks. First, it is necessary to dispose of a considerable quantity of solvent vapor. Second, the detection limit is reduced when the solution comes into contact with a powdered substrate, as it can spread rapidly by capillary action. Therefore, most work has focused on the solvent removal technique based on the use of microbore columns, where the amount of solvent is greatly reduced [49-51].

2.1.7 Electrochemical detectors

Modern liquid chromatography has relied heavily on the development of suitable detection systems that are capable of determining the separated compounds rapidly, reliably and with a minimum sample volume [52-53]. The ideal detectors are those that have a high sensitivity, high selectivity, and minimal effect on peak width, and do not significantly attenuate the separation achieved by the column. While no universally accepted detector satisfies all of the requirements for high performance liquid chromatography, electrochemical detectors have found widespread application and a variety of indicator electrodes and flow-cell designs have been developed for use in combined LCEC methods [54].

All the electrochemical detector devices depend on Faraday's law and can be divided into two extreme modes of operation in electrochemical monitoring: coulometric and amperometric. In the first mode, the electrolysis is taken to completion for each solute. Since the rate of reaction at the electrode surface may be limited by the rate of diffusion of reactants through the solvent in the flow cell, great attention to the design is required. The electrode must have a large surface area. This can be achieved in practice only at the expense of a large dead volume and residence time. Such cells are difficult to construct [55-56]. Despite the analytical advantage of coulometric detectors which give a direct measure of the total amount of reacting solute, electrochemical detectors which appear to be gaining the widest acceptances are those using the amperometric mode. In the amperometric mode, the detector typically consists of a working electrode, a reference electrode, and an auxiliary electrode. The potential applied to

working electrode is kept constant with respect to the potential of reference electrode and for maximum sensitivity and reproducibility is preferably chosen in the limiting current range of substance to be detected. The detection potential is generally found from a hydrodynamic voltammogram. An amperometric current is produced which is proportional to the concentration of analyte entering the electrochemical cell. The concentration changes as a function of time due to elution of the analyte from the chromatographic column and so does the current. Amperometric detectors have the advantage of being easier to construct, can be more specific, and lower detection limits are feasible. Because thin-layer cells have excellent flow characteristics and a high ratio of electrode surface area to solution volume, the most popular electrochemical detectors to date have been based on the amperometric detection of analyte in thin-layer cells. Presently, considerable effort in the field of LCEC is being devoted to the development of more selective, sensitive and stable detection systems to supplement the rapid advances taking place in separation methods. For example, it is possible to apply fast-scanning voltammetric detection, instead of amperometric detection [57-60]. Serious drawbacks, however, are the significant increase in background (mainly charging current) and the shift in the voltammetric wave toward more extreme potentials if the electrode reactions are not fast. These problems can be partly overcome by application of more sophisticated potential wave forms and data acquisition methods. These include the differential pulse [61] and square wave [62-65] and coulostatic compensation of charging current [66-68]. Another approach is the use of microelectrodes [65,69,70]. These have been found to offer advantages over conventionally sized electrodes in LCEC work such as small volume and time independent current response. The

steady state current response has a small diffusion layer (analytical response is significantly less dependent on flow rate), less ohmic IR drop, and little or no supporting electrolyte is needed. Chemically modifying the surface of an electrode has been used to improve the specificity of electrochemical detection for certain classes of compounds [71-72]. The use of dual-electrode electrochemical detectors has also been explored [73-76]. The advantage of two working electrodes with potentials E1 and E2 is that several kinds of experiments can be done. In one, different potentials are applied to E1 and E2 so that current response is different and permits discrimination between species, even though they may be incompletely resolved chromatographically. In another type of experiment, the down stream electrode of the dual-series electrode is used to collect the product generated at the upstream electrode. Thus, the downstream electrode is sensitive only to electrochemically reversible species generated at the upstream electrode. The analyte can thus be "derivatized" and detected within the detector cell. This circumstance is similar to that of rotating ring-disk electrodes. Several efforts to obtain three-dimensional information have been made. The potential of the working electrode is linearly varied in scanning eletrochemical detection, with or without superimposed voltage pulses [77-79]. The resulting current vs. voltage curves can be displayed as a function of the time forming a three dimensional chromato - voltammogram [80-81]. This provides information about the electrochemical characteristics of eluting substances and the possibility to detect each component in a mixture at an optimum detection potential in a single chromatographic run.

During the last ten years, electrochemical detectors for liquid chromatography have reached a level of maturity such that thousands of

these devices are in routine daily use for a variety of purposes. Although this detection scheme offers several inherent advantages over spectroscopic techniques in terms of selectivity, linear dynamic range, response time, cost and versatility, it still suffers from certain drawbacks. For example, the mobile phase must be very pure and special care taken to exclude oxygen in the negative potential range. For this reason, significantly fewer applications have been made in HPLC using a Hg electrode detector which has a suitable voltage range for reductive electrochemistry. The purpose of this part of my thesis was to explore a sensitive Hg detector for a system in which a catalytic redox hydrogen kinetic current was used as a detection signal.

2.2 Basic introduction to the catalytic hydrogen current

2.2.1 Diffusion current and kinetic current

There are two kinds of currents in polarographic measurements which are called diffusion and kinetic current. A current whose magnitude is controlled only by the rate of diffusion is called a diffusion current. Diffusion may be described as a spontaneous process leading to equilibration of concentration differences in a concentration gradient. If a concentration gradient arises in a solution, the solute starts to move from areas of high to those of lower concentration. The rate of diffusion is proportional to the concentration gradient. On the other hand, there are an appreciable number of electrode processes where the current is controlled by a chemical reaction taking place in the vicinity of the electrode. These currents are called kinetic currents. The quantitative investigation of these kinetic currents was initiated by Wiesner in 1943 [82]. Chemical reactions

may be combined with electrode processes in three ways [83-84]: a) the reaction precedes the electrode process proper, b) the reaction follows the electrode process, or c) the reaction runs parallel to the electrode process. Both preceding and following reactions are frequently not suitable for analytical applications since the limiting currents in these cases are not dependent on the concentration or do not provide high sensitivity. However, when the reaction is in parallel to the electrode process, the starting material can be generated by a chemical reaction occurring subsequent to the initial charge step. Thus, the electroactive material is effectively reduced more than once, and starting material is produced at the electrode surface by both diffusion and the chemical step. The limiting current is proportional to concentration of starting material if the solution conditions and instrumental conditions are carefully controlled. Remarkable increases in limiting current can occur, and these high currents are obtained if the rate of chemical reaction is very fast.

2.2.2 Catalytic hydrogen current

The catalytic hydrogen current is the most important catalytic current for use as a high sensitivity method in analytical chemistry. Catalytic hydrogen waves are those in which the normally irreversible and very negative reduction wave involving hydrogen ions is shifted to more positive potentials by the presence of a catalyst. The limiting current of the hydrogen ion reduction wave is a function of the concentration of the catalyst. The polarographic method has been used to obtain a large number of experimental observations that have helped to explain the catalytic activity of substances. The types of catalyst may be divided into two groups:

a) electroactive species, which after reduction form catalytically active clusters of atoms on the electrode surface, and b) certain classes of substances containing groups capable of protonation that are adsorbed on the electrode surface. The first group of catalyst includes platinum metal salts that, even at trace level, cause a catalytic hydrogen wave. The wave appears at a potential about 250 mV more positive than that for normal evolution of hydrogen and grows with increasing concentration of these salts. At constant salt concentration, the current rises with increasing acid concentration to a limit. The sensitivity of this kind of catalytic current is very high in certain cases. A metal concentration as low as 10^{-10} M can be detected [82]. The second group of catalysts comprises a large number of organic substances that at low concentration also shift the reduction potential of hydrogen ions to positive values and thus yield catalytic hydrogen waves. The catalytic current is a function of pH and buffer composition. A well-buffered medium must be employed for the investigation of the catalytic current. For unbuffered neutral media, where during the catalytic evolution of hydrogen a pH change occurs in the vicinity of the electrode, the conditions are especially complicated and water molecules function as proton donors. It has been found that this type of catalyzed process shows sensitivity of as high as one thousand times the limiting currents on the noncatalyzed waves [84].

It can be expected that such a catalytic process has the possibility of being a sensitive detector for HPLC. However, very few papers have reported the use of a catalytic process in HPLC electrochemical detection. Heuser and Girar [85] reported a dramatic electrocatalytic effect that was applied to the detection of transition - metal ions. These ions are easily

oxidized at low positive oxidation potentials. For example, the signal obtained for Co(II) was 50 times that predicted by Faraday's law. Voltammetric studies indicate that the effect involves an electron-transfer reaction between the metal cation and the tartrate anion with which it is complexed. This effect provided enhanced detection for Co(II) and Mn(II) in ion chromatography. It is clear, this electrocatalytic effect does not belong to a hydrogen catalytic system. In our laboratory, studies using the vitamin B_{12} catalyzed hydrogen reduction reaction have demonstrated the feasibility of using this type of kinetic current for sensitive EL-LC determination. Using an acetonitrile/water (pH=5.0) mobile phase, a detection limit of 1.2 pmol of vitamin B_{12} was found [86]. The objective of the experiments presented in this chapter is to demonstrate the suitability of a mercury electrode as a working electrode in a hydrogen catalytic system for determination of chloroquine and other compounds. For this purpose, both the electrochemistry and chromatography of chloroquine have been studied in detail.

2.3 Overview of the experiment

For an EC-HPLC study the experimental set-up consists of the solvent delivery system, the chromatographic column and the electrochemical detector. The solvent delivery system was a very basic pump from Bio-Analytical Systems or a Waters M-6000A pump. The column was a C-18 reversed phase column from either Water Associates or Supelco. The electrochemical detector consists of a computer controlled system that can apply the potential wave form and acquire and analyze the data and an

electrochemical cell in which a static mercury drop electrode SMDE) was used as a working electrode.

2.3.1 Computer controlled system [87].

A Digital Equipment Corporation (DEC) 11/73 computer was used to produce a large variety of pulse waveforms for output to a potentiostat through a 16-bit digital to analog converter (D/A), to acquire electrode current through a 12 bit analog to digital (A/D) converter, and to control a Metrom Multi-Mode Mercury Electrode via an air valve and drop knocker. The diagram of the overall experimental set-up is shown in Figure 1.1. The parallel output of the DEC 11/73 computer is connected to a Burr-Brown 729K (D/A) converter that is used to output an electrode potential. This potential was applied to the control potential input of a Venking model 68 FR 0.5 potentiotat. The potentiotat controls the potential between a SCE reference electrode and the Multi-Mode Mercury Electrode(MME). Current at the MME is measured via a Keithley 614 electrometer that serves both as a current to voltage (I/V) converter and as an amplifier. The current data are stored in the computer in normal form. Difference or summed currents may be displayed and listed, and the original normal form is available for examination. When the experiment is completed, the data may be displayed on a Tektronix 4014 compatible monitor and plotted on a Hewlett-Packard 7475 pen plotter.

The program for the computer control system is called HSWAVE. The computer along with the program HSWAVE is the heart of the instrument, serving as the operator's control panel for running an experiment. HSWAVE is a waveform generation program for HPLC

detection and general voltammetry. It is the main program used in this instrument for data acquisition, experimental control, and output of the voltage waveforms. The HSWAVE program is controlled by commands that are entered through the terminal keyboard. Some of the commands include changing parameters, running an experiment, and displaying data. Activating a command may change a parameter, a menu or start some action (such as initiate a waveform scan). The ranges of control potentials are +/- 2.5 volts, +/- 5.0 volts, or +/- 10.0 volts. Normally, the range is set to +/- 2.5 volts as this is the most common range of potentials used in electrochemistry. The 4096 data points in an experiment can be stored automatically.

In this instrument, the scan rate is a value that is meaningful only when viewed together with data acquisition resolution or the number points of data per scan. Scan rate is not related to the slew rate as in analog instruments. Obviously, if greater resolution is desired, along the voltage axis , the value of scan rate can be decreased; conversely, if fewer data points are required, the rate can be increased. A limit of the scan rate is imposed due to the fact that the data acquisition is performed under software control.

The current of interest at the working electrode is measured by an electrometer that converts the current to a proportional value of voltage. This voltage output is then connected via a 12 bit (1 part in 4096 resolution) differential input A/D converter with programmable gain. In this instrument, the input of the A/D converter is connected to the output of the Keithley electrometer. The electrometer has an output voltage which is proportional to input signal. When it is set to current mode, it serves as a current to voltage converter. When the electrometer is set on the 20 μA

scale, the resolution of current is 0.00488 μA. To increase current resolution and compensate for the limited offset current of the electrometer, a current injector has been placed in parallel at the input of the electrometer. This device is simply a potentiometer across a stable DC voltage source (a mercury battery) shielded in a box with appropriate triaxial connector and a switch that controls both polarity and power to keep the input current from going out of range.

2.3.2 Electrochemical cell

The electrochemical cell for flow detection in HPLC consists of two parts: the flow cell and polarographic cell as shown as Figure 2.2. The polarographic cell is a Brinkman 6.1415.250 electrochemical cell with a hole drilled in the glass about 20 mm from the top to provide for overflow of liquid. Eluent from the column was carried by Teflon tubing and introduced in the immediate vicinity of the suspended mercury drop. The flow cell is made out of Teflon and fits on the electrode glass capillary which is optimized for small dead volume. The eluent flow from the column capillary tubing fits through the other end of the flow cell and is brought as close as possible to a static or dropping mercury drop in a wall jet configuration. The flow cell is immersed in the polarographic cell which contains the reference and counter electrodes, degassing tube, and the same buffer as the mobile phase. In operation, solution eluting from the column flows across the mercury drop and diffuses into the bulk solution. The bulk solution is deoxygenated by bubbing with nitrogen or argon gas. The overflow hole is loosely coupled to a pipette that draws overflow into a

large collection vessel. This overflow can be used to collect excess solution for disposal or used for measurement and determination of the flow rate.

2.3.3 Working electrode

The working electrode is connected to the input of the I/V converter. The choice of working electrode depends upon the experiment. In this experiment, the hydrogen-catalytic currents were determined at relatively low pH and very negative potential. Thus a mercury electrode was selected as the working electrode. There are several modes of operation for the mercury electrode. In this experiment, the static mercury electrode (SME) was used. The difference between a static mercury electrode and traditional dropping mercury electrode (DME) is that with the DME, mercury is flowing all the time while in the SME mode, a mercury drop is grown quickly and then held at a constant size for a period of time when a potential is applied to it. When used as a static electrode, the theories describing electrode current are simpler than that for the DME since it is possible to neglect complicating terms such as that due to the continually changing DME area. In this instrument, the mercury drop growth does not depend upon height of the mercury column and capillary length. It was controlled by an air valve to provide a gas pressure to push out the drop. When the valve is off, there is no pressure applied and the mercury flow is cut off. While the air valve is energized, tank pressure will provide a pressure which allows the mercury to flow freely. There is an air valve and control circuit which is used to provide a voltage controlled interface to the computer.

2.3.4 Experimental procedure for electrochemical detection in HPLC

The mobile phase used was a mixture of water and acetonitrile containing 0.05M sodium acetate and was titrated to a pH of 5.0 using glacial acetic acid. The mobile phase is deoxygenated by sparging helium in a custom made flat bottom flask with an air-tight glass cover. The helium is presaturated with acetonitrile from the mobile phase. The mobile phase is then pumped through the column at a flow rate of around of 1.0 ml/minute. The eluent exits directly below the mercury drop in the polarographic cell. The bulk solution in the cell is maintained oxygen-free by bubbling nitrogen through a specially constructed bubbler that has a fine frit at the tip and hood covering the frit. The hood vents directly above the liquid level in the cell. This arrangement allows continuous bubbling of nitrogen even as the chromatogram is being recorded. Any disturbance due to bubbling is contained with the hood and will not contribute to noise at the mercury drop. Complete deoxygenation is very important in reductive electrochemistry as dissolved oxygen is easily reduced at mercury.

Samples of size about 25 µl were injected into a 20 µl sample loop, with the overflow discarded. The computerized instrument and HPLC were synchronized manually.

2.3.5 Apparatus for electrochemistry study

Several instruments were used in electrochemistry studies. A BAS-100 analyzer was used for cyclic voltammetry experiments. A three-electrode cell system with a glassy carbon working electrode, a silver chloride (saturated potassium chloride) reference electrode and a platinum

auxiliary electrode were used. Classic polarographic experiments were carried out on a Tacussel PRG-5 polarographic instrument. A dropping mercury electrode was used a working electrode, a platinum electrode as the auxiliary electrode, with a saturated calomel electrode as the reference electrode.

All chemicals were analytical-reagent grade (Fisher Scientific Co or J.T.Baker Chemical Co.) and were used as received. All solutions were prepared with pure water obtained by passing tap water through a carbon filter, a multiple ion exchange system followed by distilling.

2.4 Results and Discussion

2.4.1 Electrochemical study

The prerequisite for the detectability of organic compounds in a reductive Hg electrochemical detector is the presence of a functional group which can be reduced directly at the electrode or a functional group which will act indirectly by catalyzing a simple reduction process such as the conversion of hydrogen ion to hydrogen gas. In this research, the determinations were based on the indirect method utilizing the catalytic hydrogen process which can greatly enhance determination sensitivity. In terms of the indirect method, virtually all nitrogen heterocycles or amine compounds which are capable of binding a proton with a lone pair should catalyze the hydrogen reduction reaction. Chloroquine consists of a heterocyclic ring and amine groups as shown in Figure 2.3. It can be expected that chloroquine will catalyze the hydrogen reduction reaction and should be detectable in acid mobile phases.

Chloroquine was first discovered by German scientists in the late 1930's who were attempting to develop a synthetic antimalarial drug. They never tested it because they thought it would be too toxic. It was rediscovered by American scientists in the 1940's and was soon in widespread use [87]. Among several antimalaria compounds of the aminoquinoline class that possess significant activity against hepatic amoebiasis in hamster and in man, the most important is chloroquine since chloroquine has found acceptance in the treatment of many types of malaria. Chloroquine is used for the treatment of extra-intestinal amoebiasis in man, but has poor activity against the intestinal form, presumably because it is so readily absorbed that it does not reach effective concentration [88]. There are only a few papers reported for chloroquine measurement. The US. Pharmacopoeia [89] recommended that chloroquine in pharmaceutical preparations be determined by extraction with chloroform followed by spectrophotometry at 343 nm. Using a PVC membrane electrode Cosofret and Buck [90] showed a near Nernst response in the 10^{-2} - 10^{-6} M range and a detection limit of $2*10^{-7}$M.

2.4.1.1 Cyclic voltammetry

The electrochemical behavior of chloroquine was studied by several different electrochemistry methods with different electrodes. At first, the BAS 100 was used to study chloroquine by linear scan cyclic voltammetry in a conventional electrochemical cell. Cyclic voltammetry is the most effective and versatile electroanalytical technique available for the mechanistic study of redox system [83]. The triangular potential signal for cyclic voltammetry causes the potential of the working electrode to sweep

back and forth between two designated values(the switching potentials). To obtain a cyclic voltammogram, the current at the working electrode in unstirred solution is measured during the potential scan. A cyclic voltammogram was obtained with a glassy carbon working electrode immersed in a $2.0*10^{-4}$M chloroquine solution with 50% acetonitrile/water (pH=5.0) supporting electrolyte as shown at Figure 2.4. The electrochemical process is irreversible when the potential of the working electrode was scanned in the range of 0.0V to -1.0V vs. SCE as only one reduction peak was found at -0.64V with no peak in the reverse scan. An interesting observation is that when the negative scan potential is extended to -1.60V, one high sensitivity reduction peak can be observed followed by a curve for the normal evolution of hydrogen. The high sensitivity reduction peak arises from the catalytic hydrogen current because chloroquine can bind protons with its nitrogen lone pair. The bond hydrogen ion can be reduced at a more positive potential than the free hydronium ion giving rise to a catalytic current.

2.4.1.2 Squarewave voltammetry

To characterize the catalytic hydrogen current, squarewave voltammetry with a static mercury electrode was also used. As the name implies, a symmetrical small-amplitude square voltage is added to a staircase with a fix period. The response current is sampled at the end of both the forward and reverse half cycles. A difference current is determined by subtracting the current measured on the reverse cycle from that measured on the forward cycle. Squarewave voltammetry is a very powerful technique, since it can be used with fast scan rate. When a

dropping mercury electrode is used one can apply the entire excitation waveform during one drop period. Besides being fast, the technique is more sensitive than the popular differential pulse technique because both forward and reverse currents are measured in squarewave voltammetry [91]. The squarewave voltammetry experiments were carried out by the computer system described in the experiment section. The Metrohm multimode static mercury electrode was used as a working electrode. Figure 2.5 shows the squrewave voltammetry curves of chloroquine in 50% acetonitrile/water (pH=5.0) with a static mercury drop electrode. The potential scan started -1.0V with a step height of 10 mV and squarewave amplitude of 25 mV. When the solution contains chloroquine as low as $1.0*10^{-6}$M, there is a sensitive reduction peak at -1.53V. This is, obviously, a chloroquine catalyzed hydrogen wave since in the absence of chloroquine, the current does not begin to rise until -1.60V. A similar behavior was observed in same solution by using differential pulse polarography.

2.4.1.3 Direct current polarography

The electrode process of chloroquine was also studied by direct current (DC) polarography. The greatest advantage of DC polarography is probably the relative simplicity of the theory and its use [83]. An understanding of the nature of the electrode process is essential in the systematic use of any polarographic analytical method. Since Faraday's time, mercury has been used in electrochemistry as the most suitable material for electrodes because of its chemical nobility, its high hydrogen overvoltage and ease of purification. Moreover, in the dropping electrode used in polarography, these properties are combined by the continuous

renewal of the electrode surface; consequently, the dropping mercury electrode is remarkably convenient for investigating electrode processes and chemical change in solution. With a dropping mercury electrode, the current-potential characteristics of chloroquine in DC polarography (Figure 2.6) show a wave that rises in an irreversible fashion and reaches a limiting plateau at -1.52V, where there is no peak in the solution without chloroquine. This clearly demonstrates that the presence of chloroquine accelerates the hydrogen evolution. The electrode process of chloroquine has been studied further by using a dropping mercury electrode in the following experiments.

2.4.1.4. Current - time curves

Important information on the electrode process can be obtained from current-time curves recorded by applying the potential successively to the drop at different phases during its life. With diffusion-controlled currents, a large increase in current, caused by accumulation of depolarizer in the vicinity of the drop, occurs after interrupting and again applying the potential; this current, however, rapidly sinks to the value associated with the current obtained by applying the voltage at the beginning of the drop-life. According to the Ilkovic equation for a polarographic wave [83]

$$i_d = 0.732\, nFC\, D^{1/2}\, m^{2/3}\, t^{1/6} \qquad (2-1)$$

where i_d is diffusion current; n is the number of electrons involved in the charge transfer process; F is the Faraday constant; C is the concentration of electroactive species at the electrode surface; D is the diffusion coefficient;

m is the flow rate of mercury and t is the drop time. The instantaneous current time curves(i-t) should be parabolas with the exponent 1/6 independent of potential, regardless of whether the reaction product diffuses back into the bulk of the solution or into the mercury drop. This is a consequence of the concept of the linear character of diffusion as postulated in the derivation of the Ilkovic equation. In the case of a kinetic current, the instantaneous currents at all phases of the drop-life are equal to those obtained at constant voltage, regardless of the instant when the voltage is applied. The exponent of the current time curves has been found to be 2/3[83]. For hydrogen catalytic current, the exponents of current time curves were found to be in the range 0.5 ~ 0.6 [82]. In this experiment, the current time curves as shown in Figure 2.7 for chloroquine in 50% acetonitrile (pH =5.0) was tested with a mercury drop with an applied potential at -1.53V (vs. SCE). Figure 2.8 shows that plot of log i vs log t is a straight line The slope calculated from the plot was 0.60 which is greater than 1/6 and corresponds quite well to values for kinetic currents. This experiment provided additional evidence that the instantaneous current is controlled by a kinetic electrode process rather than a linear diffusion process.

2.4.1.5 Dependence of current on height of the mercury head

The study of dependence of current on capillary characteristics is an another method for investigating the electrode process. In the Ilkovic equation (2-1), m is directly proportional and t inversely proportional to the height of the mercury head.

$$m=k'h; \qquad (2-2)$$

and $t=k''(1/h)$ (2 - 3)

where k' and k" are constants. Substitution in the Ilkovic equation, leads to

$$i_d = k\, m^{2/3}\, t^{1/6} = k\, (k'h)^{2/3}\, (k''/h)^{1/6}$$

and on combining all constants

$$i_d = k(h)^{1/2} \qquad (2 - 4)$$

where k is a constant, i.e., the diffusion current is directly proportional to the square-root of the height of the mercury head (reservoir). This linear dependence provides an easily accessible experimental test for a diffusion controlled current. With a diffusion controlled current, the plot gives a straight line, which passes through the origin. However, the catalytic current is proportional to $m^{2/3}\, t^{2/3}$ [4]. Therefore a catalytic current can be easily recognized because of the independence of i_c on the mercury column height. Since m is directly proportional to the height of the mercury head but t inversely proportional to the height of the mercury head, the $m^{2/3}t^{2/3}$ result is independent of h. The experiments for chloroquine in the 50% acetonitrile (pH=5.0) were measured with the height of the mercury head from 37.5cm to 87.5cm. The experimental results indicate that the DC limiting currents are not proportional to the square-root of the height of the mercury head (reservoir) which indicates this system is not a diffusion controlled electrode process. In viewing data from Figure 2.9, it can be seen that the limiting currents increase very slowly with the height of the mercury head. This can be explained from the mechanism of the hydrogen catalytic current. Substances that lower the hydrogen overvoltage may be divided into two groups: (a) electroactive species which after reduction form catalytically active clusters of atoms on the electrode surface, and (b) certain classes of substances containing groups capable of protonation that

are adsorbed on the electrode surface; chloroquine belongs to the second group. Because chloroquine is adsorbed on electrode surface, the limiting current increases slowly with the height of the mercury head.

2.4.1.6 Dependence of current on concentration of buffer solution

The variations of the peak current with a buffer at constant pH=5.0 were also examined. It was found from Figure 2.10 that the current rises with increasing buffer capacity. When the concentration of buffer at pH=5.0 was raised from 0.01M to 0.50M, the current for chloroquine is increased around 7 times. The limiting current is proportional to the square root of the buffer concentration, since a log-log plot gives an exponent of 0.49 with a linear correlation coefficient of 0.998. This behavior of the limiting current with buffer concentration is consistent with an electrode mechanism involving a homogeneous rate determining step in which the conjugate acid of the buffer participates. A well buffered medium must be employed for the investigation of catalytic current. This precaution prevents possible complications due to pH changes in the vicinity of the electrode.

In general, viewing the electrochemical behavior of chloroquine from cyclic voltammetry, squarewave voltammery and direct current polarography, it is found that chloroquine will give a catalytic hydrogen wave in the 50% acetonitrile/water (pH=5.0) buffer solution. The application of this catalytic hydrogen current to HPLC detection, allows a sensitive electrochemical detector to be developed. Combining these two techniques should provide a new area which couples electroanalytical chemistry and liquid chromatography. One obtains the high separation resolution of

HPLC which can distinguish among many analytes and the high sensitivity of hydrogen catalytic current which can increase detection limits.

2.4.2 Chromatography study

As expected from the electrochemistry, a high sensitivity HPLC method can be developed by using a mercury electrode as a detector in a catalytic electrochemical system. Figure 2.11 shows the chromatogram of chloroquine in a mobile phase of 50% acetonitrile/water (pH=5.0). A differential pulse potential technique was applied to the static mercury electrode to detect the catalytic current of chloroquine eluting from the column. Figure 2.12 shows the dual pulse waveform. The mercury drop grows during the t_{air} time under constant pressure and is kept static at t_1 and then the potential is stepped from V_1 to V_2 at t_2. The current sampling takes place at the end of t_1 and t_2. The mercury drop is renewed by knocking it off at the end of t_2. Obviously, the drop size of static mercury electrode can be controlled by changing the value of either t_{air} or the pressure. The longer the period of t_{air}, the larger will be the size of mercury drop under constant pressure. When the t_{air}= 300 ms was selected under constant pressure (46 mm Hg), the diameter of each static mercury drop was 1.5 mm which is larger than the bore of Teflon tubing (0.3 mm) from which the eluent comes out from the column. Therefore, the configuration of this flow cell meets the definition of a wall-jet cell system.

2.4.2.1 Effect of drop size of electrode

The electrode drop size was varied to examine the sensitivity dependence on drop size. According to the theory of the wall-jet cell system, the current characteristics are expressed by the following equation [92-93].

$$i_{wj} = 0.439n\pi F a^{-1/2} v^{-5/12} V_f^{3/4} C_o R^{3/4} \qquad (2-5)$$

Where V_f is the flow rate; a is the inlet diameter; v is the kinematic viscosity; R is the radius of the electrode; all other terms have their usual meaning. Figure 2.13 shows the peak currents as a function of the radius of the electrodes. The response currents increased linearly with $R^{3/4}$ from 0.81mm to 1.32mm which corresponds to t_{air} time from 300 ms to 1300 ms under constant pressure (48 mm Hg). These results are consistent with that expected from equation (2-5). It is obvious that the sensitivity can be increased when larger drop sizes are used. In the other words, in this experiment the response currents will increase with t_{air} at constant pressure.

Application of a long t_{air} time in flow-injection and chromatographic systems can result in fewer data points needed for accurate determination of true peak shape. Perone and Hsi [94-95] recommended that a minimum of 10 points are needed for each peak to prevent peak distortion. In work described here, the base line widths of the peak virtually always exceeded 25 seconds, therefore, the droptime ($T=t_{air} + t_1 + t_2$) can be selected as 2.5 seconds as a maximum value. If t_1=650ms and t_2=50ms are used in the experiment, the t_{air} value can be selected as a value up to a maximum of

1800 milliseconds. In our experiment, to prevent peak distortion and to obtain an accurate determination, a t_{air} = 300 milliseconds was used in all the experiments.

2.4.2.2 Optimization of detection pulse potential

In order to determine the optimum applied potential for chloroquine detection in HPLC with a mercury electrode, the peak current response as a function of applied potential was studied. The relationship between the peak height of the differential current and pulse height of the potential is shown in Figure 2.14. In this experiment, the voltage of the first potential, V_1, was set at -1400 mv and the potential pulse V_2, was set for a duration of 50 ms for each injection to values in the range from -1425 to -1825 mV in 25 mV increment. It can be seen that the differential current of chloroquine increases slowly with the potential pulse V_2 at the beginning and then increases at a more rapid rate but afterward reaches a plateau. It is clear that the curve of the peak current vs. pulse height potential is sigmoidal which is in good agreement with the theory.

For any given analyte, the optimum polarization voltage is given by the value of pulse magnitude (V_2 -V_1), where the useful signal/noise ratio reaches its highest attainable value. If V_2 is set at the height of the plateau in Figure 2.14, the maximun sensitivity might be obtained although voltammetric peaks are broadened as pulse magnitude increases. On the other hand, because the experimental result is the difference between the currents flowing through the working electrode at potential V_1 (before the pulse) and V_2 (after the pulse), both values, V_1 and V_2 are important. In choosing V_1 and V_2, it is logical to examine the current vs. potential curves

in electrochemical experiments. This is similar to utilizing information from the UV-VIS spectrum of a compound in choosing the wavelength setting of a UV-VIS detector. In order to give the highest sensitivity, V_1 and V_2 should be set at the values which give the largest slope of difference current vs. potential curves. The DC polarography and squarewave electrochemical experiments have shown that the chloroquine catalytic current did not rise before the -1400mV and had a maximum differential current around -1530 mv. Therefore, in order to get the highest sensitivity, V_1 and V_2 were selected as -1400mV and -1600 mV, respectively.

2.4.2.3 Elimination of interference from dissolved oxygen

Significantly fewer applications have been made in HPLC using a mercury electrode which has a suitable voltage range for electrochemical reduction. One important consideration for a reductive technique is the interference from dissolved oxygen. In air-saturated aqueous solution, the concentration of oxygen in the mobile phase is about 0.5 mM. This results in a high reduction background current. Also hydrogen peroxide, an intermediate in the reduction process may chemically react with compounds in the mobile phase. In this experiment, several methods have been used to eliminate interference from dissolved oxygen. Sparging with an inert gas is probably the most frequently used method for oxygen removal. The mobile phase in the HPLC reservoir and in the electrochemical cell is continually degassed with the argon or nitrogen. During the experiment, the flow of gas was held just above the liquid to prevent turbulence. In addition, the differential technique also was used which discriminates against oxygen interference in our experiment, since

in this experiment, the voltages V_1 and V_2 are -1400 and -1600 mv which are on the plateau of the oxygen wave. Before the difference is taken, a similar current response is obtained at V_1 and V_2; thus, after the difference is taken, equal responses will cancel out. For a very small amount of sample solution, it is impossible to remove all oxygen dissolved in the sample by bubbling with an inert gas. An elution peak of oxygen was always observed and is close to chloroquine peak in 50% acetonitrile/water (pH=5.0) as shown in Figure 2.15. The retention time is 5.68 minutes for chloroquine and is 5.02 minutes for oxygen. In this case, it is difficult to determine low concentrations of chloroquine in the solution since there is an oxygen peak in front of it. However, changing the ratio of composition of mobile phase would help in the separation of chloroquine and oxygen. With a mobile phase of 65% acetonitrile and 35% water (pH=5.0), oxygen elutes from the column faster (t_{oxygen}=4.35 min.) and the chloroquine come out at little longer time($t_{chloroquine}$=7.05). Figure 2.16 shows in this mobile phase the two eluent peaks are well separated. This is because a weaker polarity of mobile phase was used which favors oxygen over chloroquine since the polarity of chloroquine is larger than oxygen.

2.4.2.4 Analytical precision

Ten replicate injections of a standard solution containing 1.0 μg of chloroquine were carried out separately to determine the precision of the LC method with the static mercury drop electrode (SMDE). The relative standard deviation was 0.73% (RSD). It is well know that mercury electrodes are quite reproducible because the electrode surface is clean and easily renewed. However, there are few applications in which a mercury

electrode is used as an electrochemical detector in HPLC. Two reasons for this are probably important. First, the dropping electrode does not provide high sensitivity in a polarography determination without a catalytic system. Second, the continuously changing area of the drop results in large capacitance current. Kok [95] compared the sensitivity and reproducibility of three electrochemical detection systems, the mercury (DME), amalgamated gold electrode, and system in which iodine is generated electrochemically in the column effluent, and found that the DME had the best reproducibility. The day to day variance was within 1.0% for a standard solution. However, the method lacked the sensitivity for real trace analysis in that system. In our experiment, the peak currents were based on the hydrogen catalytic redox cycle. It was evident that such a redox cycle has a high sensitivity, around one thousand times the limiting currents on the noncatalyzed wave. On the other hand, the static mercury electrode was used in our system which provides less capacitance current compared with dropping mercury electrode. Mercury is flowing all the time with DME mode while in the SMDE mode a mercury drop is grown quickly and then held at a constant size when sampling the current. Because of the dislodgment of the drop after each sampling, the static mercury electrode is also renewable. The high sensitivity, good reproducibility and lower capacitive current should make HPLC with such a mercury electrode system a very powerful technique for trace analysis.

2.4.2.5 Detection limit

The detection limit can be expressed in various ways. Normally, it can be defined based on the standard derivation in the regression curves.

An often used rule is that the minimum detectable concentration corresponds to an instrument reading which is three standard deviations larger than that observed for the blank. Alternatively, a criterion can be used of that quantity of solute introduced into the detector which produces a peak current two times the noise level. The implicit assumption here is that the detector, and not the analytical method, limits the precision of the determination. In this experiment, the noise was measured as the full peak to peak variation in the baseline. Under conditions of the flow rate of 1.0 ml/min and applied potentials as V_1=-1400 mV and V_2=-1600 mV vs. SCE, the noise levels were 0.006 μA, with negligible drift. Figure 2.17 shows that with chloroquine in as low as 2.0 ng in an injection, the peak current, still is detectable.

There are several factors which affect the detection limit of the detector. The detector is based on the hydrogen catalytically current produced on the electrode surface which is highly sensitive to the mass transfer rate in the well-jet configuration. Even using a steady pump, the solution movement from the column to the cell due to the regular pumping can cause a change of the mass transfer rate. The other factor that can add to the noise is mercury drop oscillation causing vibration. In our experiment, each sampling of current is done on a new drop which is dislodged by the arm of the drop knocker hitting the capillary. The differential current is the another factor which affects the detection limit because in the differential method, the level of random noise increases by a factor of two. This is the price to be paid for use of the differential technique.

2.4.2.6 Squarewave detection in HPLC

Application of the voltammetric fast-scan technique of squarewave voltammetry (SWV) as a chromatographic detection method appears to have the advantage over other methods, such as staircase scanning methods of better charging current discrimination [96-98]. A chromatovoltammogram of chloroquine with a mercury electrode coupled with squarewave detection is shown in Figure 2.18. A 20 µl solution containing 1.0 µg chloroquine was injected onto the column with a mobile phase of 50% Acetonitrile/water (pH=5.0). The squarewave potential was scanned every 2.7 sec from -1300 mV to -1900 mV with a step height of 5 mV and squarewave amplitude of 25 mV. Several papers have reported [97-99] using SWV in combination with a solid electrode and HPLC. It was pointed out that the pretreatment of the electrode was crucial to the signal response. In comparison with a solid electrode, the mercury electrode is reproducible and easy to use. But chromatographic resolution is worse than with thin-layer ECLC flow cell. Also, with computer control of an ECLC system, SWV can be run in a both a two dimensional mode, signal (cell current) response vs. retention time, or a three dimensional mode called chromatographic voltammetry where current vs. both potential and retention time is measured. The use of potential as a variable should help in identification of compounds which have the same retention time.

2.4.2.7 Gradient elution to separate chloroquine and other compounds

The application of catalytic hydrogen reduction in an electrochemical-HPLC method opens up an area of electroanalytical chemistry that has long been under utilized because with straight polarographic methods there is no simple way to distinguish among analytes which catalyze hydrogen reduction. Based on the indirect method, all compounds, such as nitrogen hetercycles or amine compounds with a lone pair electron on nitrogen will catalyze hydrogen reduction and should be detectable in acid mobile phase. Clearly, there will be many compounds that are detectable by combining the catalytic technique with HPLC. In the present experiment, gradient elution has been studied to achieve a better separation for a mixture of chloroquine, 3-quinolinecarbonitrile and 4-chloroquinoline. The different sensitivities of the three compounds in this catalytic system are also discussed.

Chloroquine, 3-quinolinecarbonitrile and 4-chloroquinoline, have the same skeleton ring but different substitutes as shown in the Figure 2.19. To separate these compounds with gradient elution, the relationships between retention time of the compounds and polarity of mobile phase were first investigated. Figure 2.20 shows that the retention times of these compounds varys with polarity of the mobile phase. It is clear, from the Figure 2.20, that 3- quinolinecarbonitrile and 4-chloroquinoline are not very polar since the retention times for both compounds increase as the polarity of mobile phase is increased. Since the structure of 4-chloroquinoline is more symmetric than that of 3-quinolinecarbonitrile, it has the longest retention time of the three compounds. For the same reason, as the polarity of the mobile phase gets weaker, both compounds come out of the column

faster. However, the retention time of chloroquine is not changed as much as these two compounds when the polarity of the mobile phase is changed over the same range. This is because chloroquine has two different functional groups. The two amine groups are easily protonated in the acid buffer solution and it can be expected to have a large polarity. On other hand, chloroquine has a long sidechain and ring that are favorable to a less polar environment. Combining the two different functional groups results in retention times which do not change very much with polarity of the mobile phase.

Since 3-quinolinecarbonitrile and 4-chloroquinoline are of similar structure, a larger polarity of the mobile phase has to be used to get separation of both two compounds. However, using a large polarity in the mobile phase will cause longer retention time. In this experiment, gradient elution was used and 10% and 65% acetonitrile were selected as solvent A (initial condition) and solvent B (final condition), respectively. The gradient elution program has a 10 minute period to go from the initial condition to the final condition. To select the optimization condition, the effect of varying the ratio of solvent A and B was investigated. Figure 2.21 shows the retention times change as solvent B goes from a 30% ramp to 60% when keeping 10% solvent A constant. In general, the three compounds were well separated using the above conditions. The retention times of the three compounds decreased with increased polarity. It interesting that when 60% solvent B is selected as a final condition, the compound which elutes from the column first is 3-quinolinecarbonitrile and not chloroquine. For a good separation and an acceptable separation time, a 40% system of solvent B is selected to use for the gradient program.

There is one more condition that can affect the separation after selecting initial and final conditions for the gradient elution program. This is the shape of the gradient curves, which can be concave, convex or linear gradient curves. The results show that the linear and concave gradient curves were unable to separate chloroquine and 3-quinolinecarbonitrile. Figure 2.22 is an elution curve for a solution mixture containing the three compounds with a convex gradient curve.

2.4.2.8 Different sensitivity in the heterocyclic compounds

Although chloroquine, 3-quinolinecarbonitrile and 4-chloroquinoline are heterocyclic compounds that have same aromatic skeleton, the sensitivities of the three compounds in HPLC with the electrochemical detector are very different. Chloroquine has the highest sensitivity in this experiment with a current that is about 160 times larger than 3-quinolinecarbonitrile. The 4-chloroquinoline has lower sensitivity compared with chloroquine but it is about 20 time more sensitive than 3-quinolinecarbonitrile. Their differential sensitivity can be explained by the mechanism of the hydrogen catalytic reaction. The mechanism of an indirect EC-LC method utilizing the catalytic hydrogen process for a compound containing nitrogen with a lone pair can be related to the following set of reactions:

$$2x \quad H^+ + RN: = RNH^+$$

$$2x \quad RNH^+ + e = RNH\cdot$$

$$2RNH\cdot = H_2 + 2RN:$$

$$2H^+ + 2e = H_2$$

where RN: is an organic molecule capable of binding a proton with a nitrogen lone pair. The compound with a bound proton, RNH^+, will be reduced at a more positive potential than the free hydronium ion giving rise to the catalytic current. Variations of this mechanism are possible and further study is necessary to work out the exact details of the process.

It is clear, based on the mechanism of the catalytic hydrogen process, discussed above, that a high electron charge density for nitrogen is of benefit in the ability of the base to bind a proton. The structures of these compounds can be used to explain the different sensitivities for the different compounds.

Compared with other two compounds, chloroquine has two amine groups along with the same heterocyclic quinoline ring. These two amine groups on the sidechain can be protonated very easily in the acid buffer solution since they have large pK_a values. In addition, the resonance structures shown in Figure 2.23 are stable which provides for more electron density of the nitrogens. That may be why the chloroquine has the highest sensitivity of the three compounds. Both the 3-quinolinecarbonitrile and 4-chloroquinoline have only one amine group in the quinoline ring which is a weaker base than the one on the sidechain of chloroquine. This is because there is a sp^2 hybrid orbital for the nitrogen atom on the quinoline ring while there is sp^3 hybrid orbital for the nitrogen atom on the sidechain of chloroquine. On the other hand, there are different ring substituents in the two compounds. Both of them are electron withdrawing functional groups making a lower electron density on the nitrogen atom. Since the -CN is a stronger withdrawing functional group than -Cl, 4-chloroquinoline is more sensitive than 3- quinolinecarbonate. On the other

hand, the resonance structure of the 4-chloroquinoline can enhance the charge density of the electrons on the nitrogen. However, there is no stable resonance structure in the 3- quinolinecarbonate. Therefore, the 3-quinolinecarbonate provides less sensitivity in these three compounds.

2.5 Conclusions

Liquid chromatography with a static mercury electrode has been investigated to detect chloroquine based on a catalytic hydrogen wave. Both the electrochemical properties and optimized HPLC conditions have been studied in this set of experiments. The results show that this method can be used as an electrochemical detector for HPLC trace determination because of high sensitivity and good reproducibility. Since nitrogenous compounds are widely used and many of these compounds have been reported to exhibit a catalytic hydrogen wave at a mercury electrode, the method may be of practical value.

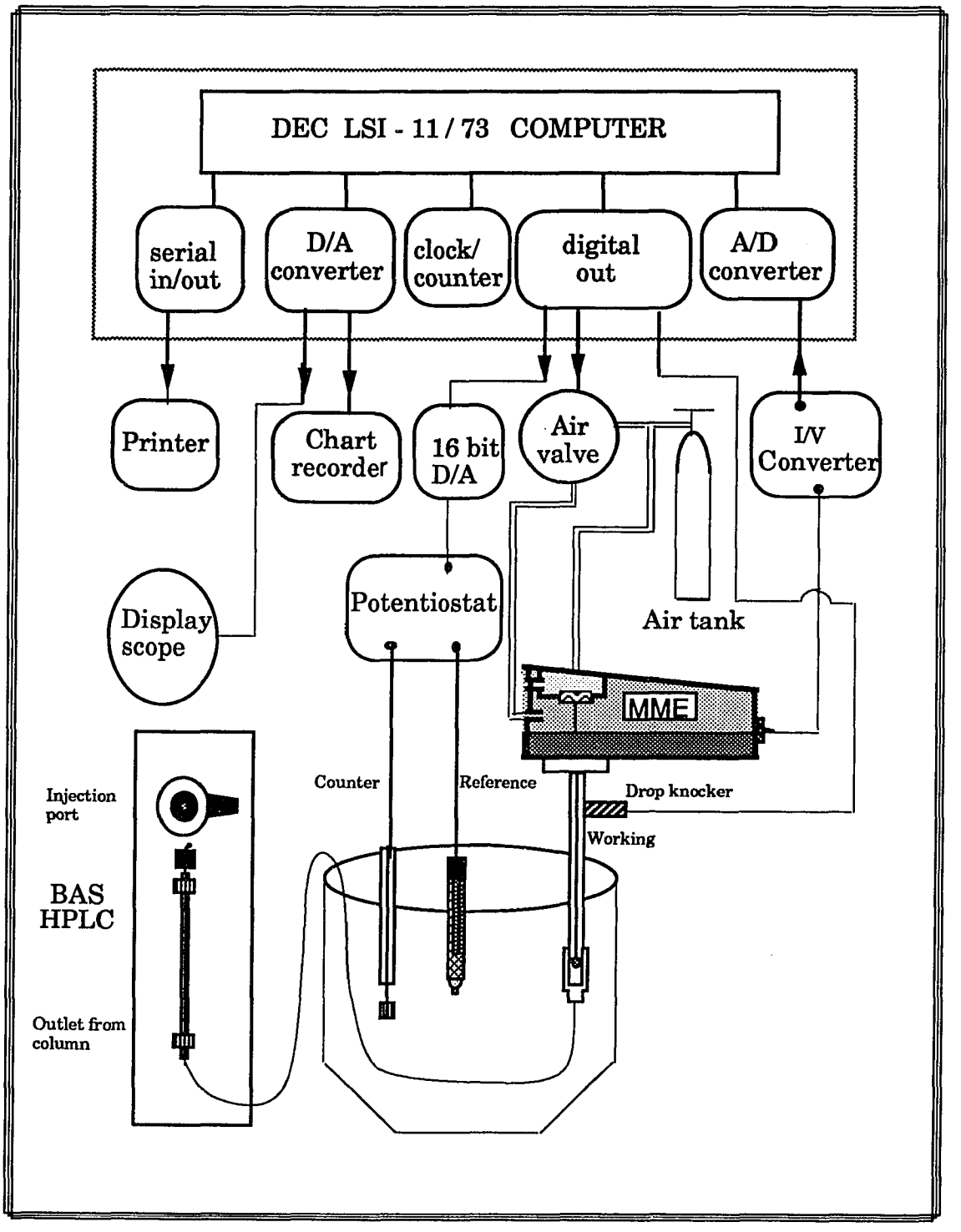

Figure 2.1 Diagram of the instrument and experimental set-up.

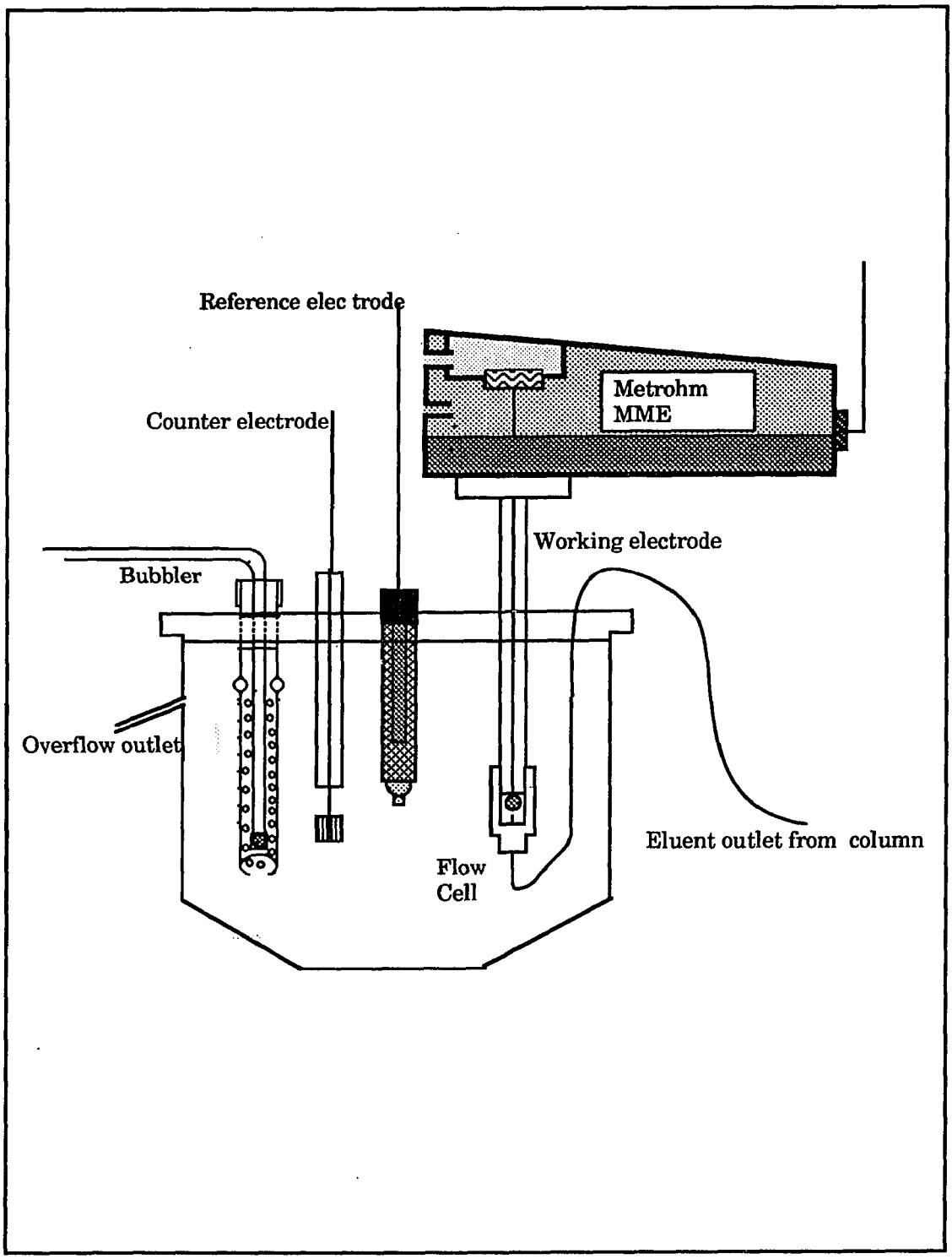

Figure 2.2 Diagram of HPLC electrochemical cell

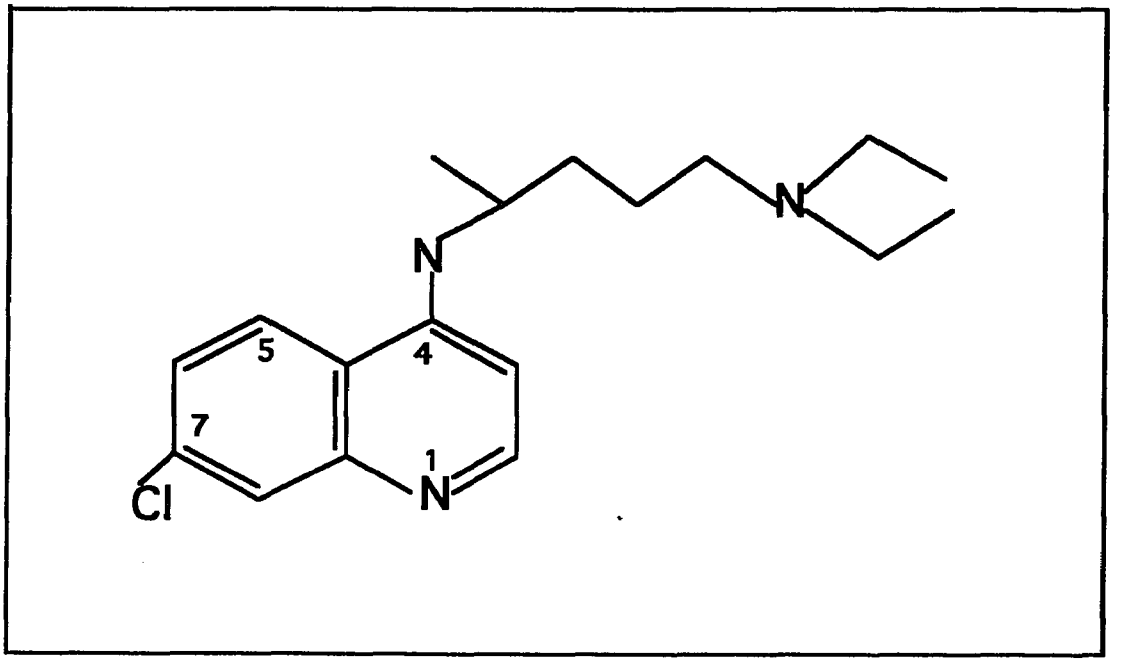

Figure 2.3 Structure of chloroquine

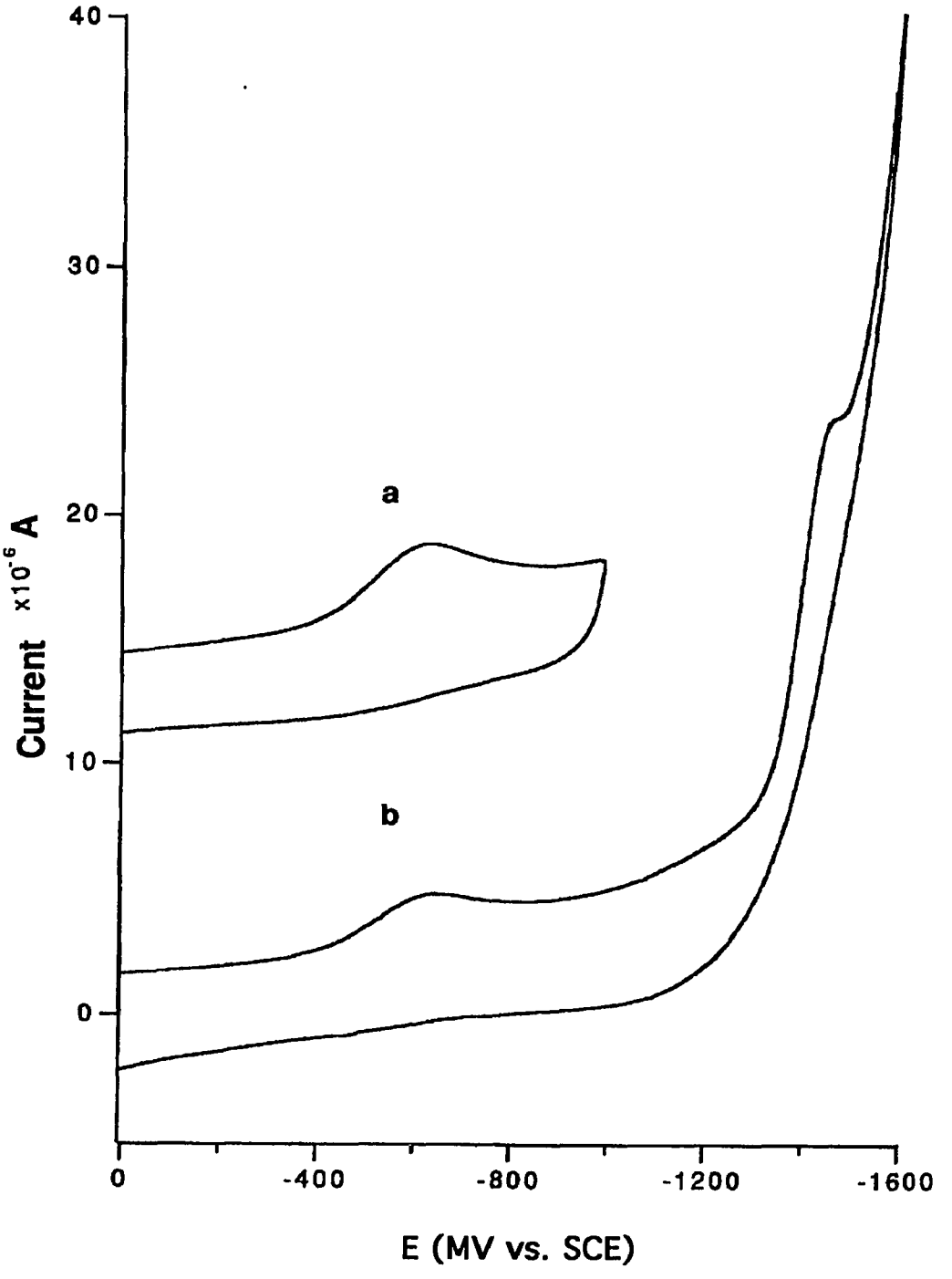

Figure 2.4 Cyclic voltammogram of 2.0*10-4M of chloroquine at a carbon disk electrode. Conditions : 50% acetonitrile 50% acetate buffer solution (0.02M, pH=5.0), Scan rate 100mv/Sec. (a) scan from 0 to-1000 mv; (b) scan from 0 to -1600 mv.

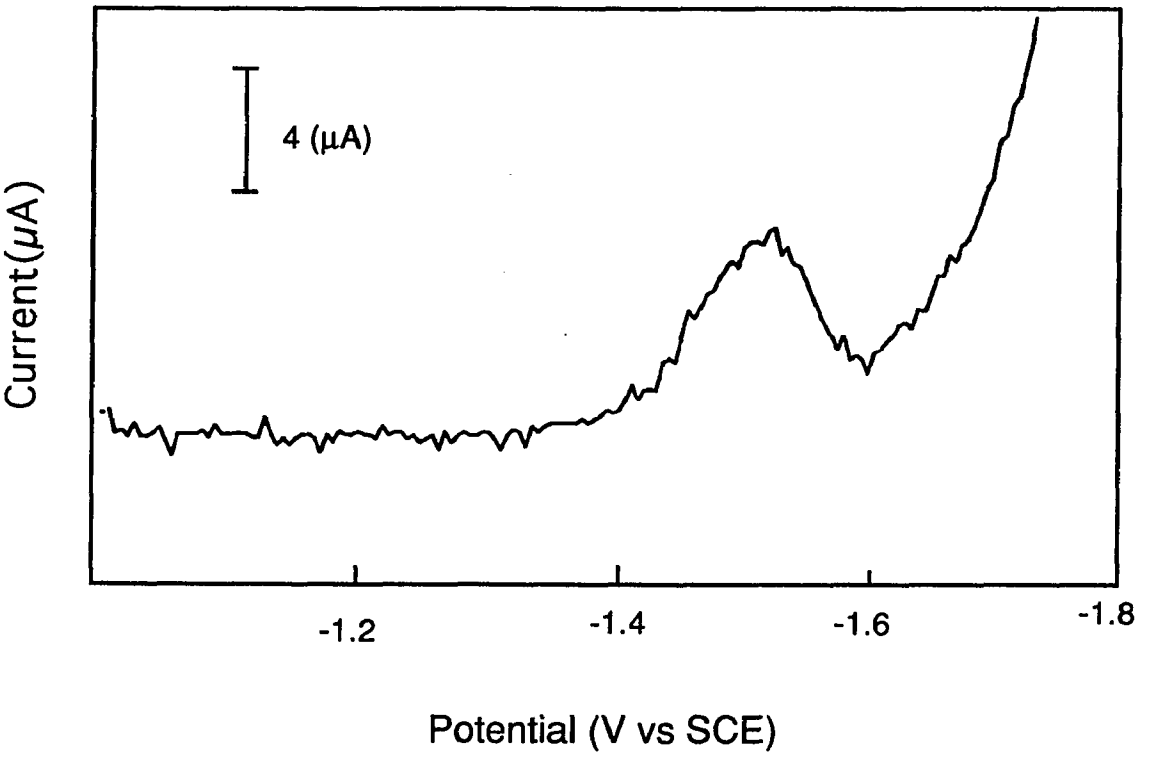

Figure 2.5 Squarewave voltammogram of 1.0*10-6M of chloroquine at static mercury electrode in 50% acetonitrile 50% acetate buffer solution (0.02M, pH=5.0). Scan from -1.0V with a step height of 10 mv and squarewave amplitude of 25 mv.

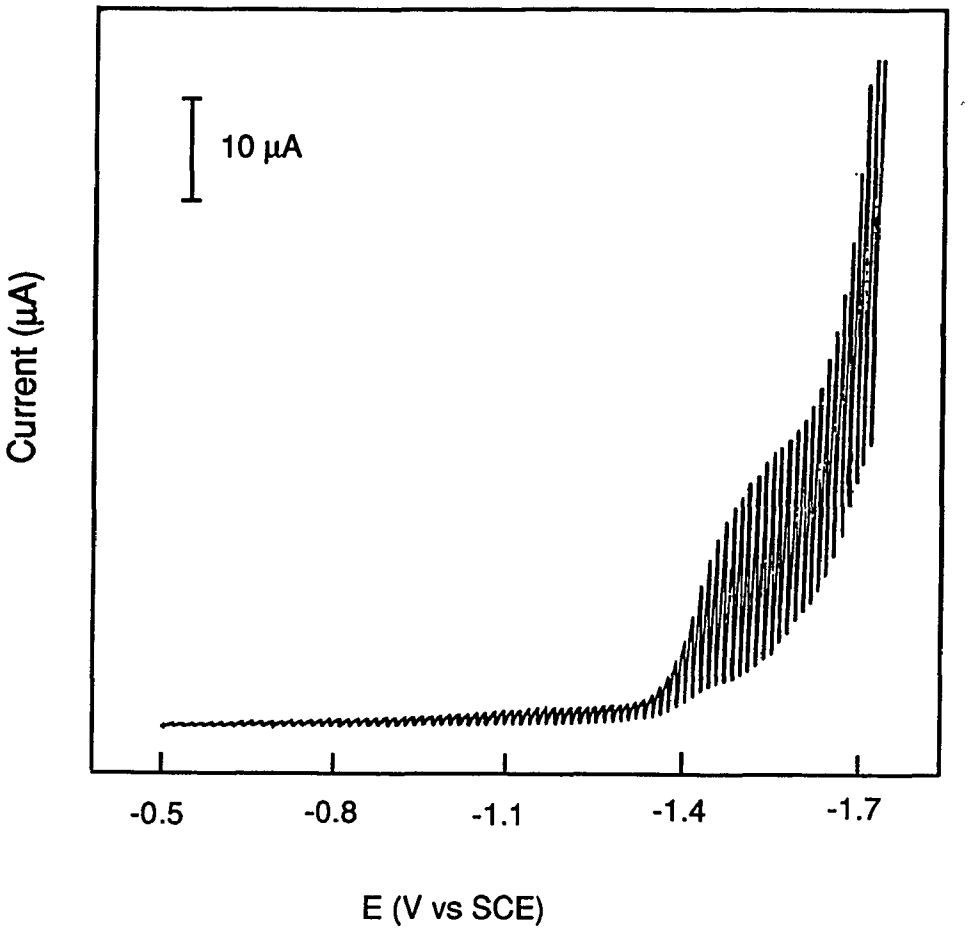

Figure 2.6 D.C polarography of 5.0*10-5M chloroquine in 50% acetonitrile 50% acetate buffer solution (0.02M, pH=5.0), scan rate 4.0 mv/sec.

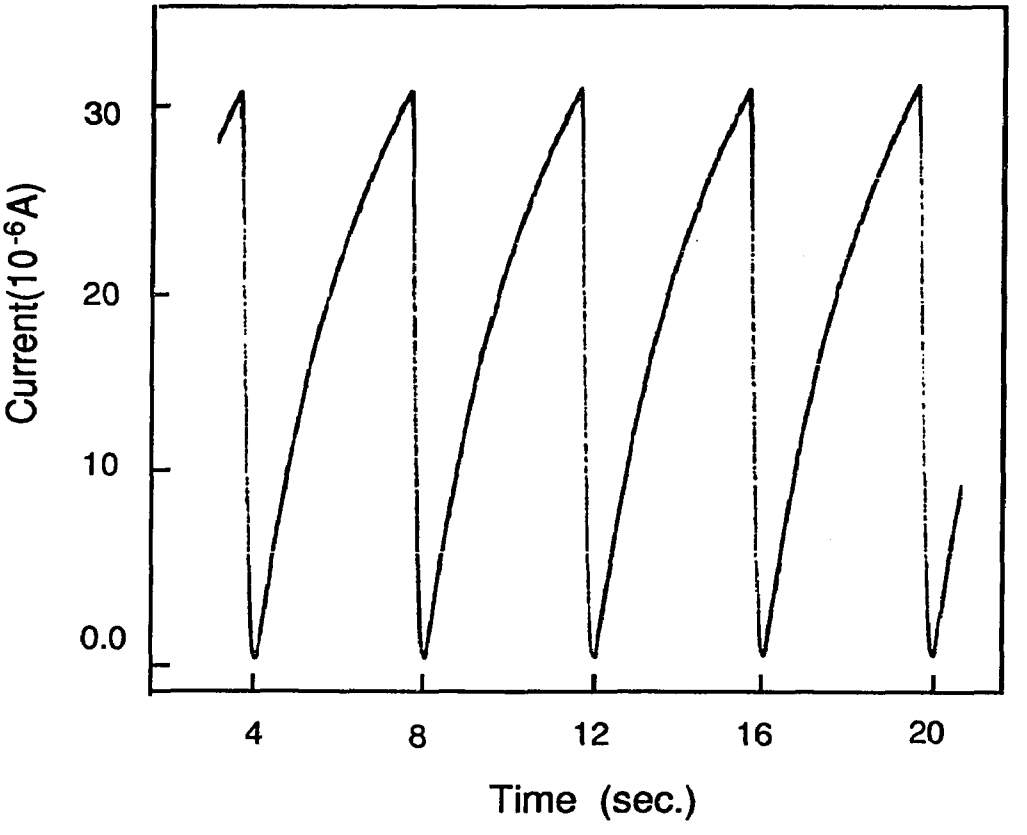

Figure 2.7 Current-time curve for chloroquine in 50% Acetonitrile 50% acetate buffer solution (0.02M, pH=5.0) at potential of the limiting current, E=-1.53V(vs SCE).

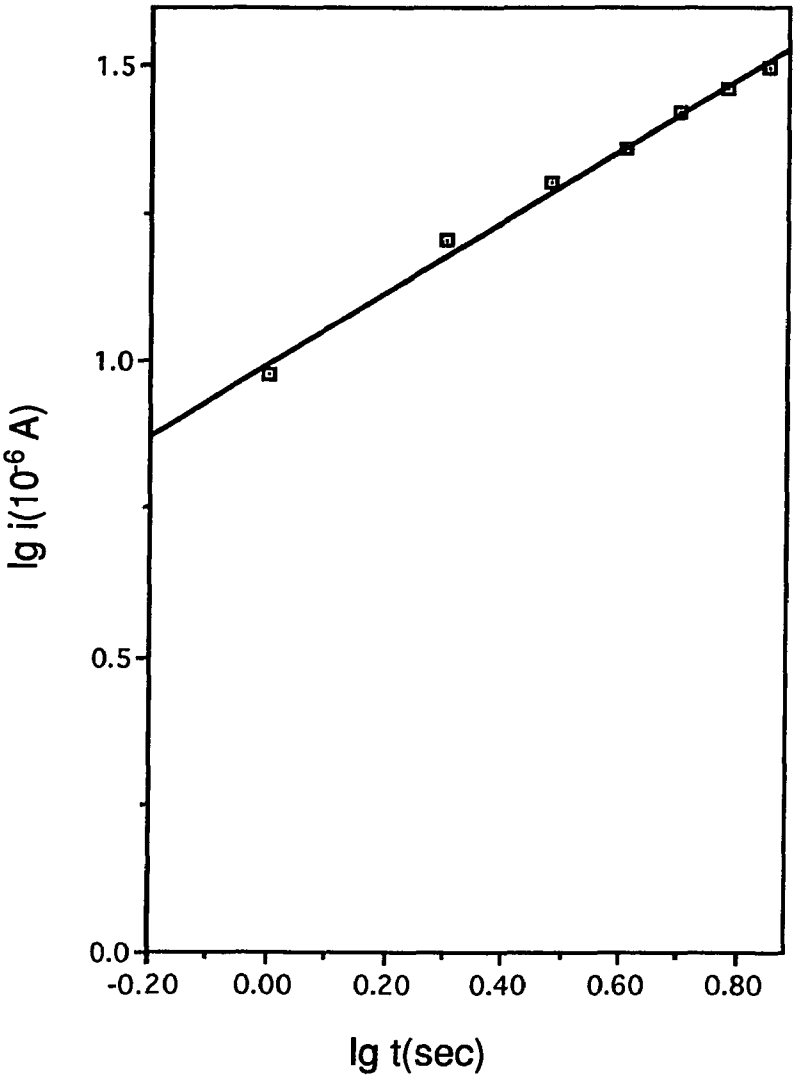

Figure 2.8 log i vs. log t plot for the current-time curve of chloroquine in 50% Acetonitrile 50% acetate buffer solution (0.02M, pH=5.0) at potential of the limiting current, E= -1.53V (vs SCE).

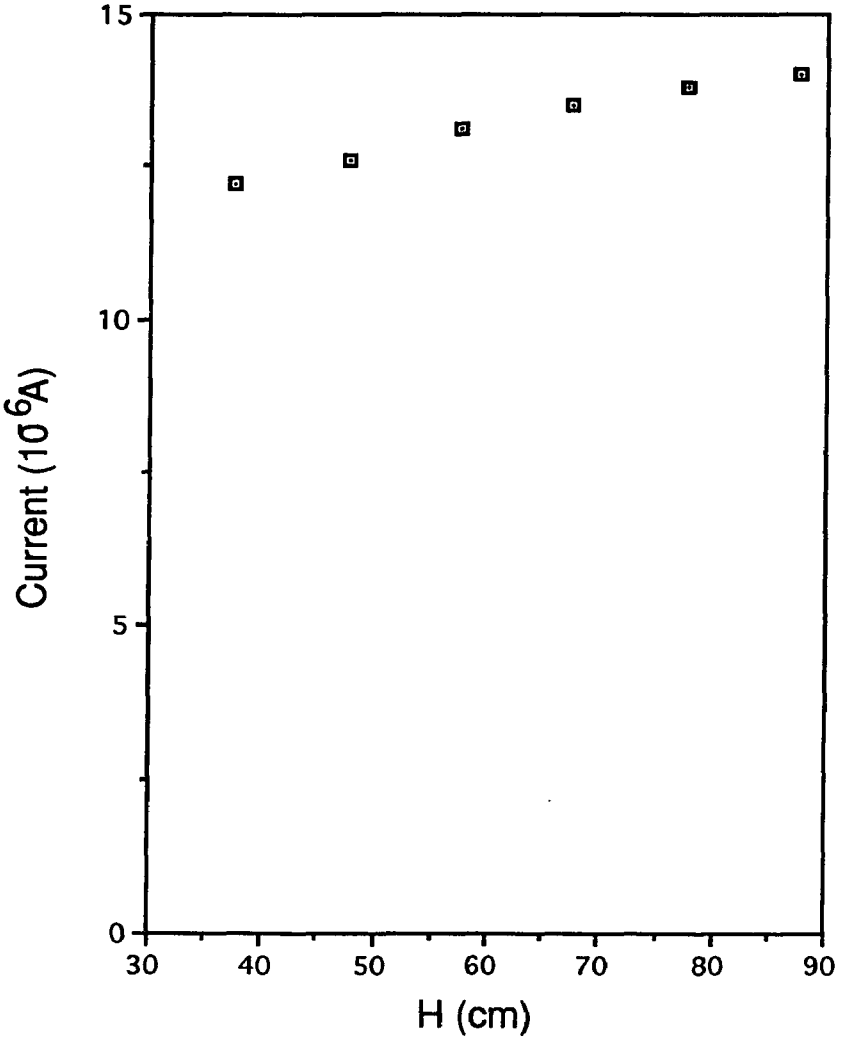

Figure 2.9 The variation of the limiting current with the height of the mercury head for chloroquine in 50% Acetonitrile 50% acetate buffer solution (0.02M, pH=5.0).

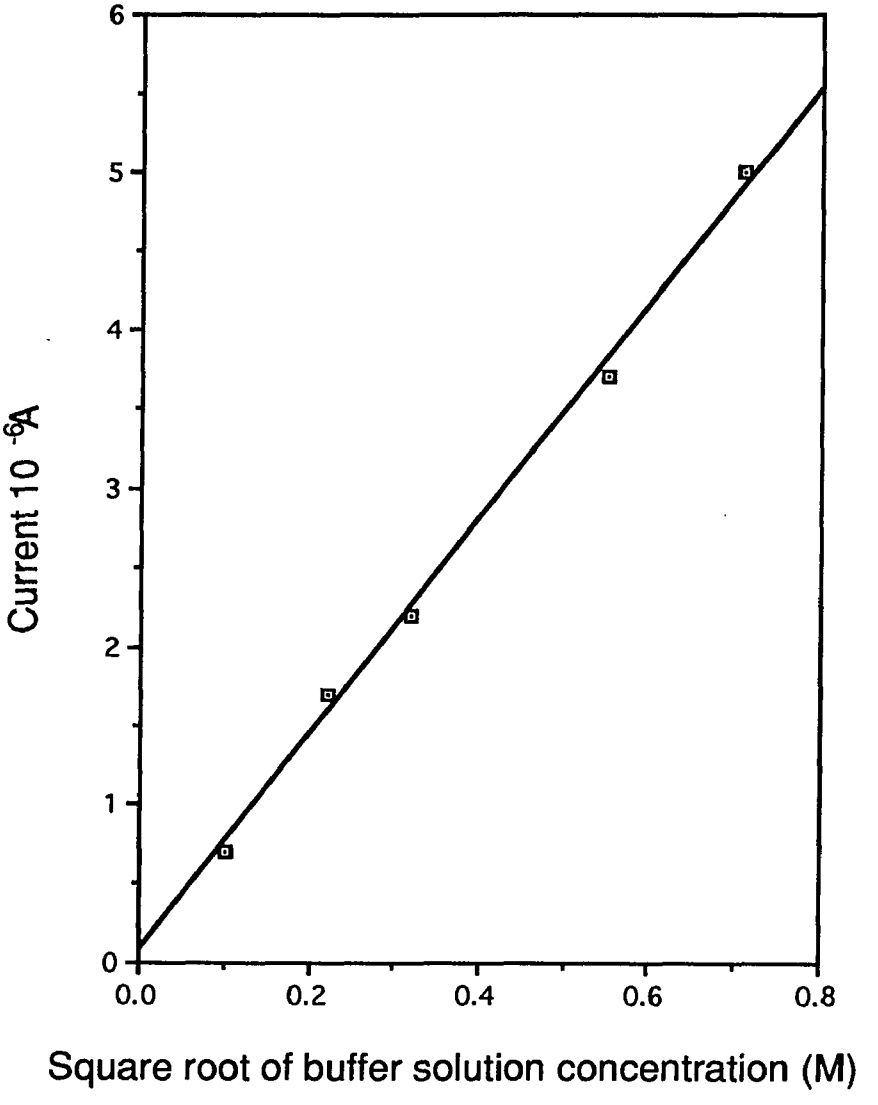

Figure 2.10 The variation of the limiting current of chloroquine with buffer concentrations at constant pH=5.0.

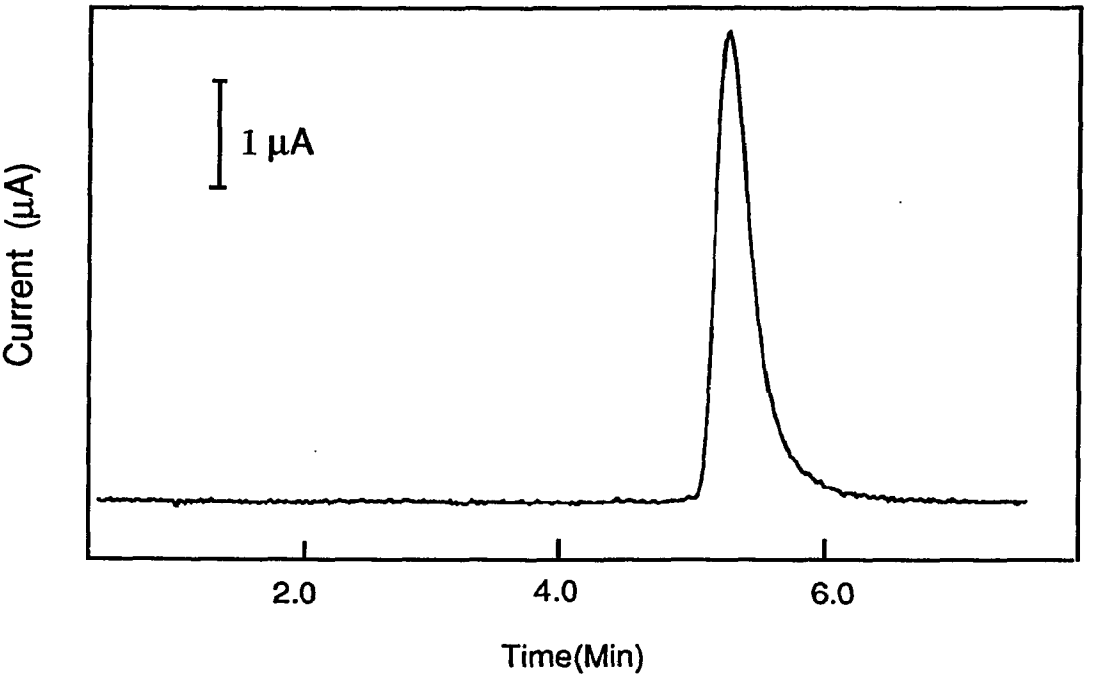

Figure 2.11 Chromatogram of 1.0 µg of Chloroquine in 20µl. Column C-18 ; mobile phase, 50% acetonitrile 50% acetate buffer solution (0.02M, pH=5.0). Flow rate 1.0ml/min. Differential pulse potential (DPP) detection with initial potential of -1400mv and a pulse amplitude of -200mv. Static mercury drop electrode: t_{air}=300ms, t_1=650ms and t_2=50ms. Mercury electrode is renewed by knocking at the end of t_2.

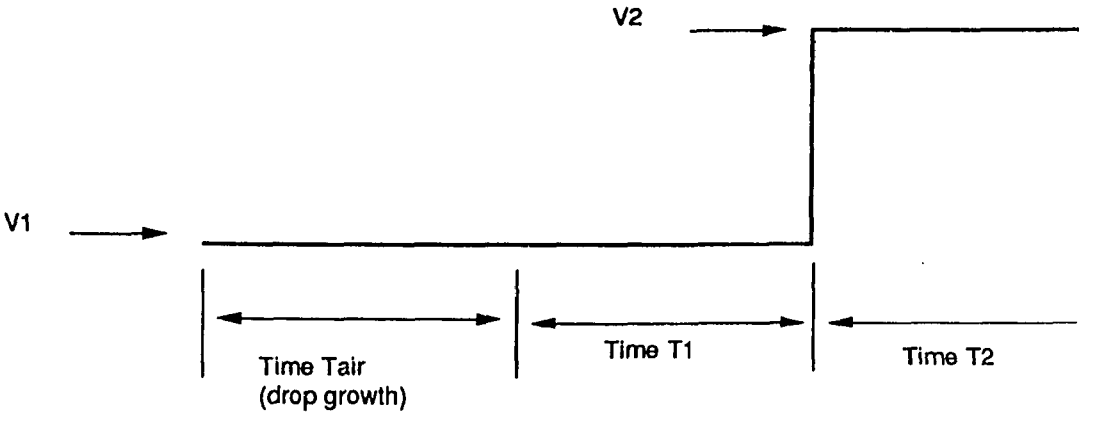

$$T_{total} = T_{tair} + T_1 + T_2$$

Figure 2.12 Differential pulse potential waveform for the detection. Mercury drop growth during the t_{air} under constant pressure and kept constant at t_1. Potential is stepped from V_1 to V_2 during t_2. The current sampling will be at the end of t_1 and t_2. Mercury electrode is renewed by knocking it off at the end of t_2.

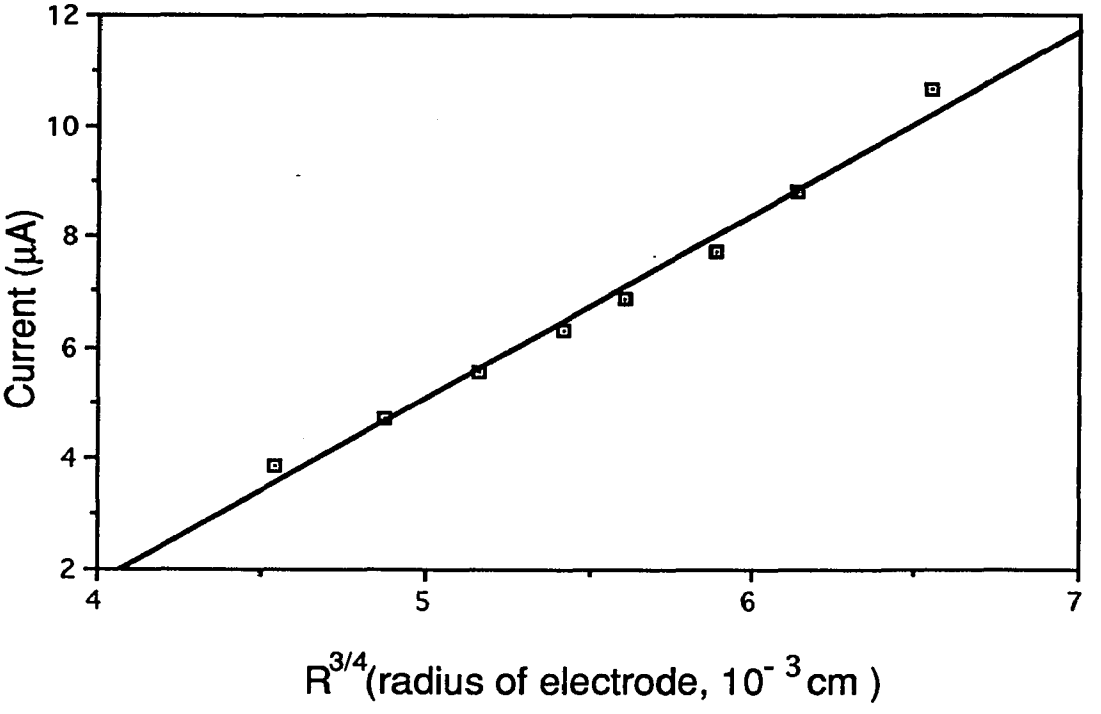

Figure 2.13 Differential current as a function of the size of the electrode. DPP detection with a t_{air} value from 300ms to 1300ms. Other conditions: Column C-18 ; Mobile phase: 50% acetonitrile 50% acetate buffer solution (0.02M, pH=5.0); Flow rate 1.0ml/min; Static mercury drop electrode: t_1=650ms, t_2=50ms.

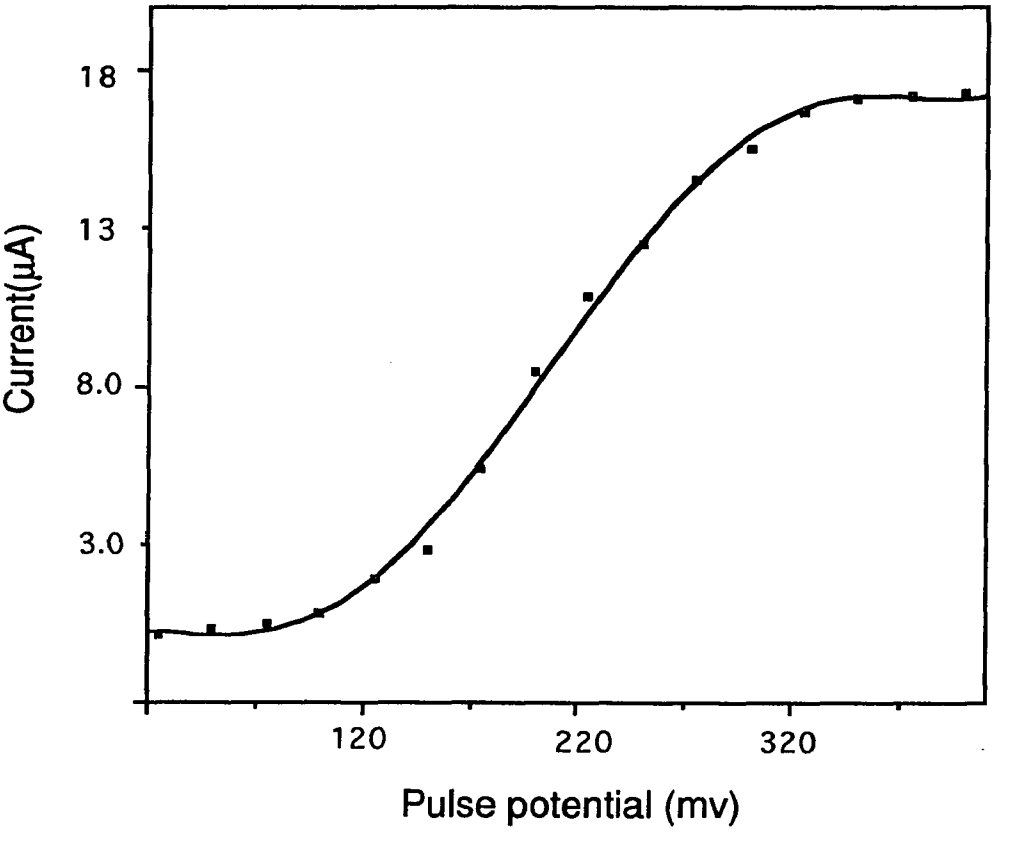

Figure 2.14 Differential current as a function of applied pulse potential. Conditions: initial potential -1400mv and pulse amplitude varies from 25 to 400 mv. Column C-18 ; mobile phase, 50% acetonitrile 50% acetate buffer solution (0.02M, pH=5.0). Flow rate 1.0ml/min. Static mercury drop electrode, t_{air}=300ms, t_1=650ms and t_2=50ms. Mercury electrode is renewed by knocking at the end of t_2.

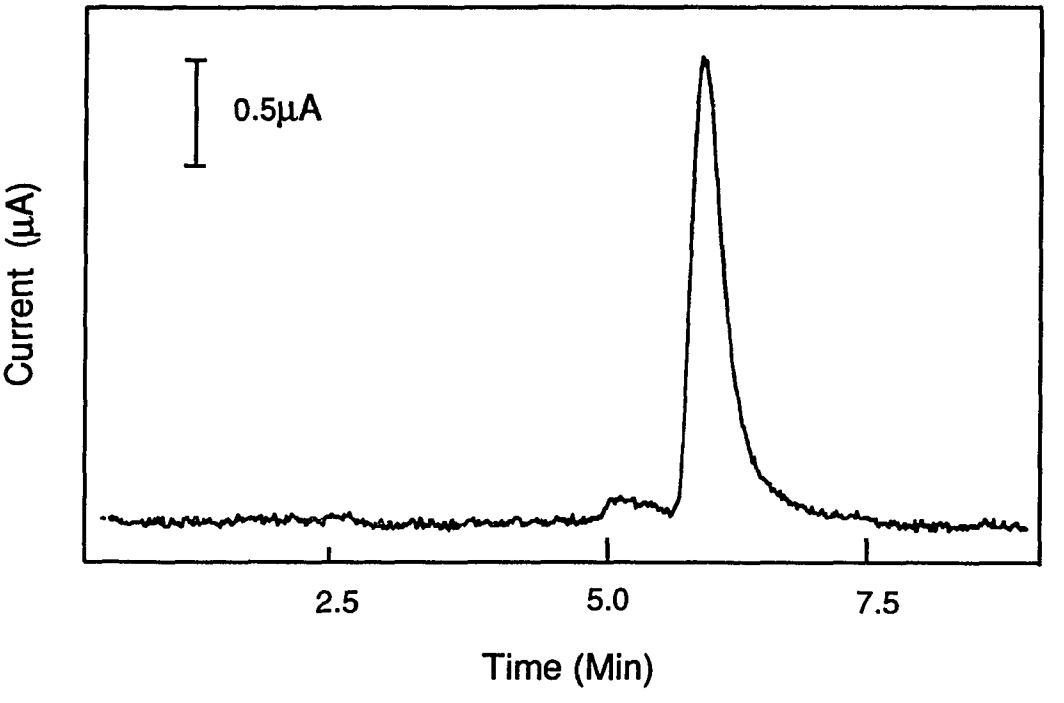

Figure 2.15 Chromatogram of 0.5 µg of Chloroquine and trace oxygen in sample solution(injected solution was not sparged by helium).Column C-18 ; Mobile phase: 50% acetonitrile 50% acetate buffer solution (0.02M, pH=5.0). Flow rate 1.0ml/min. Differential pulse potential detection with a initial potential of -1400mv and a pulse amplitude of -200mv. Static mercury as working electrode, t_{air}=300ms, t_1=650ms and t_2=50ms. Mercury electrode is renewed by knocking at the end of t_2.

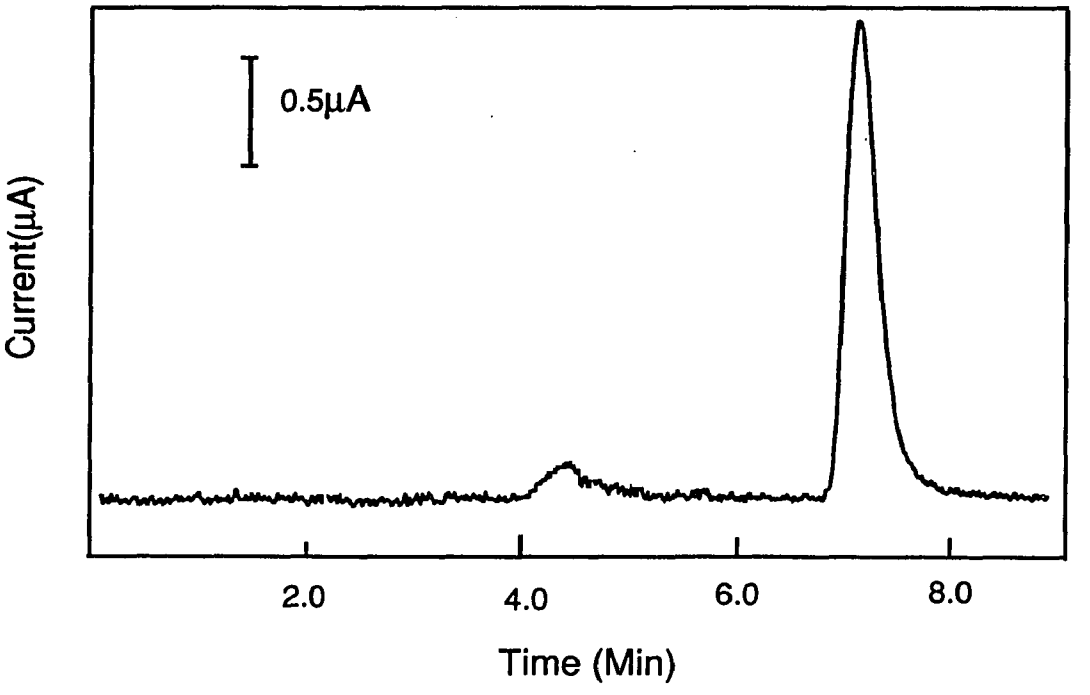

Figure 2.16 Chromatogram of 0.5 μg of Chloroquine and trace oxygen in sample solution(injected solution was not sparged by helium). Column C-18 ; Mobile phase: 65%acetonitrile 50% acetate buffer solution (0.02M, pH=5.0). Flow rate 1.0ml/min. Differential pulse potential detection with initial potential of -1400mv and a pulse amplitude of -200mv. Static mercury drop electrode: t_{air}=300ms, t_1=650ms and t_2=50ms. Mercury electrode is renewed by knocking at the end of t_2.

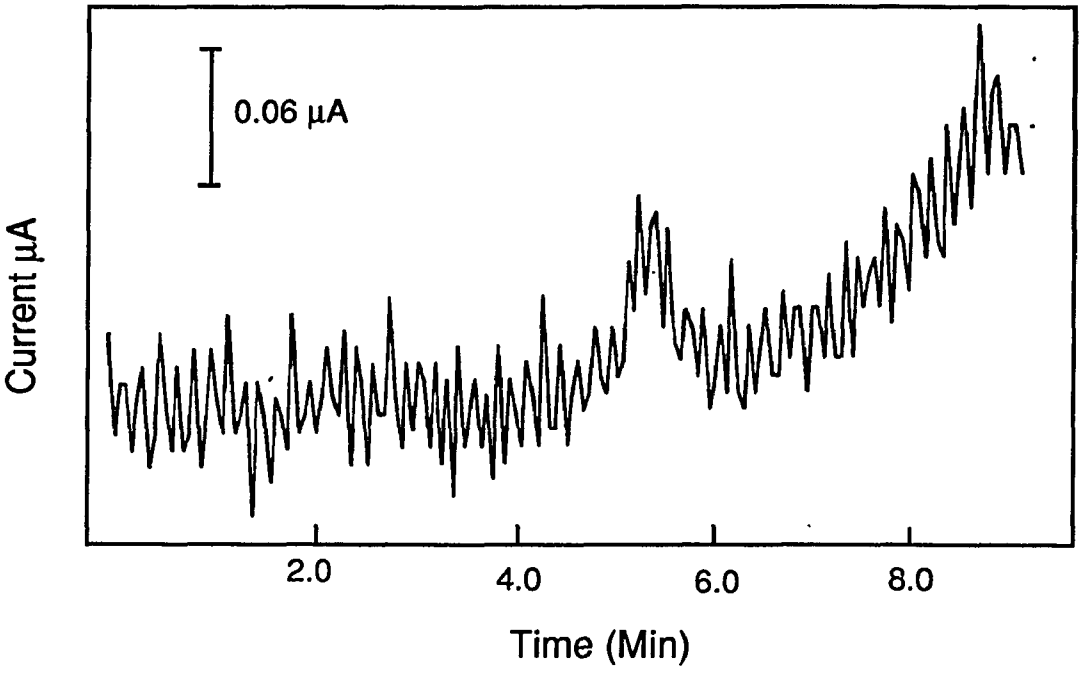

Figure 2.17 Chromatogram of 2.0 ng of chloroquine. Column C-18 ; mobile phase, 50% acetonitrile 50% acetate buffer solution (0.02M, pH=5.0). Flow rate 1.0ml/min. Differential pulse potential detection with a initial potential of -1400mv and a pulse amplitude of -200mv. Static mercury as working electrode, t_{air}=300ms, t_1=650ms and t_2=50ms. Mercury electrode is renewed by knocking at the end of t_2.

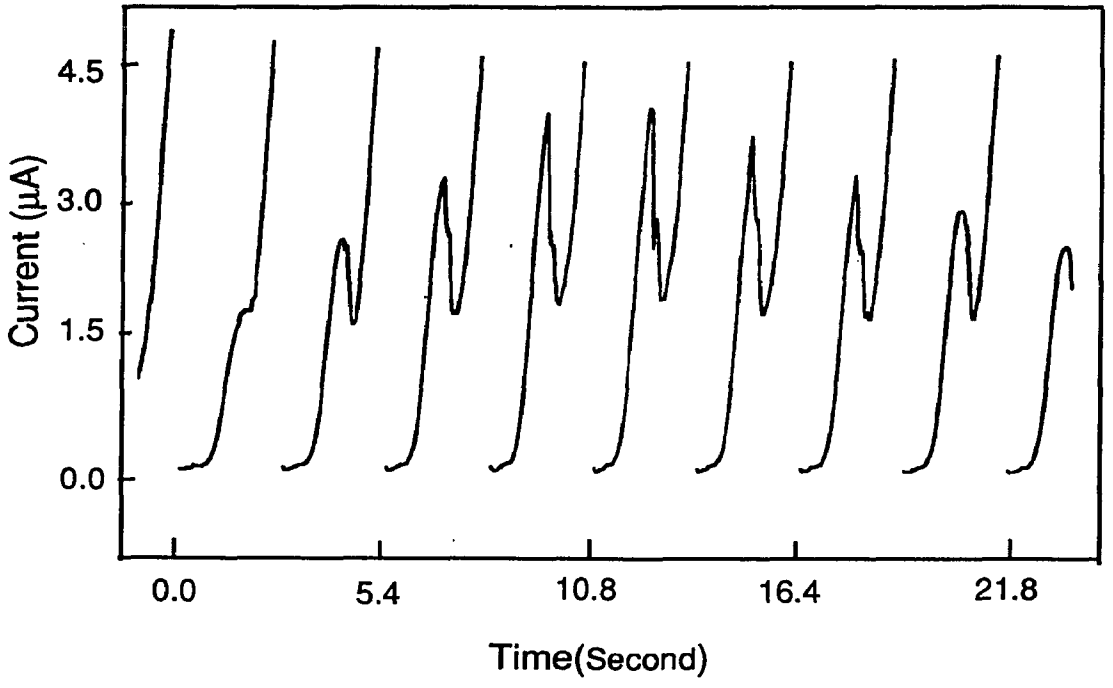

Figure 2.18 Square wave chromatovoltammogram of 1.0 µg chloroquine. Potential scan every 2.7 second from -1300 mv to -1900 with a step height of 5.0 mv and squarewave amplitude of 25 mv. Column C-18 ; Mobile phase, 50% acetonitrile 50% acetate buffer solution (0.02M, pH=5.0). Flow rate 1.0ml/min.

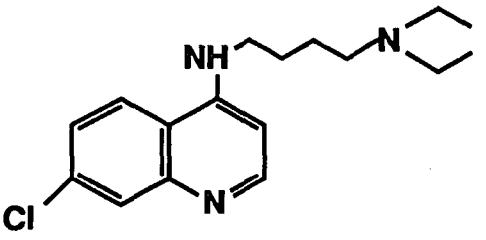

CHLOROQUINE

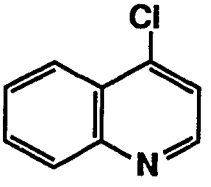

4-CHLOROQUINOLINE

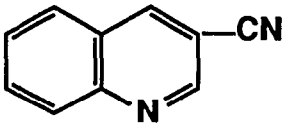

3-QUINOLINECARBONITRILE

Figure 2.19 Structure of three compounds

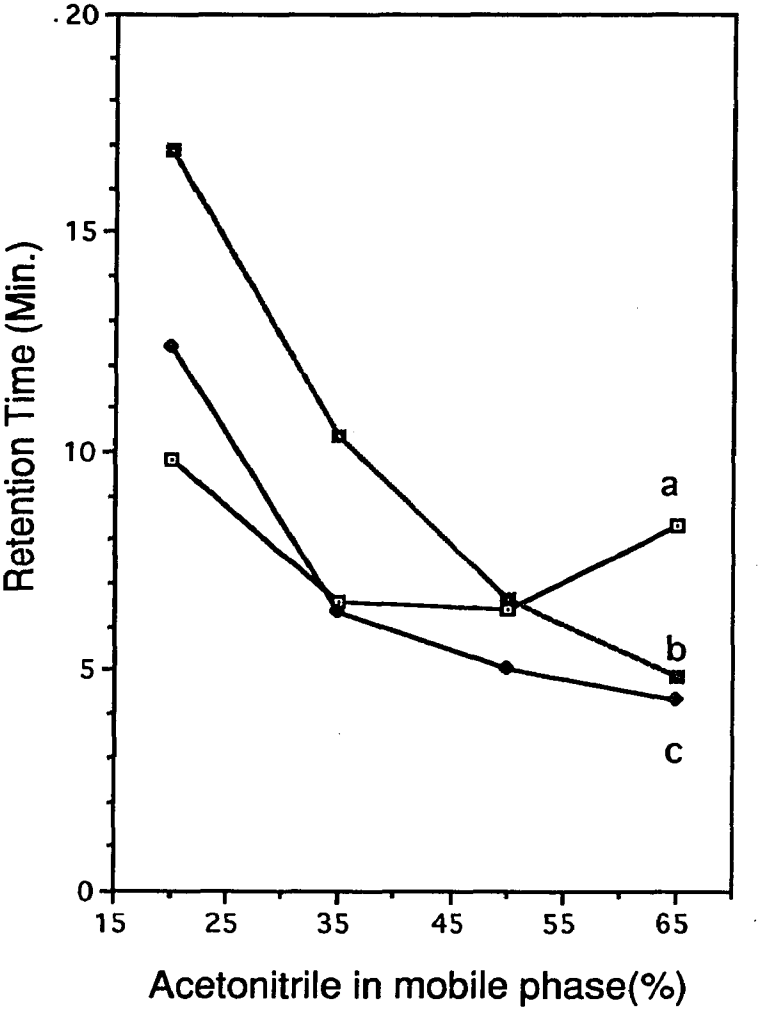

Figure 2.20 Relationship of retention times of three compounds with polarity of mobile phase. (a) chloroquine; (b) 4-chloroquinoline;(c)3-quinolinecarbonitrile.

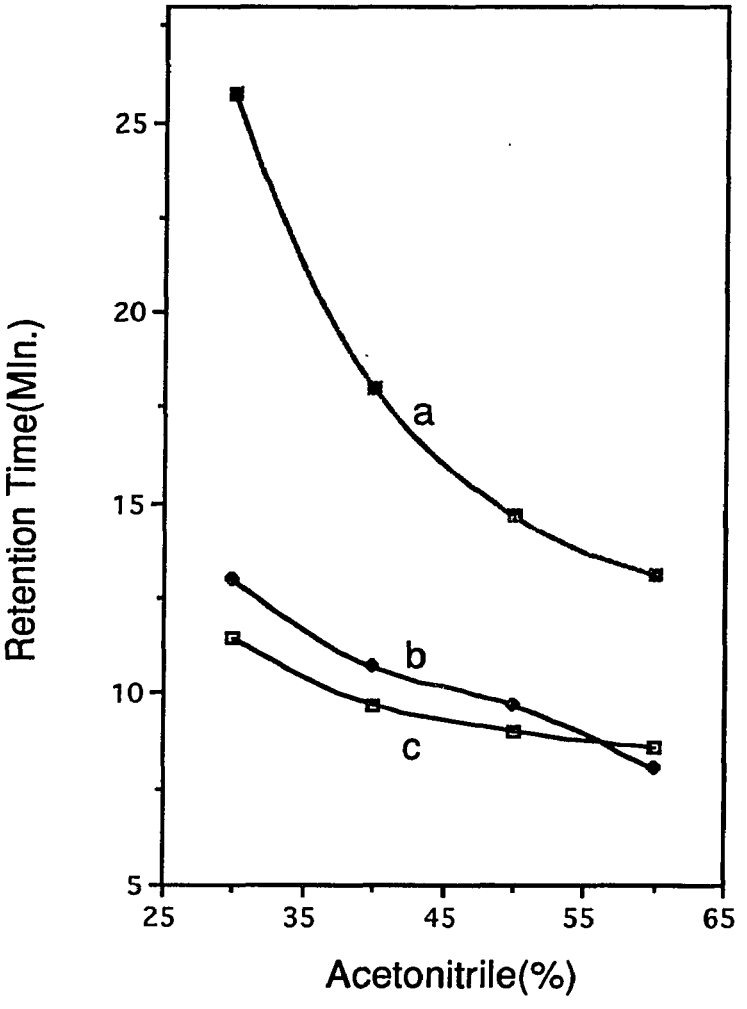

Figure 2.21 Retention time as solvent B changes from 30% ramp to 60% during gradient elution program with solvent A constant. (a) 4-chloroquinoline, (b)3-quinolinecarbonitrile and (c) chloroquine.

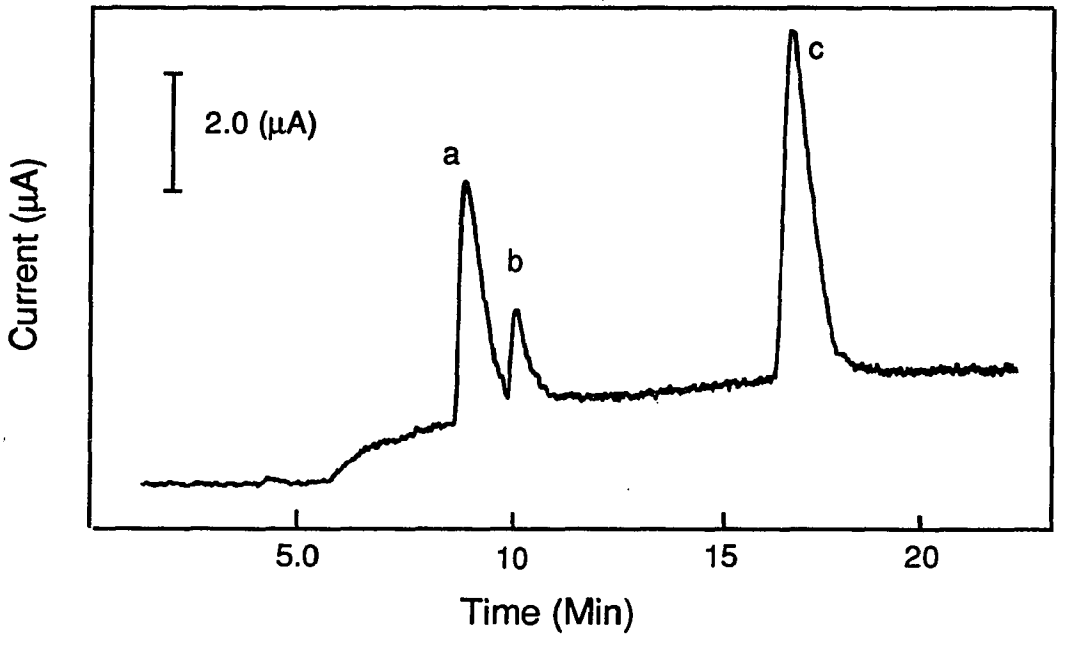

Figure 2.22 Separation of three compounds with gradient elution. Mobile phase:Solvent A, 10% Acetonitrile ; Solvent B, 65% Acetonitrile. Program:0-10 min. Inject 20 μl; (a)$5.0*10^{-5}$ M chloroquine; (b)$3.0*10^{-3}$ M 3-quinolinecarbonitrile and (c) $6.0*10^{-5}$ M 4-chloroquinoline. Other conditions: Column C-18; Flow rate 1.0ml/min. Differential pulse potential detection with a initial potential of -1400mv and a pulse amplitude of -200mv. Static mercury drop electrode: t_{air}=300ms, t_1=650ms and t_2=50ms. Mercury electrode is renewed by knocking at the end of t_2.

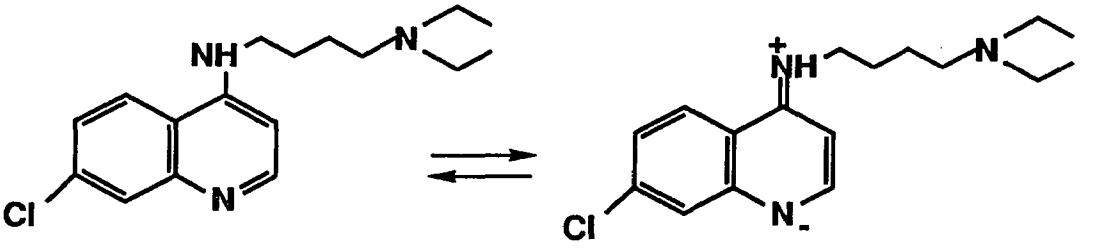

CHLOROQINE

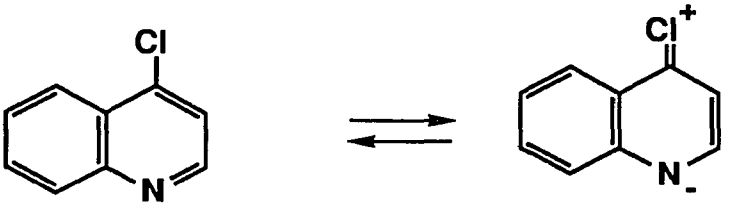

4-CHLOROQUINOLINE

Figure 2.23 Resonance structures of Chloroquine and 4-chloroquinoline.

Part III

Determination of Copper, Nickel, and Cobalt in Rock Samples by HPLC with Thin Layer Cell Electrochmical Detector

3.1 Introduction

The most common methods for determining metal ions are atomic absorption spectrometry (AAS) [1] and various colorimetric methods [2]. Techniques involving AAS have often including extraction of the metal's complexes [3-6] as a preliminary step in the analysis. All of the methods based on AAS or colorimetry have been designed to be selective, and are thus time consuming if more than one element is to be determined. The determination of metal ions through polarographic voltammetry, and other electrochemical techniques is extremely sensitive [7,8]. However, many determinations are subject to interference by overlapping waves[7-10]. The determination of metal ions by various chromatographic methods have become increasing popular owing to the speed, simplicity and low cost of such methods. An attractive approach is to add an appropriate complexing reagent to the sample and separate the metal complexes by liquid chromatography. For example, dithiocarbamate compounds have been known since the last century and form an extensive area of complexation in analytical chemistry [11,12]. Their ability to form stable chelates with a number of metal ions makes them ideal for this application. Separations have been reported by use of both normal phase [13-19] and reversed phase

[20-23] HPLC. Applications have included the analysis of electroplating solution [24], the automated analysis of wastewater [25-27], the determination of trace metals in rice flour and citrus leaves [28], and the determination of low levels of precious metals [30].

The literature, especially from Bond and co-workers, illustrates that in situ dithiocarbamate complexations, combined with liquid chromatography using electrochemical detection, can be used to develop a system capable of determining metal or organometallic species [25-28]. The success of the electrochemical detection method, depends upon the availability of a well-defined metal-complex oxidation process. The problem associated with removal of oxygen, important in reduction processes is less bothersome for oxidation processes. In addition, the electrochemical detection method is known to be more selective than the spectrophotometric one [31,32]. In the present work, the determination of metal ions of copper, nickel and cobalt as dithiocarbamate complexs by reversed phase HPLC with electrochemical detection has been applied to rock samples. A amperometric detection using a thin-layer cell and glassy carbon electrode serves to monitor the separation. Since only around a 25 μl sample is injected into the column for simultaneous multielement determination, this technique provides an additional advantage for trace metal analysis when only small amounts of sample are available.

3.2. Experimental Section

3.2.1 Reagents and Standard Solutions

All chemicals used were of analytical grade purity. All organic solvents were liquid chromatography grade from Fisher Scientific. Metal stock solutions were prepared by dissolving appropriate metal salts in distilled, deionized water. The chromatographic solvent employed was a mixture of water and acetonitrile containing 0.02M sodium acetate and was titrated to a pH of 6.0 using glacial acetic acid. Then 0.005M sodium nitrate was added to the solvent to provide adequate conductivity for electrochemical detection. The pH value of the buffer ensured no interference from the reduction of hydrogen ion and conformed to the pH restrictions applicable to the reversed phase column employed in this work. Pure water was obtained by passing tap water through a carbon filter and a multiple - ion exchange system, and then distilling.

3.2.2 Instrumentation

A Tacussel PRG-5 polarographic instrument was used for measurements in the thin layer electrochemical flow cell. A glassy carbon electrode was employed as working electrode. The electrode was cleaned at least once a day using alumina polishing powder (0.03μm) obtained from Buehler Ltd. The auxiliary electrodes were either platinum or glassy carbon and the reference electrode was Ag/AgCl (3M KCl). A Bioanalytical Systems (BAS) thin-layer flow cell was used in all LCEC work. The column was a C-18 reversed phase column from either Waters Associates or Supeleco. A Houston model 200 X-Y recorder was used for determining the peak current and retention time. After each working period, the pump and columns were flushed with acetonitrile.

Atomic absorption measurements were performed with an air acetylene flame on a Perkin Elmer model 4000 atomic absorption spectrometer.

3.2.3 Experimental procedure

The mobile phases were continually degassed with argon or helium. Samples of about 25 µl were injected into a 20 µl sample loop, with the overflow discarded. The Tacussel PRG-5 polarographic instrument and the HPLC were synchronized manually. This was accomplish by turning the knob on the BAS HPLC from "load" to "inject" while the instrument is switched to the "external cell" after all polarographic parameters have been selected and the sample has been injected with a syringe into the loop. The HPLC was run for at least 30 minute before work each day . The flow rate of the eluent from the HPLC column was determined by measuring the volume of mobile phase output for a given time.

3.3 Results and Discussion

3.3.1 Chromatographic behavior of diethyldithiocarbamate complexs

Literature reports indicate that metal dithiocarbamate complexes are electroactive at various working electrodes [33-35]. Both processes of oxidation and reduction would appear to be available for direct electrochemical detection in a nonaqeous solvent. The responses for diethyldithiocarbamate complexes of copper, nickel, and cobalt were first examined in this experiment. A small, well defined wave for oxygen was

always observed using DC detection at - 0.9V with glassy carbon electrodes despite extensive endeavors to eliminate oxygen from the mobile phase and injected solution. However, satisfactorily response was obtained when using the oxidation process and DC polarographic technique. Figure 3.1 shows the chromatogram of copper, nickel, and cobalt diethyldithiocarbamate complexes. The eluent baseline is smooth since the contribution of trace oxygen and trace impurities found in mobile phase have been minimized. The first two peaks observed correspond to oxidation of the ligand which results from decomposition of complex. These elute before the peaks for the three metal complexes and do not interfere in the determination. Since the measurement is an electrochemical current in response to a fixed electrode potential, the choice of applied potential is critical. In practice, the potential limits depend on an acceptable background current and the sensitivity required. For simultaneous determination of copper, nickel, and cobalt, an applied potential which is less positive than 0.7 V will result in a decrease in sensitivity for determination of copper and nickel and no response for cobalt. However, monitoring the current at potentials more positive than 1.00V is not effective since such potentials are sufficient to cause the second oxidation step of the free ligand [36]. Therefore, the potential was selected as 1.0 V in these experiments.

3.3.2 Complex formation

All three metal ions react very rapidly with diethyldithiocarbamate to form the corresponding complexes. However, an excess of ligand was required for fast, complete complex formation. Figure 3.2 shows the

variation of DC peak current with the concentration of diethyldithiocarbamate when the concentration of metal ion is constant. The peak currents were not increased after the concentration ratio of ligand and metal ion was 6.8:1. At least a 10-fold excess of ligand was used in all the experiments. Peak current measurements were repeated over a period of 24 hours and showed the complex to be stable over this period.

3.3.3 Peak current and flow rate

Figure 3.3 shows the variation of DC peak current with flow rate for the glassy carbon electrode in a thin-layer cell. An increase in flow rate leads to an increase in sensitivity because of increased convection. To achieve good separation with acceptable retention times for the simultaneous determination of the three metal ions, flow rates in the range of 1.0 - 2.0 ml/min were found to be suitable.

3.3.4 Reproducibility

The reproducibility in peak current measurement for the three complexes is shown in Table 3.1. This was determined by making 7 repeat injections each of 20 μl solutions of the complexes containing 40 ng of copper and cobalt and 120 ng of nickel. The reproducibility can be considered in terms of the coefficient of variation and the mean value. Typical values of test metal were 1.5% for 120 ng nickel and 3.0% for 40 ng copper and cobalt, respectively.

3.3.5 Calibration and detection limits

The Figures 3.4 - 3.6 show the calibration plots prepared from the chromatographic data obtained after reaction of known amounts of a mixture of the three metal ions with the ligand. All plots show good linearity for nanogram amounts of the metals injected into the column. Table 3.2 shows the linearity range and detection limits. In general, lower detection limits were observed for all the three complexes in the thin layer cell. However, it was also noted that smaller linear ranges of the plot of peak height vs. concentration were obtained in comparison with a large cell. These indicate higher ohmic IR drop in the Bioanalytical Systems cell. This is probably caused in part by the fact that the reference electrode is not situated as close to the working electrode as in the usual electrochemical cell.

3.3.6 Determination of Cu, Co, and Ni in rock samples

3.3.6.1 Tests for interferences

The effects of possible interfering ions were studied by adding varying amounts of selected foreign ions to samples of metal ions to be determined. A foreign ion was considered to interfere when the peak height of a metal complex was changed by more than 5.0 %. Zn, Cr, Mn, Pb, Hg, Mg, Fe, K cations were added as their nitrate salt; NO_3^-, Cl^-, Br^-, SO_4^-, PO_4^- anions were added in the form of the sodium salt. All foreign ions were added

separately in a 10 -fold weight excess. None of these compounds altered the current response for the Cu, Co, and Ni complexes. These data suggest that this is a relatively interference-free method for the determination of copper, nickel, and cobalt using the electrochemical detector system.

3.3.6.2 Procedure to dissolve rock sample

Weigh accurately about 0.050g rock sample into 20 ml beaker add 10 ml HNO_3 and HCl (1:1). Cover the beaker with watch glass and keep the solution just below the boiling point on a hot plate until the sample dissolves. This may require 60 to 90 min. Remove the watch glass and add 10 ml water. Then evaporate the solution until all of the residual acid is removed. This may be repeated several times. Transfer the solution to a 25 ml volumetric flask and rinse with 70% acetonitrile (pH=6.0 buffer solution) and dilute to mark.

Figure 3.7 shows the presence, mainly, of nickel and copper in the rock sample. This is a pyroxene sample. Relative large amounts of metals such as Si(52%), Ca(15%), Mg(17%) and Fe(10%) and other common metal Al(1%), Na(1%) exist in this sample but do not interfere with the determination of Cu, Co, or Ni. The analytical results, summarized in Table 3.3, are in good agreement with the values from atomic absorption spectroscopy and indicate the potential of the method. For determination of trace metals, AAS would generally be the preferred technique except when only small volumes of sample are available. However, for extensive multielement determination on very small grains of rock where sample

volume must be kept small, LCEC could provide a distinct advantage for trace metal determination.

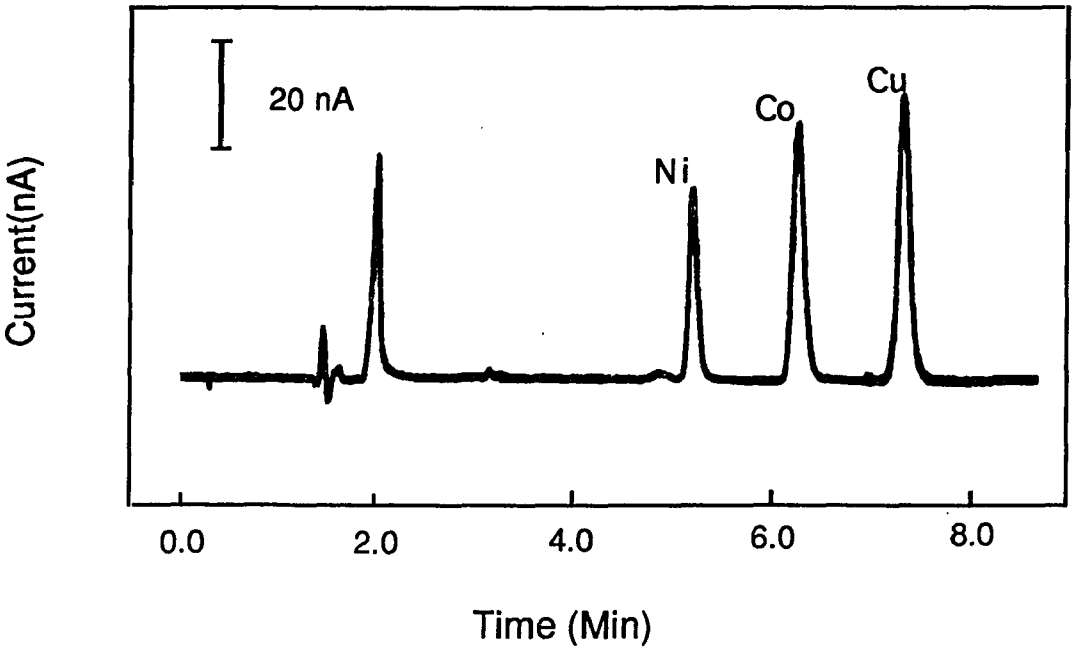

Figure 3.1 Multielement Chromatogram using HPLCEC: running solvent, 70%acetonitrile 30% acetate buffer solution(0.02 M, pH=6.0) containing 10^{-4}M $(dedtc)^-$ and 0.005 M sodium nitrate; flow rate=1.5 ml/min; detector cell, BAS, glassy carbon working electrode; dc response monitored at 1.0 V vs.Ag/AgCl; Injection 20 µl of complex containing 10ng of nickel, 20 ng of cobalt and 10ng copper.

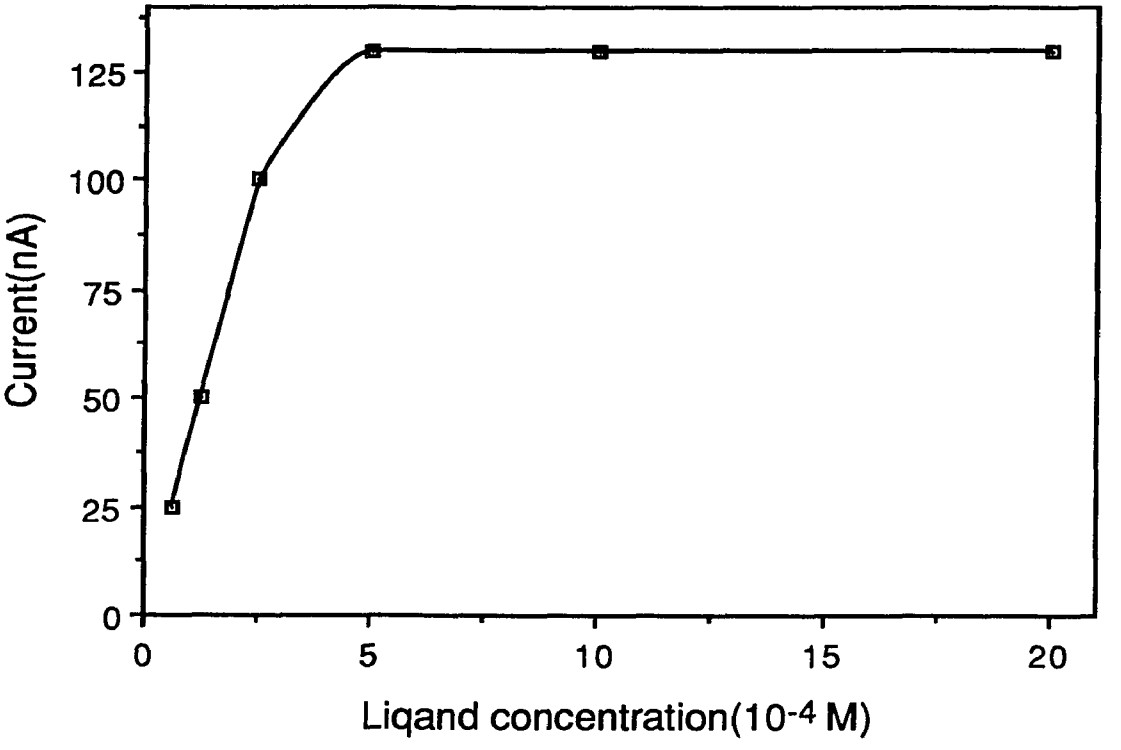

Figure 3.2 Variation of peak current with concentration of diethylcarbamate: running solvent,70%acetonitrile 30% acetate buffer solution(0.02 M, pH=6.0); flow rate=1.5 ml/min;dc response monitored at 1.0 V vs.Ag/AgCl; Injection 20 µl of complex containing 100ng copper.

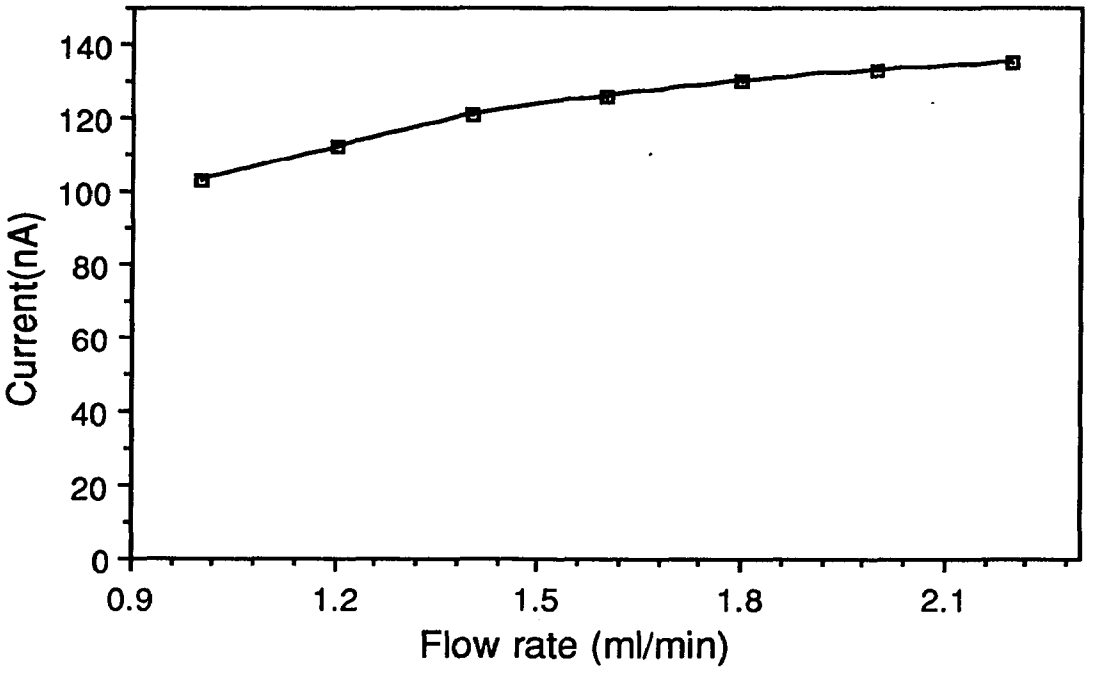

Figure 3.3 Variation of Peak current with flow rate: running solvent, 70% acetonitrile 30% acetate buffer solution (0.02 M, pH=6.0) containing 10^{-4}M $(dedtc)^-$ and 0.005 M sodium nitrate; dc response monitored at 1.0 V vs.Ag/AgCl; Injection 20 µl of complex containing 60 ng copper.

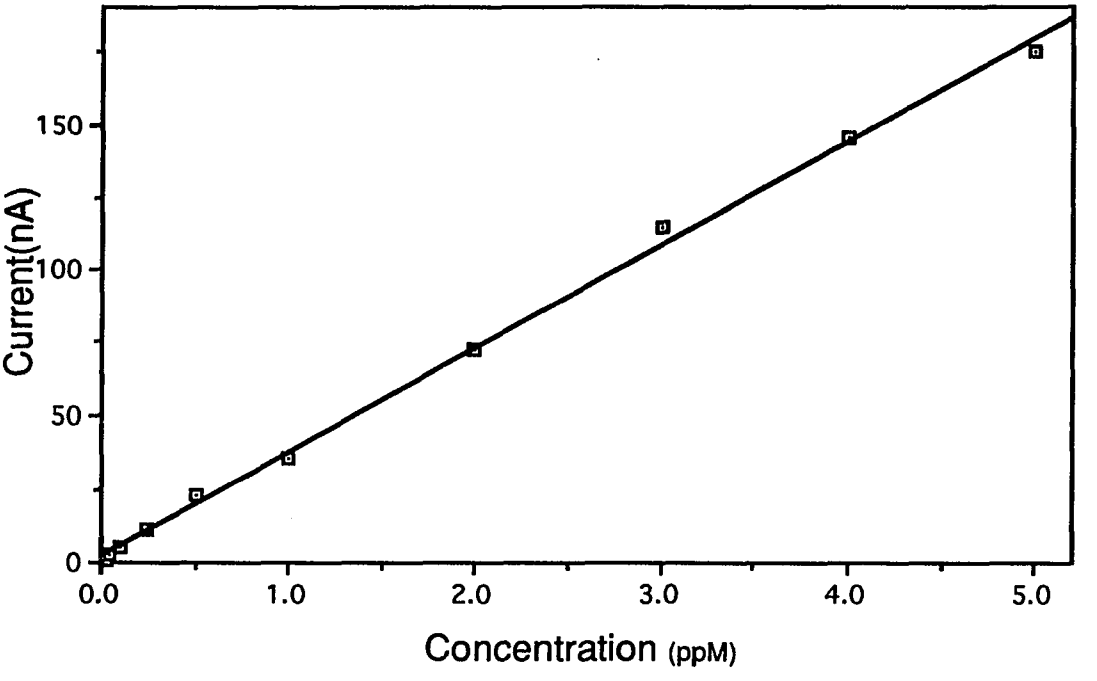

Figure 3.4 Calibration plot for nickel diethyldithiocarbamate determinated by HPLCEC: running solvent, 70% acetonitrile 30% acetate buffer solution (0.02 M, pH=6.0) containing 10^{-4}M $(dedtc)^-$ and 0.005 M sodium nitrate; flow rate=1.5 ml/min; detector cell, BAS, glassy carbon working electrode; dc response monitored at 1.0 V vs.Ag/AgCl; each Injection 20 µl of nickel diethyldithiocarbamate solution.

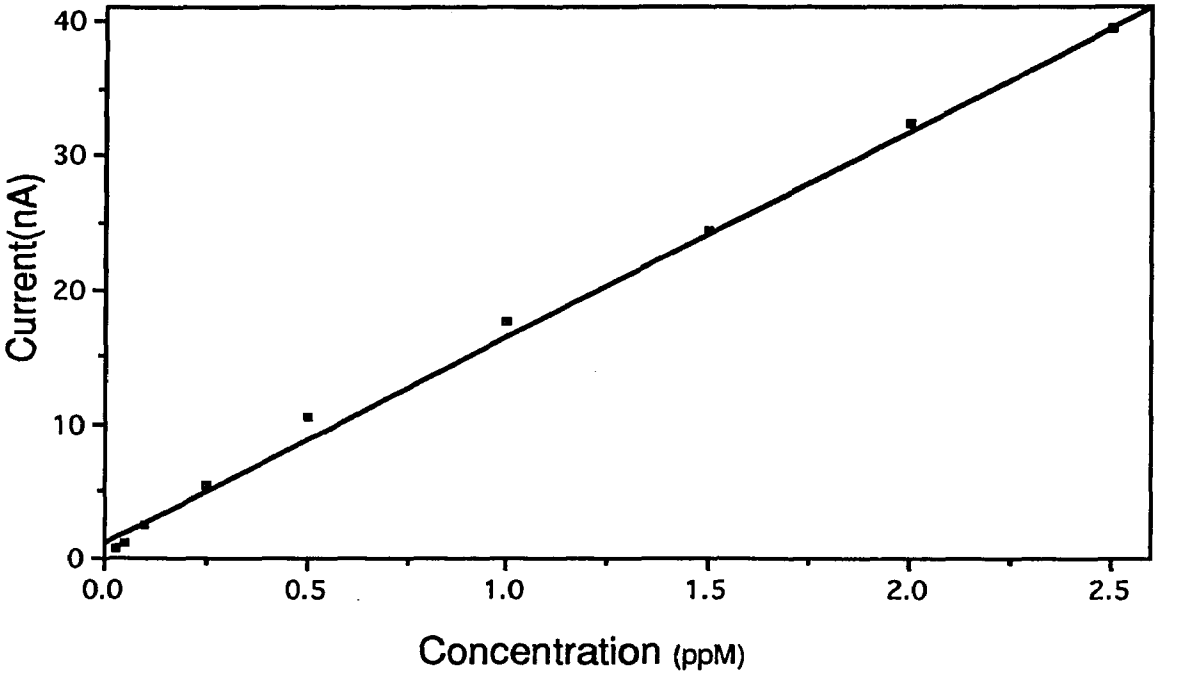

Figure 3.5 Calibration plot for cobalt diethyldithiocarbamate determinated by HPLCEC: running solvent, 70% acetonitrile 30% acetate buffer solution (0.02 M, pH=6.0) containing 10^{-4}M $(dedtc)^-$ and 0.005 M sodium nitrate; flow rate=1.5 ml/min; detector cell, BAS, glassy carbon working electrode; dc response monitored at 1.0 V vs.Ag/AgCl; each Injection 20 µl of cobalt diethyldithiocarbamate solution.

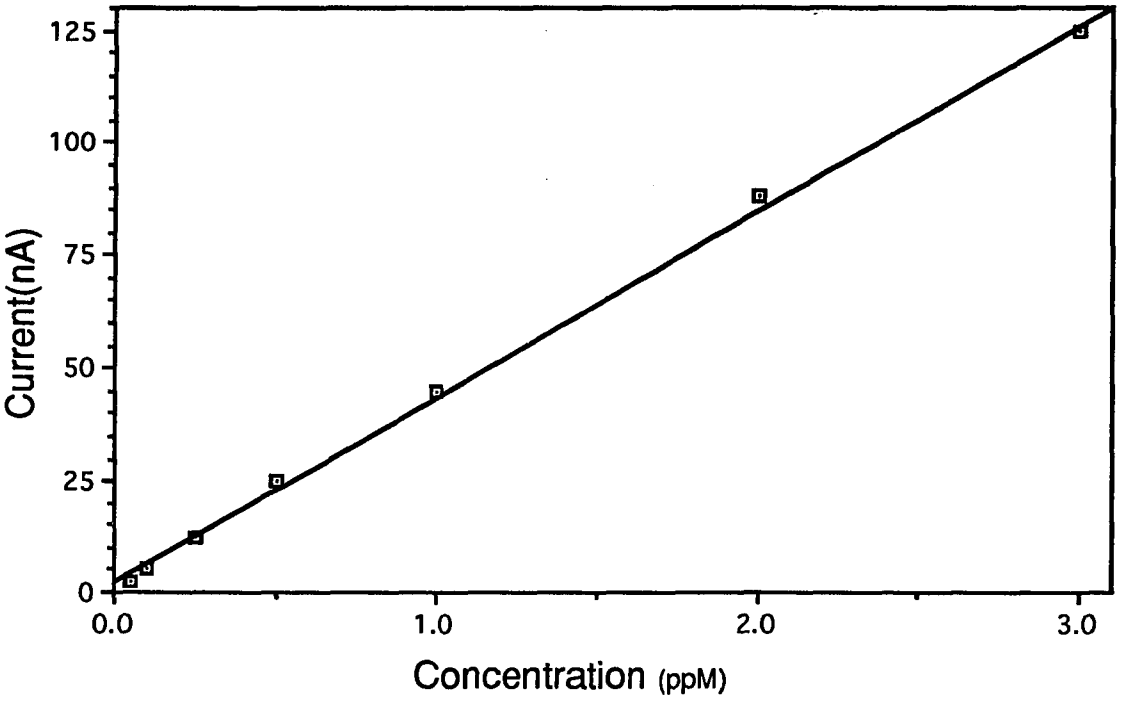

Figure 3.6 Calibration plot for copper diethyldithiocarbamate determinated by HPLCEC: running solvent, 70% acetonitrile 30% acetate buffer solution (0.02 M, pH=6.0) containing 10^{-4}M $(dedtc)^-$ and 0.005 M sodium nitrate; flow rate=1.5 ml/min; detector cell, BAS, glassy carbon working electrode; dc response monitored at 1.0 V vs.Ag/AgCl; each Injection 20 μl of copper diethyldithiocarbamate solution.

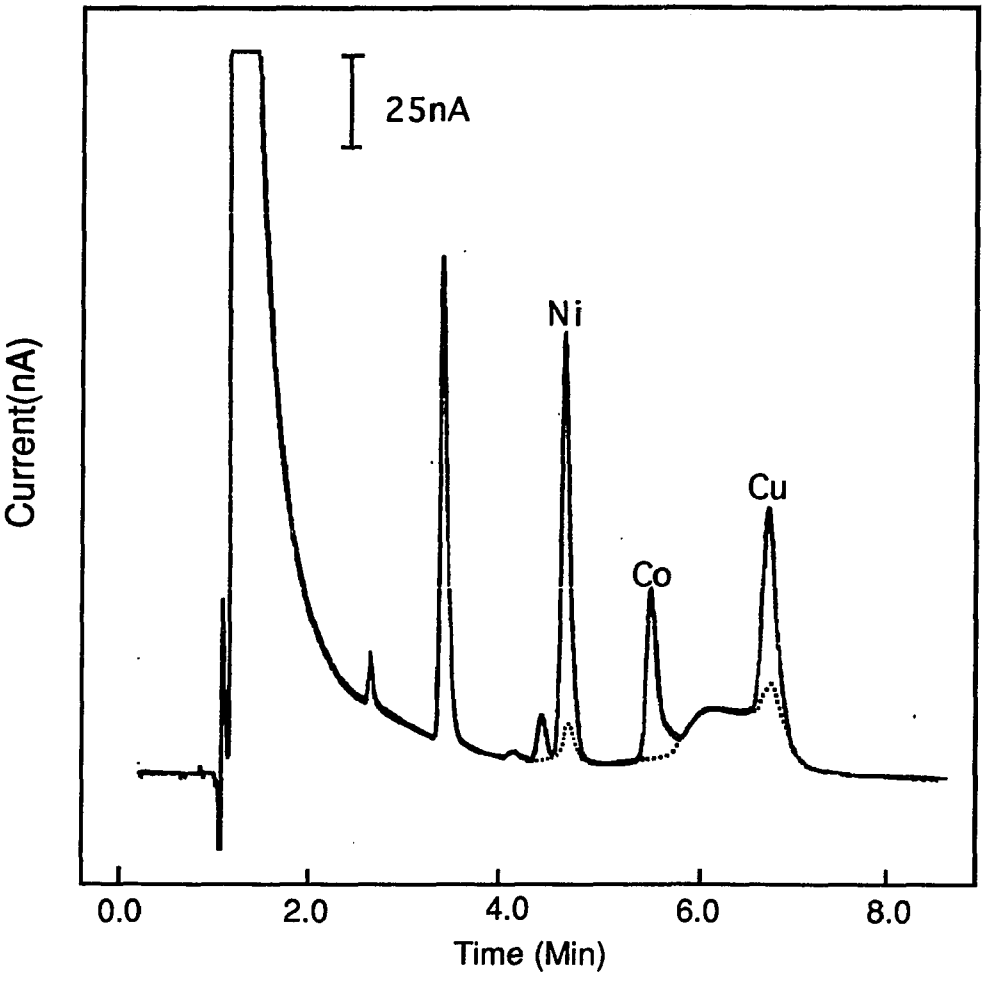

Figure 3.7 Determination of Cu, Co, and Ni in rock sample: running solvent, 70%acetonitrile 30% buffer solution 10 $^{-3}$M $(dedtc)^-$; flow rate=1.5 ml/min; glassy carbon woring electrode; dc response monitored at 1.0 V vs.Ag/AgCl; Injection 20 µl slution: (-----) rock sample; (——) added standard solution to rock sample.

Table 3.1

Data showing the precision of peak current measurements for metal diethyldithiocarbamates

Metal ion	Peak current (nA)				Mean (nA)	Standard deviation
Nickel	201 208	206 207	210 210	205	206.7	3.15
Copper	72 72	70 70	72 72	74	72.8	1.80
Cobalt	40 38	38 38	40 40	40	38.7	1.25

Injection volume = 20 µl; Solvent flow rate=1.5 ml/Min; solvent system 70%:30% acetonitrile: acetate buffer(0.02M) pH=6.0 containing 10^{-4}M $(dedtc)^-$ and 0.005 M sodium nitrate; the DC response was monitored at 1.00 V vs. Ag/AgCl.

Table 3.2

Linear calibration range and detection limits of metal ions

Metal ions	Linear range (ng)	Detection limit (ng)*
Copper	0.2 - 60	0.2
Cobalt	0.5 - 50	0.5
Nickel	0.2 -100	0.1

* Detection limits based on the signal to noise ratio of 2.

Table 3.3

Comparison of liquid chromatographic technique (LCEC) and atomic absorption spectrometry (AAS)

Method	Amount of Ni(%)	Amount of Cu(%)
LCEC *	0.020	0.11
AAS **	0.017	0.10

* LCEC: Injection volume = 20 µl; solvent flow rate 1.5 ml/Min;solvent system 70%:30% acetonitrile: acetate buffer(0.02M, pH=-6.0) containing 10^{-4}M $(dedtc)^-$ and 0.005 M sodium nitrate; DC response was monitored at 1.00 V vs Ag/AgCl.

** AAS: air-acetylene flame; slits are 0.7mm; wavelength: 324.8 nm for Cu, 232.0 nm for Ni.

Reference for Part 1

[1] Rolison, D.R.; Fleischmann, M.; Pons,S.; Rolison, D. R.; Schmidt, P. P., Eds "Ultramicroelectrodes"; Datatech Systems Inc: Morganton, N. C., **1987.**

[2] Birke, R. L. *J. Electroanal. Chem.* **1989,** 274, 297.

[3] Myland, J. C.; Oldham, K. B. *J. Electroanal. Chem.* **1990,** 288, 1.

[4] Colyer, C. L.; Oldham, K. B.; Fletcher, S. *J. Electroanal. Chem.* **1990,** 290, 33.

[5] Wehmeyer, K. R.; Wightman, R. M. *Anal.Chem.* **1985,** 57, 1989.

[6] Chen, X.; Zhuang, J.; He, P. *J. Electroanal. Chem.* **1989,** 271, 257.

[7] Colyer, C. L.; Luscombe, D.; Oldham, K. B. *J. Electroanal. Chem.* **1990,** 283, 397.

[8] Stojek, Z.; Osteryoung, J. *Anal. Chem.* **1989,** 61, 1305.

[9] Hirayama,C., Galus, Z., Guminski, C.; Metals in Mercury; Solubility data series; Pergamon Press: London, 1987.

[10] Bard, A. J., Faulkner, L. R."Electrochemical Methods"; Wiley: New York, 1980.

[11] Bobbert, P. A.; Wind, M. M.; Vlieger, J. *Physica.* **1987,** 58, 141A.

[12] Adams, R. N. "Electrochemistry at Solid Electrodes"; Marcel Dekker: New York, **1969.**

[13] Private discussion with Davis K. Cope, North Dakota State University, **1991.**

[14] Saveant, J. M.; Tesser, D. J. *J. Electroanal. Chem.* **1975,** 65, 57.

[15] Oldham, K. B.; Zoski, C. G. *J. Electroanal. Chem.* **1988,** 256, 11.

[16] Oldham, K. B.; Myland, J. C.; Zoski, C. G.; Bond, A. M. *J. Electroanal. Chem.* **1989,** 270, 79.

[17] Galus, Z.; Golas, J.; Osteryoung, J. *J. Phys. Chem.* **1988,** 92, 1103.

[18] Oldham, K. B.; Zoski, C. G. ; Bond, A. M. *J. Electroanal. Chem.* **1988,** 256, 11.

[19] Weast ,R.; C, Selby,S. M.; Hodgman, C. D. "Handbook of Chemistry and Physics"; Chemical Rubber Co.: Ohio, 1964.

[20] Aoki, K.; Tokuda,K. ; Matsuda,H.; Osteryoung J. *J. Electroanal. Chem.* **1984,** 171, 219.

[21] Gennett , T.; Weaver, M. J. *Anal. Chem.* **1984**, 56, 1444.

[22] Wipf, D. O.; Kristensen, E. W; Deakin, M. R.; Wightman, R. M. *Anal. Chem.* **1988,** 60, 306.

Reference for Part II

[1] Giddings, J. C. "Dynamics of Chromatography " Part I; Marcel Dekker: NewYork, **1965.**

[2] Hamilton, P. B.; Bogue, D. C.; Anderson, R. A. *Anal. Chem.,* **1960,** 32, 1782.

[3] Horvath, C.; Preiss, B.; Lipsky, S. R. *Anal. Chem.*, **1967,** 39, 1422.

[4] Huber, J. F. K.; Hulsman, J. A. R. J. *Anal. Chim. Acta*, **1967**, 38, 305.

[5] Kirkland, J. J. *J. Chromatogr. Sci.* **1969**, 7, 7.

[6] Dolan, J. W. *LC - GC* **1986,** 4, 528.

[7] Spino, L. A.; Han, S. M.; Armstrong, D. W.; Parrott, A. R. *J. Liq. Chromatogr.* **1987**, 10, 1603.

[8] Brooks, H. B.; Thrall, C.; Tehrani, J. J. *Chromatogr.* **1987**, 385, 55.

[9] Conlon, R. D.; Vandemark, F. L.; Dong, M. W.; Schmidt, G. *Am. Lab.* **1987**, 19, 96.

[10] Strasters, J. K.; Billet, H. A. H.; De Galan, L.; Vandeginste, B. G. M.; Karterman, G. *J. Liq. Chromatogr.* **1989**, 12, 3.

[11] Verzele, M.; Steenbeke, G.; Vindevogel, J. *J. Chromatogr.* **1989**, 477, 87.

[12] Wheals, B. B.; White, P. C.; Paterson, M. D. *J. Chromatogr.* **1985**, 350, 205.

[13] Pawliszyn, J. *Anal. Chem.* **1986**, 58, 243.

[14] Pawliszyn, J. *Anal. Chem.* **1986**, 58, 3207.

[15] Pawliszyn, J. *Anal. Chem.* **1988**, 60, 766.

[16] Hancock, D. O; Synovec, R. E. *J. Chromatogr.* **1989**, 464, 83.

[17] Hancock, D. O; Synovec, R. E. *Anal. Chem.* **1988**, 60, 1915.

[18] Renn, C. N.; Synovec, R. E. *J. Chromatogr.* **1991**, 536, 289.

[19] Pfeffer, W. D.; Yeung, E. S. *Anal. Chem.* **1986**, 58, 2103.

[20] Sauda, K.; Imasaka, T.; Ishibashi, N. *Anal. Chim. Acta* **1986**, 187, 353.

[21] Lingerman, H.; Van de Nesse, R. J.; Brinkman, U. A. T.; Gooijer, C.; Velthorst, N. H. *Methodol. Surv. Biochem. Anal.* **1990**, 20, 355.

[22] Van de Nesse, R. J .; Hoornweg, G. P.; Gooijer, C.; Birnkman, U. A. T.; Velthorst, N. H. *Anal. Chim. Acta* **1989**, 227, 173.

[23] Sepaniak, M. J.; Young, E. S. *Anal. Chem.* **1977**, 49, 1554.

[24] Van de Nesse, R. J.; Mank, A. J. G.; Horrnweg, G. P.; Gooijer, C.; Brinkman, U. A. T. *Anal. Chem.* **1991**, 63, 2685.

[25] Van de Nesse, R. J.; Gooijer, C.; Hoornweg, G. P.; Brinkman, U. A. T.; Veltorst, N. H.; Van der Bent, S. J. *Anal. Lett.* **1990**, 23, 1235.

[26] Weinberger, R.; Mannan, C.; Cerchio, M.; Grayeski, M. L. *J. Chromatogr.* **1984**, 288, 445.

[27] De Jong, G. J.; Lammers, N.; Spruit, F. J.; Frei, R. W.; Brinkman, U.A.T. *J. Chromatogr.* **1986**, 353, 249.

[28] Andrew, J. W. ; Grayeski, M. L. *Anal. Chem.* **1987**, 59, 1452.

[29] De Jong, G. J.; Lammers, N.; Spruit, F. J.; Dewaele, C.; Verzele, M. *Anal. Chem.* **1987**, 59, 1458.

[30] Chang, H. C.; Tayor, L. T. *Anal. Chem.* **1991**, 63, 486.

[31] Schreurs, M; Gooijer, C.; Velthorst, N. H. *Anal. Chem.* **1990**, 62, 2051.

[32] Jones, P.; Willams, T.; Ebdon, L. *Anal. Chim. Acta* **1990**, 237, 291.

[33] Arpino, P. J.; Guiochon, G. *Anal. Chem.* **1979**, 51, 682.

[34] Hayes, M. J.; Lankmayer, E. P.; Vouros, P.; Karger, B. L.; McGuire, J. M. *Anal. Chem.* **1983**, 55, 1745.

[35] Yinon, J.; Hwang, D. G. *J. Chromatogr.* **1985**, 339, 127.

[36] Lee, E. D.; Henion, J. D. *J. Chromatogr. Sci.* **1990**, 23, 253.

[37] Covey, T. R.; Lee, E. D.; Brulins, A. P.; Henion, J. D. *Anal. Chem.* **1986**, 58, 1451A.

[38] Koropchak, J. A.; Aryamanya-Mugisha, H. *Anal. Chem.* **1988**, 60, 1838.

[39] Van der Greef, J.; Niessen, W. M. A.; Tjaden, U. R. *J. Chromatogr.* **1989**, 474, 5.

[40] Moseley, M. A.; Deterding, L. J.; De Wit, J. S. M.; Tomer, K. B.; Kennedy, R. T.; Bragg, N.; Jorgenson, J. W. *Anal. Chem.* **1989**, 61, 1577.

[41] Ilkonomou, M. G.; Blades, A. T. ; Kebarle, P. *Anal. Chem.* **1990**, 62, 957.

[42] Kawabata, K.; Kishi, Y.; Kawaguchi, O.; Watanabe, Y.; Inoue, Y. *Anal. Chem.* **1991**, 63, 2137.

[43] Vouros, P.; Lankmayer, E. P.; Hayes, M. J.; Karger, B. L.; McGuire, J. M. *J. Chromatogr.* **1982**, 251, 175.

[44] Siegel, M. M.; Isensee, R. K.; Beck, D. J. *Anal. Chem.* **1987**, 59, 989.

[45] Brown, R. S.; Taylor, L. T. *Anal. Chem.* **1983**, 55, 723.

[46] Vidrine, D. W. *J. Chromatogr. Sci.* **1979**, 17, 477.

[47] Vidrine, D. W.; Mattson, D. R. *Appl. Spectrosc.* **1978**, 32, 502.

[48] Griffiths, P. R.; Pentoney, S. L.; Giorgetti, A.; Shafer, K. H. *Anal. Chem.* **1986**, 58, 1349A.

[49] Jlnno, k.; Fujimoto, C. *J. Chromatogr.* **1990**, 506, 443,

[50] Fraser, D. J. J.; Norton, K. L.; Griffiths, P. R. *Anal. Chem.* **1990**, 62, 308.

[51] Fujimoto, C.; Morita, T.; Jinno, K. *J. Chromatogr.* **1988**, 438, 329.

[52] Haddad, P. R.; Heckenberg, A. L. *J. Chromatogr.* **1984**, 300, 357.

[53] Snyder, L. R., Kirkland, J. J. "Introduction to Modern Liquid Chromatography " 2nd ed; Wiley-Interscience: NewYork, **1979.**

[54] Kissinger, P. T. *Anal. Chem.* **1977**, 49, 447A.

[55] Lankelma, J.; Poppe, H. *J. Chromatogr.* **1976**, 125, 375

[56] Buchta, R. C.; Papa, L. *J. Chromatogr. Sci.* **1976**, 14, 213.

[57] Janata, J.; Ruzicka, J. *Anal. Chim. Acta* **1982**, 139, 105.

[58] Caudill, W. R.; Ewing, A. G; Jones.; Wightman, R. M. *Anal. Chem.* **1983**, 55, 1877.

[59] Ploegmarkers, H. H. J. L.; Mertens, M. J. M. *Anal. Chim. Acta* **1985**, 174, 71.

[60] Gunasingham, H.; Fleet, B. " Electroanalytical Chemistry " Vol.15.; Bard, A. J. Ed.; Marcel Dekker: New York, **1988.**

[61] Elferink, F.; Van Der Vigh, W. J. F.; Pinedo, H. M. *Anal. Chem.* **1986**, 58, 2549.

[62] Wang, J; Ouziel, E.; Yarnitzky, C.; Ariel, M. *Anal. Chim. Acta* **1978**, 102, 99.

[63] Samuelsson, R.; Osteryoung, J. *Anal. Chem.* **1980**, 52, 2215.

[64] Scanion, J. J.; Flaquer. P. A.; Robinson, G. W.; O'Brien, G.E.; Sturrock, P. E. *Anal. Chim. Acta* **1984**, 158, 169.

[65] Kounaves, S. P. ; Young, J. B. *Anal. Chem.* **1989**, 61, 1469.

[66] Last, T. A. *Anal. Chem.* **1983**, 55, 1509.

[67] Last, T. A. *Anal. Chim. Acta* **1983**, 155, 287.

[68] Trubey, R. K.; Niernan, T. A. *Anal. Chem.* **1986**, 58, 2549.

[69] Goto, M.; Shimada, K. *Chromatographia* **1986**, 21, 631.

[70] White, J. G.; St. Claire, R. L. III; Jorgenson, J. W. *Anal. Chem.* **1986**, 58, 293.

[71] Bard, A. J. *J. Chem. Educ.* **1983**, 60, 302.

[72] Murray, R. C.; Ewing, A. G.; Durst, R. A. *Anal. Chem.* **1987**, 59, 379A.

[73] Hou, W.; Wang, E. *Analyst* **1990**, 115, 139.

[74] Mayer, G. S.; Shoup, R. E. *J. Chromatogr.* **1983**, 255, 533.

[75] Lunte, C. E.; Kissinger, P. T.; Shoup, R. E. *Anal. Chem.* **1985**, 57, 1541.

[76] Roston, D. A.; Shoup, R. E.; Kissinger, P. T. *Anal. Chem.* **1985**, 54, 1417A.

[77] Schneiderman, M. A.; Sharma, A. K.; Locke, D. C. *J. Chromatogr.* **1987,** 409, 343.

[78] Ashley, L.; Levine, S. L. *Talanta* 1983, 30, 515.

[79] Kowalski, Z.; Kubiak, W. *Anal. Chim. Acta* 1984,159, 129.

[80] Reardon, P. A.; O'Brien, G. E.; Sturrock, P. E. *Anal. Chim. Acta,* **1984**, 162, 175.

[81] Scanlon, J. J.; Flaquer, P. A.; Robinson, G. W.; O'Brien, G. E.; Sturrock, P. E. *Anal. Chim. Acta,* **1984**, 158, 162.

[82] Heyrovsky, J.; Kuta, J. "Principles of Polarography "; Academic Press : New York, **1966**.

[83] Bond, A. M. "Modern Polarographic Methods in Analytical Chemistry" ; Marcel Dekker: New York, **1980.**

[84] Birke, R. L.; Gu, R.; Yau,J.; Kim, M-H. *Anal. Chem.* **1984**, 56, 1716.

[85] Heuser, J. R.; Girard, J. E. *Anal. Chem.* **1985**, 57, 2847.

[86] Kumar, V. T. " Electro-catalytic Detection in High Performance Liquid Chromatography of Vitamin B_{12} and other Molecules of Biological and Enviromental Interest."; Ph. D Diss., The City University of New York, **1992**.

[87] Sukenick, G. D. "The Design and Application of Two Versatile Computer Based Electrochemical Instruments for Static and Flow Chemical Analysis"; Ph. D diss., The City University of New York, **1993.**

[88] W. J. Ross, in M. E. Wolff (Ed.), "Burger's Medicinal Chemistry" 4th edn., Part II; Wiley: New York, 1981.

[89] United States Pharmacopeia, XX Rev., U.S. Pharmacopeial Convention; Rockville: M. D., 1980.

[90] Cosofret, V. V.; Buck, R. P. *Anal. Chim. Acta* **1985,** 174, 299.

[91] Kissinger, P. T.; Heineman, W. R. "Laboratory Techniques in Electroanalytical Chemistry"; Marcel Dekker: New York, **1984.**

[92] Yamada, J.; Matsuda, H. *J. Electroanal. Chem.* **1973,** 44, 189.

[93] Gunasingham, H.; Bernard, F. *Anal. Chem.* **1983,** 55, 1409.

[94] Hsi,T.; Johnson, D. C. *Anal. Chim. Acta* **1985,** 175, 23.

[95] Perone, S. P.; Jones, D. O. "Digital Computers in Scientific Instrumentation: Applications to Chemistry"; McGraw-Hill: NewYork, 1973.

[96] Kok, W. T.; Halvax, J. J.; Frei, R. W. *J. Chromatogr.* **1986,** 352, 27.

[97] Kounaves, S. P.; Young, J. B. *Anal. Chem.* **1989**, 61, 1469.

[98] Samuelsson, R.; O'Dea, J. J.; Osteryoung, J. *Anal. Chem.* **1980,** 52, 2215.

[99] Goto , M.; Shimadada, K. *Chromatographia,* **1986,** 21, 631.

Reference for Part III

[1] Pinta, M. "Modern Methods for Trace Element Analysis"; Ann Arbor Science: Ann Arbor, M.I., 1978.

[2] Sandell, E. B.; Onishi, H. "Photometric Determination of Traces of Metals. General Aspects."; Wiley: New York, **1978.**

[3] Borggaard, O. K.; Christensen, H. E. M.; Nielsen, T. K.; Willerns, M. *Analyst* **1982,** 107, 1479.

[4] Kinrade, J. D.; Van Loon, J. C. *Anal. Chem.* **1974,** 46, 1894.

[5] Lo, J. M.; Yu, J. C.; Hutchinson, F. I.; Wal, C. M. *Anal. Chem.* **1982,** 54, 2536.

[6] Bruland, K. W.; Franks, R. P.; Knauer, G. A.; Martin, J. H. *Anal. Chim. Acta* **1979,** 105, 233.

[7] Bond, A. M. "Modern Polarographic Mrthods in Analytical Chemistry "; Marcel Dekker: New York, 1980.

[8] Fiato, J. B. *Anal. Chem.* **1972,** 44, 75A.

[9] Copeland, T. R.; Osteryoung, R. A; Skogertoe, R. K. *Anal. Chem.* **1974,** 46, 2093.

[10] Bard, A. J.; Faulkner, L. R. " Electrochemical Methods"; Wiley: New York, **1980.**

[11] Mages, R. J. *Rev. Anal. Chem.* **1973,** 1, 335.

[12] Hulanicki, A. *Talanta* **1967,** 14, 1371.

[13] Uden, P. C.; Bigley, I. E. *Anal. Chim. Acta* **1977,** 94, 29.

[14] Heizmann, P.; Ballschmlter, K. *J. Chromatogr.* **1977,** 137, 153.

[15] Liska, O.; Guiochon, G.; Colin, H. *J. Chromatogr.* **1979,** 171, 145.

[16] Schwedt, G. *Chromatographia* **1978,** 11, 145.

[17] Liska, O.; Lehotay, J.; Brandsteterova, E.; Guiochon, G. *J. Chromatogr.* **1979,** 171, 153.

[18] Lehotay, J.; Liska, O.; Brandsteterova, E.; Guiochon, G. *J. Chromatogr.* **1979,** 172, 379.

[19] Liska, O.; Lehotay, J.; Brandsteterova, E.; Guiochon, G.; Colin, H. *J. Chromatogr.* **1979,** 172, 384

[20] Haring, N.; Ballschmlter, K. *Talanta* **1980,** 27, 873.

[21] Shih, Y.; Carr, P. W. *Anal. Chim. Acta* **1982,** 142, 55.

[22] Schwedt, G. *Chromatographia* **1979,** 12, 289.

[23] Dilli, S.; Hadded, P. R.; Htoon,A. K., *J. Chromatogr.* **1990,** 500, 313.

[24] Hutchins, S. R.; Haddad, P. R.; Dilli, S *J. Chromatogr.* **1982,** 252,185.

[25] Bond, A. M. ; Wallace, G. G. *Anal. Chem.* **1981,** 53, 1209.

[26] Bond, A. M. ; Wallace, G. G. *Anal. Chem.* **1982,** 54, 1706.

[27] Bond, A. M. ; Wallace, G. G. *Anal. Chem.* **1983,** 55, 718.

[28] Bond, A. M. ; Wallace, G. G. *Anal. Chem.* **1984,** 56, 2085.

[29] Ichinoki, S.; Yamazaki, M. *Anal. Chem.* **1985,** 57, 2219.

[30] Mueller, B. J.; Lovett, R. J. *Anal. Chem.* **1985,** 57, 2693.

[31] Johnson, D. C.; Weber, S. G.; Bond, A. M.; Wightman, R. M.; Shoup, R. E.; Knull, I.S. *Anal. Chim. Acta* **1986,** 180,187.

[32] Kissinger, P. T.; Heineman, W. R. "Laboratory Techniques in Electroanalytical Chemistry"; Dekker: New York, 1984.

[33] Toropova, V. F.; Budnlkov,R. G.; Uakovich, N. A. *Tananta* **1977**, 25, 283.

[34] Wheeler, S. H.; Mattson, B. M.; Miessier, G. L.; Pignolet, L. H. *Inorg. Chem.* **1978,** 17, 340.

[35] Hendrickson, A. R.; Martin, R. L.; Rohde, N. M. *Inorg. Chem.* **1975,** 14, 2980.

[36] Cauquls, G.; Lachenal, D. *J. Electroanal. Chem.* **1973,** 43, 205.